

# Electronic and Chemical Properties of Liquids and Solutions

---

Dissertation zur Erlangung des  
naturwissenschaftlichen Doktorgrades  
der Julius-Maximilians-Universität Würzburg

vorgelegt von  
Monika Blum  
aus Aschaffenburg

Würzburg 2009

Eingereicht am: 9. November 2009

Bei der Fakultät für Physik und Astronomie

1. Gutachter: Prof. Dr. E. Umbach

2. Gutachter: Prof. Dr. K. Fauth

der Dissertation

1. Prüfer: Prof. Dr. E. Umbach

2. Prüfer: Prof. Dr. K. Fauth

3. Prüfer: PD Dr. R. Fink

im Promotionskolloquium

Tag des Promotionskolloquiums: 17. Dezember 2009

Doktorurkunde ausgehändigt am: ...

# CONTENTS

---

<b>1</b>	<b>Introduction .....</b>	<b>1</b>
<b>2</b>	<b>Spectroscopic Methods.....</b>	<b>3</b>
2.1	X-ray Absorption Spectroscopy.....	3
2.2	X-ray Emission Spectroscopy.....	6
2.2.1	Resonant Inelastic X-ray Scattering .....	7
2.2.2	RIXS Dynamics .....	9
2.2.3	Raman Shift .....	11
2.2.4	Two-Dimensional RIXS Map.....	11
2.4	X-ray Spectroscopy of Molecules .....	13
<b>3</b>	<b>Instrumentation .....</b>	<b>17</b>
3.1	Membranes .....	17
3.2	Flow-Through Liquid Cell.....	19
3.3	Further Developments of the Liquid Cell – an Outlook.....	23
3.4	The SALSA Endstation – Home of the Flow-Through Liquid Cell.....	25
3.4.1	The SALSA Chamber.....	25
3.4.2	The X-ray Spectrometer.....	26
3.5	The Beamline .....	28
<b>4</b>	<b>Sodium Hydroxide and Sodium Deuterioxide in Aqueous Solution.....</b>	<b>31</b>
4.1	Aqueous Solutions of NaOH and NaOD .....	32
4.1.1	The XAS Spectra – Isotope Effect and Concentration Dependence ....	32
4.1.2	The Non-Resonant O K Edge XES Spectra – Concentration Dependence .....	33
4.1.3	The RIXS Maps – the Electronic Structure of the Hydroxide and Deuterioxide Ions.....	34
4.2	Solid NaOH – an Investigation.....	39
4.3	Summary .....	42

---

<b>5</b>	<b>Studies of Amino Acids in a Liquid Environment .....</b>	<b>45</b>
5.1	The Smallest Amino Acid: Glycine .....	49
5.1.1	The Nitrogen K Edge Absorption – a Comparison between Solid State, Solution, and Gas Phase.....	51
5.1.2	The Nitrogen K Edge Emission of Glycine – Impact of Different pH-Values .....	53
5.1.3	The Nitrogen K RIXS Map of the pH 6 Solution .....	58
5.1.4	A Glance at the Carbon K and the Oxygen K Edge of Glycine.....	59
5.1.5	Summary .....	65
5.2	An Amino Acid with Two Amine Groups: Lysine.....	66
5.3	Summary and Outlook .....	70
<b>6</b>	<b>Simple Alcohols and Acids .....</b>	<b>73</b>
6.1	Methanol .....	73
6.1.1	The O K Edge of Methanol .....	74
6.1.2	The C K Edge of Methanol.....	76
6.2	Acetic Acid .....	79
6.2.1	The O K Edge of Acetic Acid – a RIXS Map Study .....	80
6.2.2	The C K Edge of Acetic Acid.....	83
6.3	Summary .....	84
	<b>Summary .....</b>	<b>87</b>
	<b>Zusammenfassung .....</b>	<b>89</b>
	<b>Appendix.....</b>	<b>91</b>
	<b>Bibliography.....</b>	<b>97</b>
	<b>Own publications .....</b>	<b>115</b>
	<b>Curriculum Vitae.....</b>	<b>117</b>
	<b>Acknowledgment .....</b>	<b>119</b>

## CHAPTER I

# Introduction

---

Liquids and solutions seem to be “easy” substances which surround us in our daily life, including drinks, cleaning chemicals, and medicine.

Therefore, at first sight, one would think that liquids and solutions probably are well-known “chemicals”. This is probably true, but not on an atomic scale! Indeed, the geometric structure of liquids and solutions has been investigated by neutron and x-ray scattering as well as infrared spectroscopy [e.g., Har05, Wer04] but much less is known about their electronic structure. Since it is the intermittent bonding between molecules that gives aqueous solutions their peculiar characteristics, the electronic structure plays a crucial role in understanding the properties of the liquid state. In particular the dynamical aspects, e.g., the continuous forming and breaking of bonds within the hydrogen bond network, govern the microscopic and macroscopic behavior of liquids and solutions. Thus, a detailed investigation of the electronic structure of liquids is important to understand chemical and biological processes in aqueous environments. Soft x-ray techniques are an excellent choice to perform such investigations because they probe the local partial density of states.

This thesis focuses on the investigations of the electronic and chemical properties of liquids and solutions, which is still a very young field of research but also very important. In particular, understanding biological molecules in their natural environment, i.e., in aqueous solution, is crucial to understand biological processes, e.g. in bio-medicine. One example for such processes is the mechanism of the selective permeation of ions through channels in cell membranes [Hil92, Bez08]. Among the biological molecules, amino acids in solutions play an important role since they are the building blocks of peptides and proteins.

One main obstacle for investigating liquids and solutions with soft x-rays is that very sophisticated experimental setups are needed for these measurements. Such setups are not commercially available. The measurements presented in this thesis were performed in the new synchrotron endstation SALSA (**S**olid **A**nd **L**iquid **S**pectroscopic **A**nalysis) which is dedicated to the studies of biologically relevant systems in their natural environment [Blu09]. This endstation was developed and commissioned within the framework of this thesis. In particular, a novel flow-through liquid cell was developed.

---

The new setup was used to investigate different liquids and solutions. For experiments on solutions, a detailed knowledge of the pure solvent is essential. Therefore, concentration dependent measurements of sodium hydroxide (NaOH) and sodium deuterioxide (NaOD) were performed. NaOH was used as a solvent to change the pH-values of the amino acids, which form the center of this thesis. To achieve a basic knowledge of the electronic structure of amino acids and their pH-value dependency the simplest amino acid glycine and a small amino acid lysine were investigated. With the measurements of a simple alcohol and a simple acid, namely methanol and acetic acid, two common liquids used in daily life are a further topic.

The thesis is organized as follows: in Chapter 2 an overlook of the applied measurement techniques (photon-in-photon-out) is provided, and the approach of the RIXS map is introduced. The necessary experimental equipment with the newly designed flow-through liquid cell and the SALS endstation are explained in Chapter 3. In Chapter 4 the aqueous solutions of NaOH and NaOD are in the focus of the investigation. The amino acid solutions of glycine and lysine for different pH-values are the topic of Chapter 5. In Chapter 6 first investigations of methanol and acetic acid are presented.

## CHAPTER II

# Spectroscopic Methods

---

The central topic of this thesis is the study of the electronic structure of liquids and aqueous solutions. Despite the difficulties of the experimental realization (which is the topic of chapter 3), soft x-ray photon-in-photon-out methods together with a 3<sup>rd</sup> generation synchrotron source with tunable energy and high flux appear to be an excellent choice for these studies. While x-ray absorption spectroscopy (XAS) studies the unoccupied states, x-ray emission spectroscopy (XES) probes the occupied states. Finally, both techniques can be combined as resonant inelastic x-ray scattering (RIXS) providing additional information.

The following chapter will give insight in these three measuring techniques and will explain their basic physical principles. Furthermore, an introduction into the concept of RIXS-maps will be given. These maps make it possible to get the full XAS, XES, and RIXS information in one 2-dimensional image.

### 2.1 X-ray Absorption Spectroscopy

When atoms or molecules are irradiated with photons of sufficient energy, these photons can be absorbed by exciting an electron from an occupied orbital of the molecule into unoccupied states or removing it from the system (see Figure 2.1).

Soft X-ray absorption spectroscopy (XAS, often referred to as near edge x-ray absorption fine structure (NEXAFS)) takes advantage of this process, by using tunable energy to selectively excite electrons from a core level to an unoccupied state. Every photon entering a material system has a probability  $P_{i \rightarrow f}$  to be excited from the initial state  $i$  to a final state  $f$ . With the perturbation Hamiltonian  $H_{int}$  representing the photon this process can be described by Fermi's Golden Rule [Dir27]:

$$P_{i \rightarrow f} \propto |\langle f | \mathbf{H}_{int} | i \rangle|^2 \delta(E_f - E_i \pm h\nu) \quad (2.1)$$

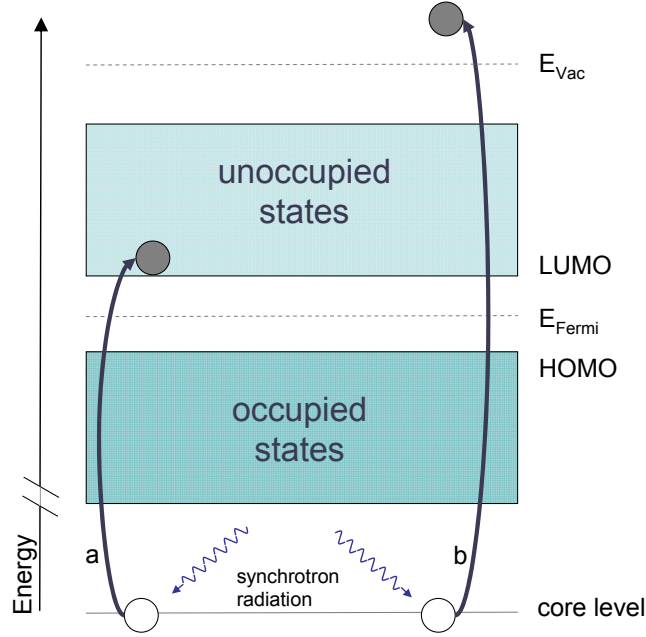


**Figure 2.1:** a) Schematic drawing of an excitation process into an unoccupied state. b) Excitation into a state above the vacuum level. The Schematic drawing is shown for a semiconductor but the processes are also possible for metals and molecules.

Where  $E_i$  and  $E_f$  are the energies of the initial and final states and  $h\nu$  represents the energy of the emitted ( $+h\nu$ ) or absorbed ( $-h\nu$ ) photon. The Dirac delta function ensures the energy conservation, i.e.  $E_f - E_i \pm h\nu = 0$ .

By applying the dipole approximation and neglecting multi-photon processes, the probability  $P_{i \rightarrow f}$  can be expressed by:

$$P_{i \rightarrow f} \propto \left| \sum_k \langle f | \hat{\mathbf{x}}_k | i \rangle \right|^2 \delta(E_f - E_i \pm h\nu) \quad (2.2)$$

Where  $\hat{\mathbf{e}}$  stands for the unit vector of the wave amplitude and  $\mathbf{x}_k$  for the linear momentum operators of the electrons. The sum accounts for all electrons interacting with the photon field and the dipole approximation considers the electric field to be constant over the spatial distribution of the affected electron wave function.



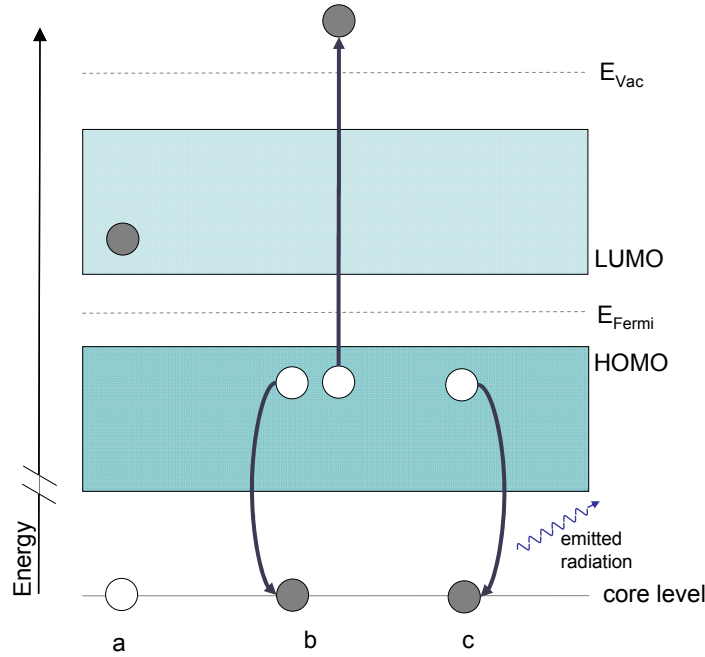


**Figure 2.2:** Schematic drawing of the decay processes. a) excited initial state, b) Auger decay process, and c) radiative decay process.

To extract an expression for the absorption intensity  $I_{XAS}(h\nu_{in})$  from the probability  $P_{i \rightarrow f}$  it has to be integrated over all possible final states  $f$ . The intensity can then be described by [Fer50]:

$$I_{XAS}(h\nu_{in}) \propto \sum_f \left| \sum_k \langle f | \hat{\mathbf{e}} \mathbf{x}_k | i \rangle \right|^2 \delta(E_f - E_i \pm h\nu) = \left| \sum_k \langle f | \hat{\mathbf{e}} \mathbf{x}_k | i \rangle \right|^2 \rho_f(E_f)$$

with  $E_f = E_i + h\nu_{in}$  (2.3)

Where  $\rho_f(E_f)$  stands for the density of states (DOS) and the matrix element makes sure that only transitions that fulfill the selection rules are allowed (symmetry and dipole selection rules [Kuk97]:  $\Delta L = \pm 1$ ,  $\Delta S = 0$ ,  $\Delta J = \pm 1, 0$  without  $J = 0 \rightarrow \Delta J = 0$ , and  $\Delta m_j = \pm 1, 0$  without  $m_j = 0 \rightarrow \Delta m_j = 0$  if  $\Delta J = 0$ ). Thus, only suitable states are probed, and the *partial* density of states can be used in equation 2.3. Furthermore, a wave-function overlap between initial and final state is needed. Caused by the localization of the core hole, only the density of states in the environment of the core

---

will be probed. Therefore,  $\rho_f(E_f)$  can be replaced by the *local* partial density of states  $\rho_p(E_f)$  (LPDOS).

After the excitation of an electron from a core level to an unoccupied state the now existing core hole can be refilled by an electron from a higher occupied level. For light elements this happens on the femtosecond time scale.

The energy gained when refilling the core hole can be “used” in two different ways:

1. The radiative decay (fluorescence): a photon with less or equal energy than the incident photon is emitted
2. The Auger decay: the energy is used to emit a weakly bound electron

Both processes are schematically shown in Figure 2.2. For light elements, the latter decay of both is usually more probable (emitted photons are  $\sim 0.1\%$  or less with respect to the total yield [Kra79]).

There are different ways to detect an absorption signal, e.g., transmission mode, electron yield (EY) mode, and fluorescence yield (FY) mode. For the transmission mode the photons passing through the sample without being absorbed are detected, and the absorption is directly inferred from this. In the soft x-ray range this method requires very thin samples. The EY mode is based on the Auger decay process and secondary processes, i.e. the method is very surface sensitive due to the mean free path of the electrons (typically a few nanometers [Tan93]). Both techniques are not suitable for the liquid flow-through cell design and the resulting measurements of liquids presented in this thesis. Therefore, the detection mode of choice is the FY mode, in which the emitted photons are detected. This method is bulk sensitive; thus it is possible to pass a membrane which is necessary to separate the liquid from UHV (see chapter 3). While in the so called total yield mode, all outgoing particles are detected, in the partial yield mode only selected energies are detected.

Apart from a small elastic contribution, most of the secondary photons have an energy below the absorption edge. Therefore, the absorption coefficient of the emitted photons is usually lower than for the absorbed ones which leads to *saturation effects* (sometime also called *self-absorption*). This effect depends on the geometry of detector and beam with respect to the sample. Very detailed information to self-absorption and saturation is given in the doctoral thesis of Oliver Fuchs [Fuc09\_Dr].

Further information on XAS/NEXAFS can be found in [Stö92].

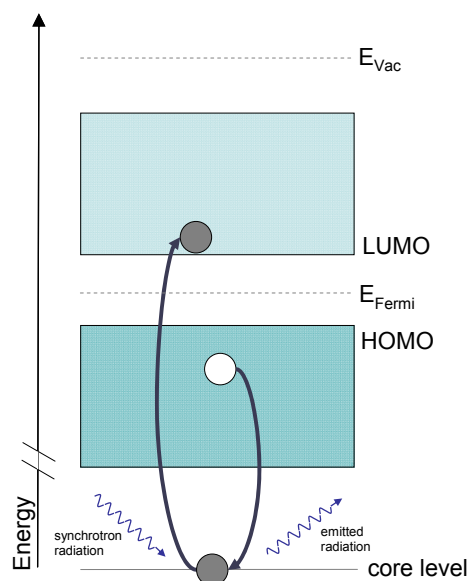


**Figure 2.3:** Schematic drawing of the non-resonant x-ray emission process.

## 2.2 X-ray Emission Spectroscopy

Whereas XAS probes the unoccupied electronic states, x-ray emission spectroscopy (XES) gives insight into the occupied electronic states. The XES process works as follows: after an electron from a core level is excited the system relaxes by filling the core hole with an electron typically from a valence level and a photon is emitted. The electrons allowed to refill the core hole are selected by the same selection rules as mentioned in 2.1; the process is schematically shown in Figure 2.3. In the case in which the core hole is filled by the excited electron, the photon is “reflected” without energy loss. The resulting peak is the so called *elastically scattered* or *Rayleigh line*.

The emission process is also described by Fermi’s Golden Rule in equation 2.1 ( $h\nu$  has to be positive) and the XES intensity can be expressed as follows:

$$I_{XES}(h\nu_{out}) \propto \left| \sum_k \langle f | \hat{\mathbf{x}}_k | i \rangle \right|^2 \rho_i(E_i) \quad \text{with } E_i = E_f + h\nu_{in} \quad (2.4)$$

---

Above, XES is shown as a simple two-step process. This gives a reasonable approximation for non-resonant excitations, i.e. the core electron is excited into a state above the vacuum level or into an occupied state, and the decay occurs without phase correlation with the absorption process. In the next section, XES will be discussed in the correct one step process which has to be applied for resonant excitation.

## 2.3 Resonant Inelastic X-ray Scattering

From the discussion of XES above it seems that the energy of the emitted photon is independent of the excitation energy. This is not valid for resonant excitations. Here, coherence between the emission and the absorption process exists, and the resonant emission has to be treated as one-step scattering process. This process, in general, is a form of electronic Raman scattering and is often referred to as resonant inelastic x-ray scattering (RIXS).

In the one-step process picture there is the probability of a transition from an initial state  $i$  with the energy  $E_i$  to a final state  $f$  with the energy  $E_f$  involves an intermediate state  $m$  with the energy  $E_m$  and the emission of a photon with the energy  $h\nu_{out}$ . The scattering process requires second order perturbation theory, leading to the Kramers-Heisenberg formalism [Kra25]. In 1992 the formalism was – for the first time – used by Ma et al. to explain resonant effects in XES spectra [Ma92, Ma94]. Disregarding the non-resonant term and multiple-photon processes, results in the cross section for the inelastic scattering process. Hereby, a photon with the energy  $h\nu_{in}$  is absorbed, and a photon with the energy  $h\nu_{out}$  is emitted into the solid angle  $\Omega$  [Ma94]:

$$\frac{d^2\sigma(\nu_{in})}{d\nu_{out}d\Omega} \propto \sum_f \sum_m \frac{|\langle f | p \cdot \hat{e}_{out} | m \rangle \langle m | p \cdot \hat{e}_{in} | i \rangle|^2}{(E_m - E_i - h\nu_{in})^2 + \Gamma_m^2/4} \cdot \delta(h\nu_{in} - h\nu_{out} - E_f + E_i) \quad (2.5)$$

where  $\Gamma_m$  identifies the lifetime broadening of the intermediate state  $m$ . The  $\delta$  function ensures the energy conservation and shows the independence of the emitted photon energy from the intermediate state. The denominator in equation 2.5 defines the resonance condition, i.e., intermediate states are preferred which have an energy of

$h\nu_{in}$  above the initial state  $i$ . If there are real states in the range of  $|E_m - E_i - h\nu_{in}| < \Gamma_m$  it is called the on-resonance case [Cal98]. Furthermore, there is a near-resonance case with  $|E_m - E_i - h\nu_{in}| > \Gamma_m$ . The probability for the latter is much lower and is interpreted as an excitation into virtual intermediate states.

For completeness it should be mentioned that RIXS can also be used for band structure studies. For crystalline samples in the one-step scattering process the wave functions in equation 2.5 can be described by periodic Bloch wave functions with a well defined crystal momentum  $k$ . If the excitation is coherent over many lattice unit cells and if the momentum of the x-ray photon can be neglected for soft x-rays the emission and the absorption process have to take place at the same position in the Brillouin zone. This crystal momentum conservation was first described by Ma et al. [Ma92, Ma94, Ma96]. The neglect of the momentum is a good approximation for photons in the very low soft x-ray range. However, for higher excitation energies the the momentum be included. This was shown for the example of the Si K edge ( $E_{Exc}=1840$  eV) by Ma et al. [Ma95].

One of the main advantages of this technique is that for soft x-rays the selection of  $k$ -vector is only chosen by the excitation energy and not by the experimental geometry and thus RIXS can even be used to study poly-crystalline samples.

A nice overview about band structure studies with RIXS with detailed information and examples was published by S. Eisebitt and W. Eberhardt [Eis00].

### 2.3.1 RIXS Dynamics

To study the electronic structure, dynamics are of interest and should not be neglect. This was illustrated in the Presentation Speech for the Nobel Prize in Chemistry 1986 given by Sture Forsén. Forsén compared a scientist with a spectator of a drastically shortened version of a classical drama, where he or she is only shown the opening scene of the first act and the last scene of the final. The main characters are introduced, then the curtain falls for change of scenery and as it rises again, on the scenery floor a considerable number of dead bodies can be seen and a few survivors. Not an easy task for the inexperienced to unravel what actually took place in between [For86]. Hereby, the core-hole lifetime can be a useful tool to study dynamics and so to unravel what took place in between.

In principle two different kinds of dynamics were found for the RIXS process, namely electron and proton dynamics. Electron dynamics are especially important for solids, where RIXS can be used for band mapping.

---

Hereby, electron-electron and phonon-electron interactions can lead to scattering processes that cause a loss of k-information, i.e. dephasing. A common approximation is to divide the spectra into a so-called ‘incoherent’ fraction, which shows no excitation energy dependence and a so-called ‘coherent’ fraction  $f$  (i.e. the ratio between coherent and total intensities), which is given by:

$$f = \frac{\tau_D}{\tau_D + \tau_L} \quad (2.6)$$

where  $\tau_D$  identifies the dephasing time and  $\tau_L$  the lifetime of the core hole. If the core hole lifetime is known, it is then possible to determine the characteristic dephasing time from the RIXS spectra [Ma96, Min98, Eis00, Rub00]. The coherent fraction is rarely more than 10% and decreases by increasing the excitation energy higher above the threshold, because the possibility of scattering processes increases with higher excitation energy [Rub00]. Furthermore, it is possible to “shorten” the core-hole lifetime by detuning the excitation energy to below the absorption onset according to Heisenberg’s uncertainly principle [Bjö97].

In addition to the scattering processes described above proton dynamics are reported [Bjö92, Bjö97, Bri99, Fuc08, Ode09, Ode09\_2] which also take place on the time-scale of the core hole lifetime. If the excitation leads to an anti-bonding intermediate state, the atoms start to move apart, i.e. the molecule starts to dissociate. This is especially valid for low-Z elements such as hydrogen atoms, which can move far enough (during the core hole lifetime) to cause a significant change in the resulting emission spectra. The results of the atom movement are two different signatures in the spectrum: an undissociated component representing the intact molecule and a dissociated component. The latter is the fraction of molecules, for which the corresponding molecular bond no longer exists, i.e. the proton has no significant overlap with the electron density of the rest of the molecule. For instance RIXS spectra of liquid water reveal a peak splitting, which is not seen in PES measurements. This splitting can be explained by proton dynamics [Fuc08, Fuc08\_co, Ode09, Ode09\_2]. The concept of proton dynamics is based on the final state rule [Bar82, Nil95], and the final state with the displaced protons can be observed in the emission spectra.

Proton dynamics are of particular importance for soft x-ray measurements of liquids, to which this thesis is dedicated. Therefore, more details on that will be given in chapters 4 and 5.

Further information about RIXS dynamics can be found in [Rub00].

### 2.3.2 Raman Shift

In most RIXS spectra right below the absorption edge a shift of the emission lines parallel to the Rayleigh line can be observed which is called *Raman shift*. It is the result of the Lorentzian resonance condition and the energy-conserving Dirac delta function (see equation 2.5): The Lorentzian makes detuned excitations into short-lived virtual states below the absorption onset possible. In the final state, however, the excited electron has to be lifted from the virtual state into a real state. The necessary energy has to be “paid” by the emitting photon leading to a shift of the emission spectrum to lower energies.

Within this work, the Raman shift will show up in different occasions (e.g. chapter 4).

### 2.3.3 Two-dimensional RIXS Map

In section 3.4.2 the novel high-transmission soft x-ray spectrometer used for the measurements in this thesis will be described. With this instrument it is possible to detect complete RIXS maps within 10 to 60 minutes instead of a small number of spectra at selected excitation energies. A RIXS map is a two-dimensional representation of the color-coded emission intensity as a function of emission (abscissa) and excitation (ordinate) energy. Thus it provides the full information accessible with soft x-ray spectroscopies. Especially, resonant effects which go along with intensity variation and energy shifts, which were always difficult to identify, since only a few emission spectra at selected excitation energies were available, can be found more easily.

Most of the data in this thesis will be presented in the form of RIXS maps. In the following, the principle of a RIXS map is explained using H<sub>2</sub>O as an example. Figure 2.4 (left side) shows the resonant series of H<sub>2</sub>O (O-K edge) measured with a state-to-the-art soft x-ray spectrometer based on the Rowland-circle geometry. The excitation energies range from 533.5 eV (bottom spectrum, cyan) to 550.1 eV (top spectrum, red). Each spectrum was measured for 600 s adding up to a total measuring time of 3 h 20 min. In comparison Figure 2.4 (right side) shows the spectra recorded with the new spectrometer. These spectra are subset of the RIXS map in Figure 2.5. Their total measuring time was approximately 5 min, i.e. a measurement time of 15 s per spectrum. No difference in statistics between the spectra can be found. The resolution of the new spectrometer is even slightly better than that of the Rowland-circle spectrometer. In Figure 2.5 the whole O-K edge RIXS map is shown. The

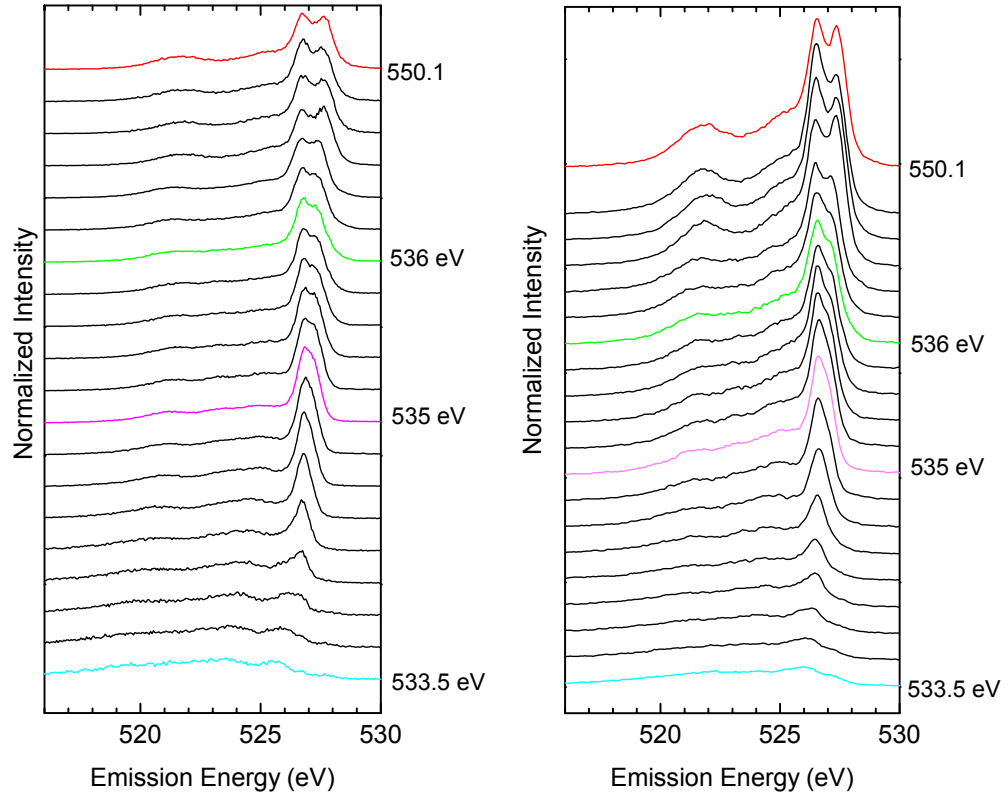


**Figure 2.4:** Left: O-K edge RIXS series measured with a Rowland-circle soft x-ray spectrometer. Total measuring time for 20 spectra: 3 h 20 min. Right: Single spectra from RIXS map. Total measuring time for 20 spectra: 5 min.

emission spectrum (non-resonant) excitation energy of 550.1 eV is shown at the top of the map (also red spectrum). The spectrum on the right hand side represents a partial (the intensity between emission energies of 516.2 and 533.8 eV were added up) fluorescence yield absorption spectrum. The elastically scattered peak (Rayleigh line) can be found as a bright diagonal line with equal excitation and emission energies in the lower right corner of the map. Every line of the map is a single spectrum at a certain excitation energy. With the color-coded intensity it is now much easier to identify resonant effects.

The results in chapter 4, 5, and 6 will be mostly presented in RIXS maps and discussed in the different sections.



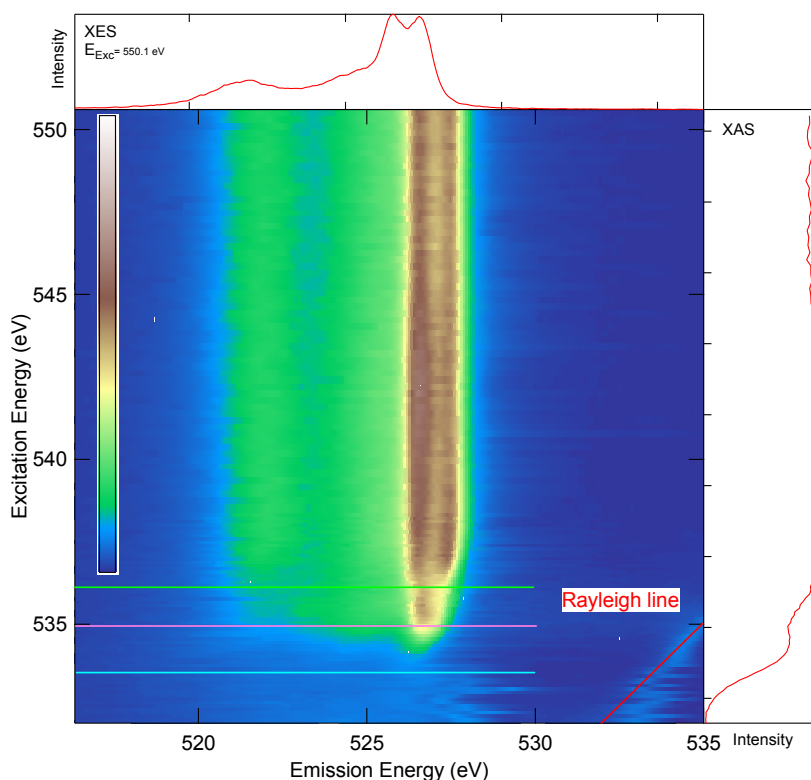


**Figure 2.5:** O-K edge RIXS map of  $\text{H}_2\text{O}$ . The horizontal axis represents the emission energy, the vertical axis shows the excitation energy, and the emission intensity is color-coded. Above the map, a non-resonant spectrum at an excitation energy of 550.1 eV is shown. The right panel corresponds to a partial fluorescence yield absorption spectrum. The Rayleigh line can be found as a diagonal line in the right lower corner of the map. The three colored horizontal lines stand for the excitation energies shown in Figure 2.5.

## 2.4 X-ray spectroscopy of molecules

The focus of the here presented thesis is on the studies of liquids and solutions with x-ray spectroscopy, which is a very young field of research. However, the study of molecules with x-ray spectroscopies (in particular with XAS) has been done for a long time. In the following section an overview is given why x-ray spectroscopy is an excellent tool to study the electronic structure of molecules. A few examples are given.

First of all XAS as well as XES are probes of the local density of states. Thus it is possible to focus the study on a specific element of the molecule. This gives detailed information about the wave functions of the unoccupied and occupied molecular orbitals [Mei89]. The element specific excitation can be used as a tool for “choosing” a

---

specific functional group, e.g., in this thesis the amine and carboxylic functional groups of glycine (see chapter 5).

Furthermore, the techniques can be used to investigate a selective excitation of chemically shifted atoms of the same element in the molecule. Hereby, the influence of a core-hole modifies the empty orbital structure in terms of symmetry and energy shifts. Core-level shifts can be observed in the absorption spectra and can be used to selectively generate core-holes on different atoms of the same element for the emission studies. E.g., N<sub>2</sub> absorbed on Ni (100), here the two chemically different N atoms can be observed in the XAS spectrum for the N1s  $\rightarrow$  2  $\pi^*$  transition [San93, Nil97, Ben98]. In this thesis such a chemically selective excitation was used in the case of acetic acid (see chapter 6).

With x-ray spectroscopy it is also possible to investigate the symmetry of well-ordered molecules on surfaces. By using dipole selection rules with suitable experimental geometries the contributions from  $\pi^*$  and  $\sigma^*$  orbitals can be separated. A good example molecule which was studied in our group in quite some detail with both XAS [Umb90, Tab95, Umb98, Sch05, Zou06, Stö92, Fri02, Fri03, Gus07] and XES [Fuc\_PT] is 3,4,9,10-perylene tetracarboxylic acid dianhydride (PTCDA).

While as discussed above x-ray spectroscopies give detailed information about the electronic and chemical properties of molecules, the measurement itself is difficult due to the sensitivity of the molecules towards soft x-rays as will be discussed in the following.

## Beam damage

Under the impact of photons organic molecules react very sensitive to x-rays [McC58, Ste70, Box71, Box72, Isa73, Box74, Lin74, Ada76, Ben82, Ebe83, Wad84, Str93, Boz94, Che96, San97, Bur00, Abd00, Feu00, Hei01, Pen01, Kem01, Cof02, San02, Che02, Dow04, Zub04, Zub04\_2]. Radiation induced damage manifests itself in the disturbance of a long-range crystalline or supermolecular order and in chemical modifications of the system under study, e.g., dissociation, free radical formation, or mass loss. The radiation-induced chemical modifications can be observed in the spectra mostly by spectral changes over time. For example amino acids decompose under radiation via several pathways, including dehydrogenation, decarboxylation, deamination, and dehydration [Zub04]. Zubavichus et al. showed on the example of phenylalanine and tyrosine which components of the molecule is influenced by the radiation. If the molecule possesses a carboxylic functional group this one is the first that decomposes [Zub04\_2].

For synchrotron based studies the flux density of the beam is very high and can cause beam damage in less than a second. To rule out possible beam induced changes in the XES and XAS spectra the samples have to be handled with special care. From beam damage series (measuring spectra on the same spot on a solid sample as a function of time) the critical exposure time after which beam damage becomes visible can be determined. To avoid significant damage the sample can be measured while continuously scanning the beam across the sample such that the critical exposure time is never reached for each single measuring position [Fuc\_PT].

In this thesis the focus is on liquids and solutions. Since many such samples consist of (organic) molecules beam damage effects will also take place. While for static cells these effects were reported [Fuc09\_Dr], they can be avoided by using a flow-through liquid cell as described in the following chapter.

---

## CHAPTER III

# INSTRUMENTATION

---

In recent years, the investigation of the electronic structure of liquids has grown to a vivid research field. Since all measurement techniques to study the electronic structure, in particular photoelectron spectroscopy (PES) as well as soft x-ray emission (XES) and absorption (XAS) spectroscopy, require ultra-high vacuum (UHV), which is incompatible with liquids, these investigations are a technical challenge. To use the wealth of information offered by these techniques sophisticated experimental setups are needed. First attempts to measure liquids with PES date back to the early seventies [Sie73] using a wetted wire or wheel and differential pumping. Today, such PES measurements can be performed with a liquid micro jet injected directly into the vacuum [Wil04, Win06] or a droplet train [Sta08]. However, this approach has two major disadvantages. First, the liquid in the jet is far away from thermodynamic equilibrium, i.e. the measured spectra are always a mixture of gaseous and liquid signal [Win06]. Second, due to the short inelastic mean free path of the electrons (typically a few nanometers [Tan93]) only the surface of the liquid can be studied, which is expected to be different from its bulk [Sie85]. These limitations can be overcome by using photon-in-photon-out techniques in the soft x-ray range with an information depth of a few hundred nanometers. The information depth of these techniques makes it possible to separate the sample liquid from the UHV and thus study the liquid of interest in thermodynamic equilibrium at normal pressure. The separation of liquid and UHV is accomplished by a thin window membrane. In the following the different membranes used in this thesis are discussed followed by a description of the designs of the flow-through liquid cell, the SALSA endstation, and the VLS spectrometer. In the last subsection of this chapter Beamline 8.0.1 at the Advanced Light Source (ALS) is described.

### 3.1 Membranes

Since 1994 Silson Ltd (UK) produces ultra-thin silicon nitride ( $\text{Si}_3\text{N}_4$ ) window membranes which are extensively used within the x-ray and e-beam communities [Sil].

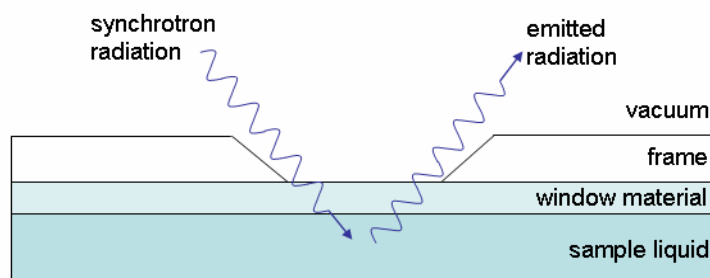


**Figure 3.1:** Schematic drawing of a window membrane.

With these  $\text{Si}_3\text{N}_4$  membranes the liquid of interest can be separated from the UHV which makes it possible to use bulk-sensitive techniques like XES and XAS for the study of liquids [Guo02, Dud04].

In principle all membranes are based on the same design which is shown in Figure 3.1. X-ray photons (with an information depth of typically a few hundred nanometers) enter through the window membrane into the liquid and the emitted photons then exit via the same opening. Even if the design of the membranes is very similar not every membrane material can be used for every measurement.

There are two main requirements for a suitable membrane material: First the membrane must not contain the studied element (i.e. to detect the nitrogen K edge one can not use a silicon nitride ( $\text{Si}_3\text{N}_4$ ) membrane) and second, the transmission should be high at and around the respective absorption/emission edge (see Figure 3.2). For this thesis the main focus is on organic samples. Thus, the most important edges are the oxygen K, the carbon K, the nitrogen K, and the sulfur  $\text{L}_{2,3}$  edges. In Figure 3.2 the total transmissions of suitable membranes are shown over a photon energy range from 10 to 650 eV (note that the energy range of the used x-ray spectrometer is between 130 and 650 eV, see section 3.4.2). Vertical colored bars identify typical excitation and emission energy ranges of the important edges.

To achieve optimal transmission,  $\text{Si}_3\text{N}_4$  membranes (Silson Ltd) with a thickness of  $\sim 100$  nm were used for the O K and C K measurements and silicon carbide (SiC) membranes (NTT group) with a thickness of  $\sim 150$  nm were used for the O K and N K measurements. The  $\text{Si}_3\text{N}_4$  and the SiC membranes have a silicon frame and a membrane size of  $1 \times 1 \text{ mm}^2$  (see Fig. 3.1). Due to the strong absorption of the Si  $\text{L}_{2,3}$  edge both membrane materials are not suited for the S  $\text{L}_{2,3}$  edge, since the theoretical transmission of  $\text{Si}_3\text{N}_4$  and SiC membranes of the required thickness is below 1% (see Figure 3.2 and [CXRO]). Instead, carbon-based (and Si-free) materials

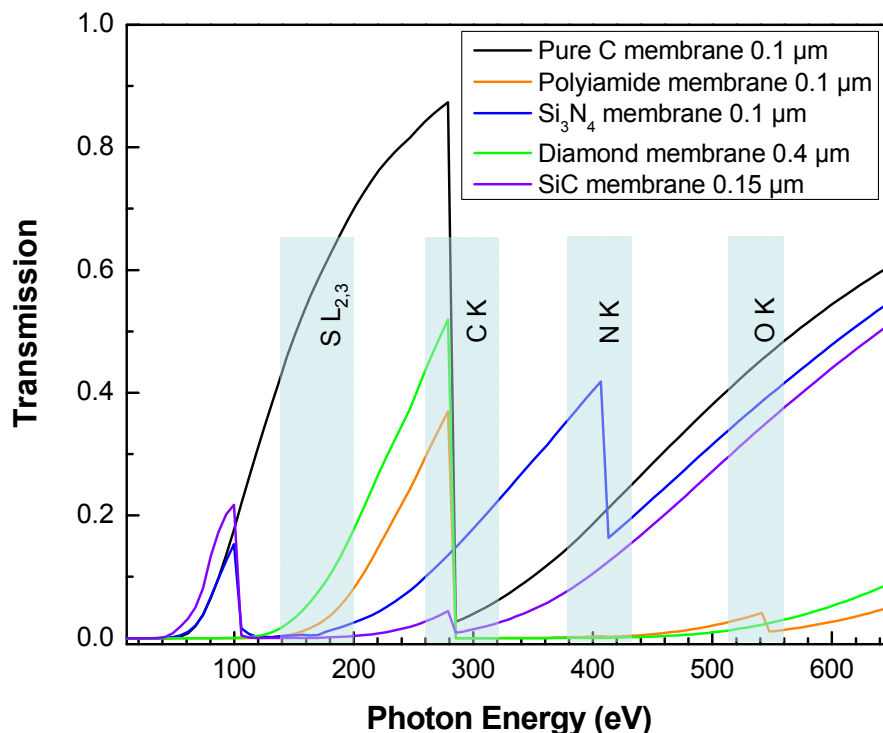


**Figure 3.2:** Calculated (total) transmissions for different window membrane materials ( $\text{Si}_3\text{N}_4$ , SiC, diamond film, Polyimide, and pure carbon) in the photon energy range between 10 and 650 eV [CXRO]. Colored vertical bars represent typical excitation and emission energies for the relevant edges (the sulfur  $L_{2,3}$  edge, the carbon K edge, the nitrogen K edge, and the oxygen K edge).

can be used [Hes03]; by now three different types were tested. First, a polyimide ( $\text{C}_{22}\text{H}_{10}\text{N}_2\text{O}_5$ ) membrane (Luxel) with a thickness of  $\sim 1 \mu\text{m}$  and a membrane size of 1mm in diameter, second, a diamond film (Applied Diamond) with a thickness of  $\sim 400 \text{ nm}$  and also an opening of 1 mm in diameter, and third, pure carbon membranes (Joakim Andersson, Uppsala University, Sweden) with a thickness of  $\sim 80 \text{ nm}$  and  $\sim 100 \text{ nm}$ . The latter will be the choice for future measurements at the S  $L_{2,3}$  edge.

### 3.2 Flow-Through Liquid Cell

The membranes described above are necessary to separate the sample liquid and the UHV and are integrated in a so called liquid cell which will be described in this section.

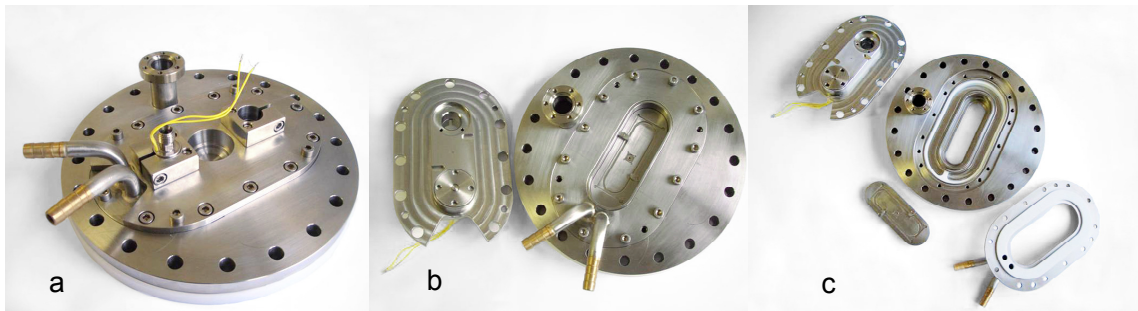


**Figure 3.3:** **a)** Flow-through liquid cell integrated into a standard CF150 flange. **b)** View onto inset, top part with liquid valves removed. **c)** Disassembled cell; view onto cooling circuit channel, inset is lying next to the flange.

First XES and XAS experiments on liquids were performed using static liquid cells [Guo02, Hes03, Dud04, Ode05]. In a static cell, a small amount of liquid is encapsulated behind the window membrane on a modified sample holder, which allows the introduction of the liquid cell into the UHV like any other (dry) solid sample. However, there are several disadvantages of the static cell concept. First, a temperature control is difficult with this design and was not implemented in any of these static cells. Furthermore, due to the (necessary) high x-ray intensity for XES measurements, an increased local temperature in the liquid near the window membrane is unavoidable, even when the liquid cell body is externally cooled. For water and many other liquids, this as well as x-ray induced dissociation processes can lead to the formation of bubbles behind the window. Furthermore, for solutions the deposition of solutes (or dissociation fragments thereof) on the inside surface of the membrane potentially occur, which can have a strong contribution to the measured spectra. Finally, chemical interactions between the liquid and the window membrane were found, e.g., the oxidation of (oxygen-free) Si-based membranes during the study of water [Fuc08\_2].

To avoid or minimize these issues a first flow-through liquid cell was developed in our group [Fuc08\_2]. This cell is integrated into a standard UHV sample manipulator with XYZ-translation. In this design, the investigated liquid is continuously sucked through the cell with a flow rate of approximately 45  $\mu\text{l/s}$ , e.g., replacing the content of the cell 15 times per second. Similar designs of a flow-through cell are used by Forsberg et al. [For07] to study atmospheric corrosion by soft x-rays and by Tokushima et al. [Tok09].

In this thesis a completely new design of a flow-through liquid cell is presented. In this new design an optical microscope can be integrated into the liquid cell. Moreover it contains an improved temperature control, its maintenance is simplified,



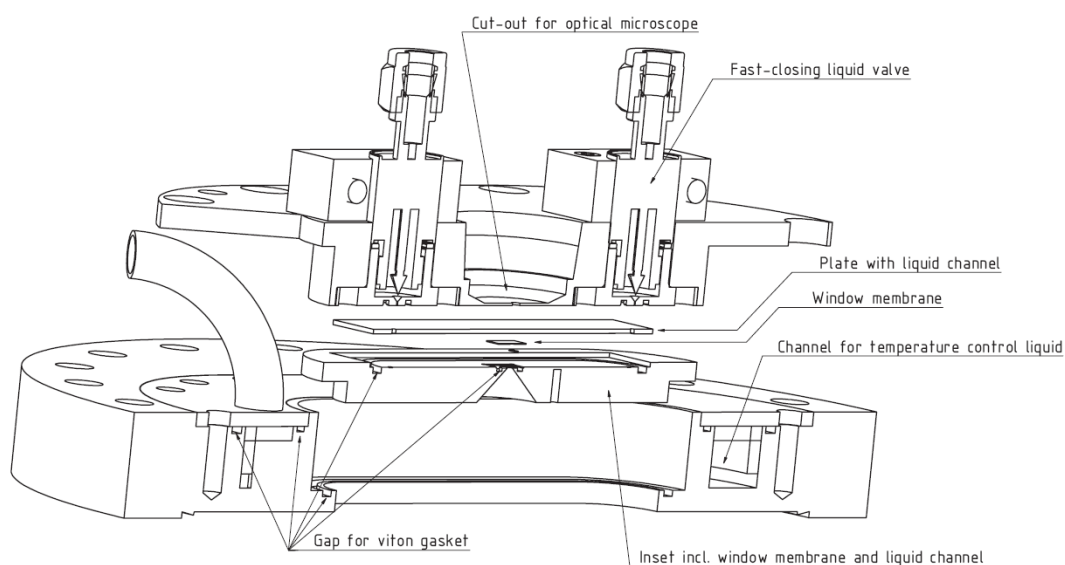


**Figure 3.4:** Exploded view of the flow-through liquid cell. For better visibility, the Viton gaskets are not shown.

and it is much more flexible for further applications (such as investigations of solid/liquid interfaces and electrochemical cells).

Figure 3.3 shows pictures of the new flow-through liquid cell and of its easy disassembly. All parts are labeled in the exploded view of the cell in Figure 3.4. The cell is integrated into a standard CF150 (8" outer diameter) flange. For temperature-controlled measurements, a separate, Teflon-insulated liquid circuit channel is milled into the flange (see Figure 3.3c and Figure 3.4). A temperature control liquid is pumped through the channel with a water chiller, resulting in a strongly improved temperature response, with respect to former liquid cells. With this setup temperatures from approximately 1 °C up to approximately 90 °C can be reached.

The “heart” of the cell is a removable inset which is vacuum-sealed with a Viton O-ring (see Figure 3.3 b, c and Figure 3.4). The inset contains the window membrane, sealed with a Viton O-ring, and a stainless steel plate with two feedthroughs (inlet and outlet) and a channel for the liquid. This is depicted in Figure 3.5, which shows a detailed sketch of the inset.

The sample liquid is sucked through the inlet into a 100 µm deep channel (65 mm long and 1.3. mm wide) and passes behind the window membrane, creating a bubble-free laminar flow. The sucking helps to reduce the pressure on the window membrane which reduces the risk of a membrane break. With respect to the

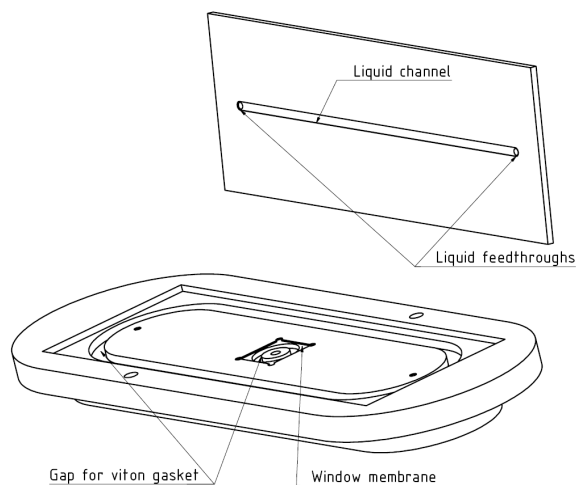


**Figure 3.5:** Detailed sketch of the liquid cell inset and the plate with the liquid channel. The plate fits into the cut-out of the inset.

previous design [Fuc08\_2], the liquid volume in the cell is reduced from 15 to 8.5  $\mu\text{l}$ . This volume can be separated from the liquid reservoir by fast-closing liquid valves (Parker; see Figure 3.3 and Figure 3.4). In the case of a membrane rupture, a fast pressure sensor closes the valves within 1.5 ms, leaving only the small sample liquid volume of the liquid cell exposed to the vacuum. Thus, the time for the recovering of the vacuum can be reduced in respect to older setups. Furthermore, the overall sample volume is minimized by this out-of-vacuum design. Due to the easy accessibility of the liquid valves, all tubes are outside the vacuum and can be kept very short reducing the total volume of the sample liquid required to less than 10 ml.

One big advantage, with respect of maintaining the liquid cell, is the easy and fast exchange of the inset and the possibility to use very different window membrane types (i.e., materials), sizes, and thicknesses (see section 3.1) by having insets adapted to the respective membrane. To exchange the inset the top part with the liquid valves has to be removed and the inset can be taken out without interference with the cooling circuit (see Fig 3.3 b).

The new flexible cell design can be used for a variety of different experiments, using different insets for variable membrane types as well as an inset for solid state samples. The latter is important to obtain reference spectra for comparison with the liquids. Furthermore, it is possible to perform optical microscopy of the liquid sample exposed to the beam. For this purpose, the stainless steel plate containing the liquid channel can be replaced by a glass plate, and a microscope is mounted between the fast-closing liquid valves (see Figure 3.4).

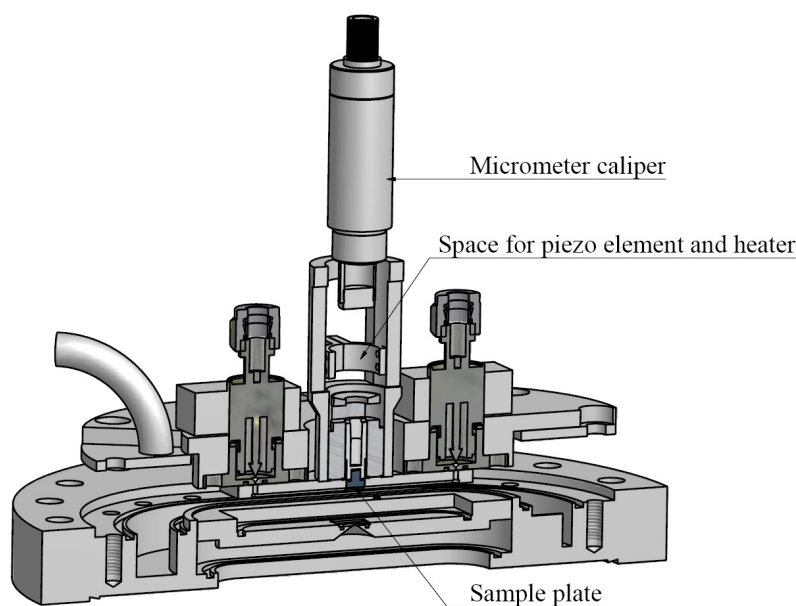


**Figure 3.6:** Modified flow-through liquid cell for the investigation of solid-liquid interfaces. The picture shows the cell with movable sample plate, micrometer caliper, piezo element, and heater.

The next section will give an insight what can be done with this new liquid cell in the future.

### 3.3 Further Developments of the Liquid Cell – an Outlook

As mentioned above, the new flow-through liquid cell is a very flexible design, and can thus be modified for the use in a variety of different experiments.

One of these further developments of the liquid cell is dedicated to study the solid-liquid interfaces (e.g. for investigating the chemical bath deposition process frequently used in thin film solar cells [Wei03, Wei03\_2, Bär05, Bär05\_2, Bär05\_3, Bär06, Enn06]). For this purpose, the top part of the cell and the plate with the liquid channel was modified as can be seen in Figure 3.6.

In this design, the sample can be moved near the window through a round cut-out in the middle of the plate with the liquid channel. For a precise movement toward the window membrane, a micrometer caliper and a piezo element are used, onto which the solid sample (e.g. a thin film solar cell) is mounted. Furthermore, the sample plate

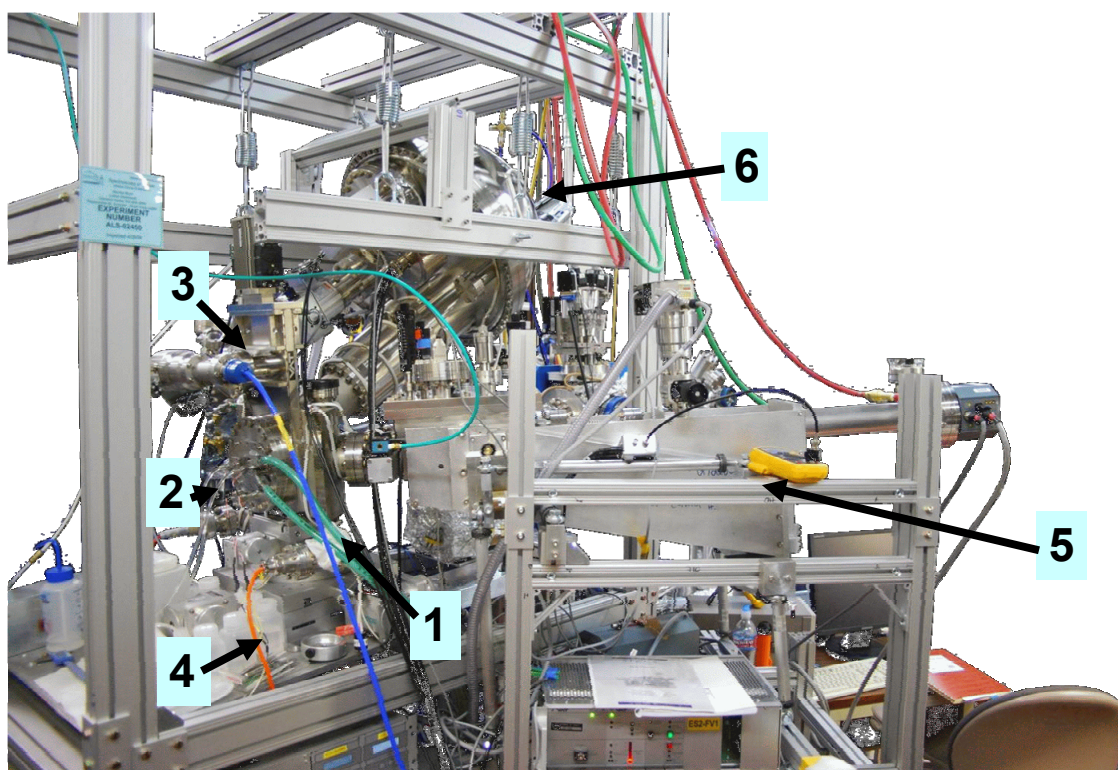


**Figure 3.7:** Picture of the SALSA endstation at Beamline 8.0.1 of the Advanced Light Source, Lawrence Berkeley National Lab. 1: analysis vacuum chamber, 2: flow-through liquid cell, 3: pneumatic valve to separate liquid cell and analysis chamber, 4: micrometer x-y-z precision stage, 5: VLS soft x-ray spectrometer, and 6: electron analyzer (Specs PHOIBOS 150MCD) suspended by springs.

can be heated from the back side. All other parts (i.e. liquid valves, inset, and cooling circuit) are identical to the flow-through liquid cell presented in section 3.2. The liquid is (again) sucked through the inlet feedthrough and passes between the window membrane and the solid sample. Systems of interest to be investigated with this setup are for example fuel cells as well as the layer growth from a solution.

Furthermore, first gas measurements were performed with cell described in this chapter. For these first experiments, a gas reservoir was installed in front of the liquid inlet. The gas is then sucked through the cell with the same system used for the liquids (for an example see chapter 5).

### 3.4 The SALSA Endstation – Home of the Flow-Through Liquid Cell

The SALSA (“Solid And Liquid Spectroscopic Analysis”) endstation with the mounted liquid cell is shown in Figure 3.7. SALSA includes a custom-built analysis (vacuum) chamber (with the attached flow-through liquid cell), a high-resolution high-transmission x-ray spectrometer described in section 3.4.2 and in [Fuc09], and a Specs PHOIBOS 150MCD electron analyzer. For solid sample measurements the cell can be replaced by a custom-built preparation chamber with a standard UHV manipulator and surface preparation equipment, as discussed below. Figure 3.8 shows a photograph of SALSA with the preparation chamber mounted.

#### 3.4.1 The SALSA Chamber

The CF150 flange of the new flow-through liquid cell is attached to the backside of the analysis chamber. It is connected to the chamber via a CF150 pneumatic valve (VAT) with an independent pumping system. With this valve the flow-through liquid cell can be separated from the analysis chamber, which is useful for two reasons. First, with the valve closed it is possible to replace the inset or the membrane without compromising the vacuum in the SALSA analysis chamber. Second, it protects the analysis chamber in the case of a membrane rupture. In this case, sample liquid is released into the vacuum leading to a fast pressure rise in the chamber. At a pressure of  $5 \times 10^{-7}$  mbar, a fast pressure sensor trips, closing not only the fast liquid valves in the cell, but also the CF150 pneumatic valve, a CF40 pneumatic valve separating the analysis chamber and the soft x-ray spectrometer, and a fast valve installed in the beamline close to the endstation. The interlock system is fast enough that the rest of the beamline is not affected by the pressure rise. With the closed CF 150 pneumatic valve the vacuum in the analysis chamber and the x-ray spectrometer can start to recover immediately after the membrane rupture. Thus the recovering time could be reduced (to approx. 30 min) in respect to older designs.

The analysis chamber is nearly a semi-cylinder, with the center point at the window membrane of the liquid cell. This center point is also the focus position of the synchrotron beam and the x-ray and electron spectrometers. To achieve this alignment, the entire analysis chamber can be adjusted with micrometer precision using an xyz-stage (Huber). The range of motion is  $\pm 25$  mm in the x and y direction and 10 mm in the z direction, respectively.

SALSA is – as the name tells – not only an endstation for liquids but also for solid state samples. As mentioned above, a preparation chamber with a standard

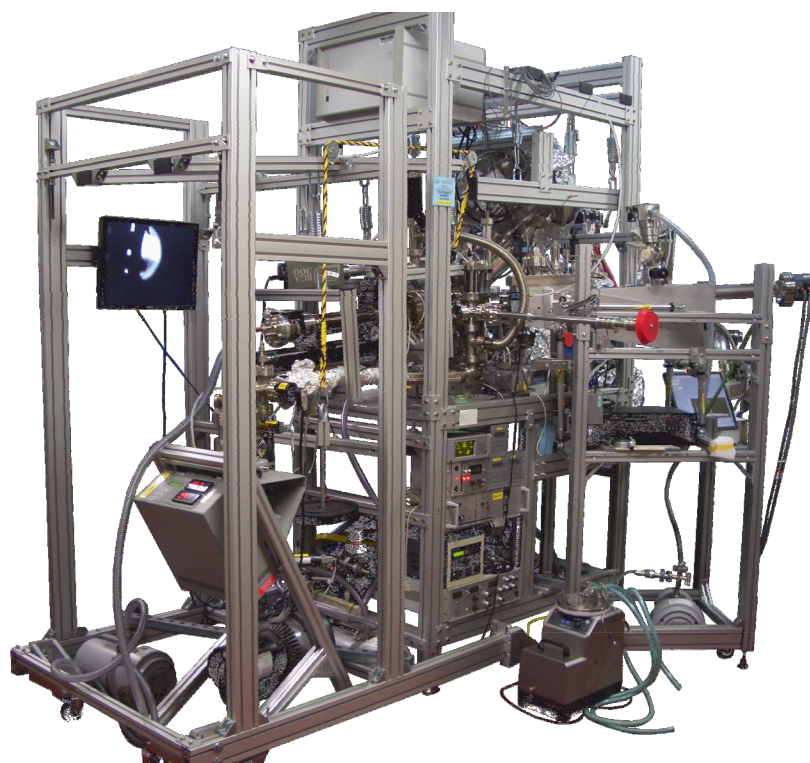


**Figure 3.8:** Picture of the SALSA endstation with connected standard manipulator for solid state samples.

manipulator can be attached to the back of the analysis chamber, replacing the flow-through liquid cell (Figure 3.8). Furthermore, an electron analyzer (SPECS Phoibos 150 MCD) is installed in the analysis chamber. Since the analyzer is rigidly attached and thus has to be moved with the entire chamber, the analyzer is suspended with six springs to remove the load from the chamber and, in particular, the xyz-stage.

The soft x-ray spectrometer (which is described in 3.4.2) is attached to the analysis chamber with a bellows, and thus maintains its position with respect to the synchrotron beam when the analysis chamber is moved to align the liquid cell with respect to the beam.

### 3.4.2 The X-ray Spectrometer

The high-resolution, high-transmission x-ray spectrometer connected to the SALSA chamber is a soft x-ray spectrometer with a variable-line-space (VLS) grating.

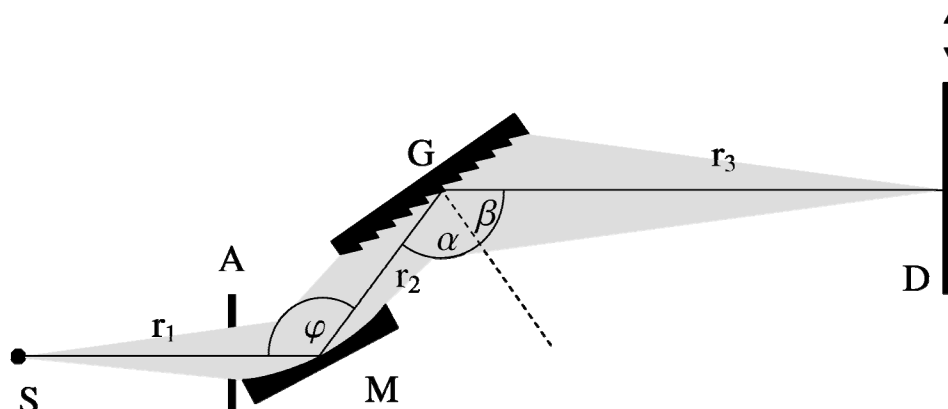


**Figure 3.9:** Schematic drawing of the x-ray spectrometer. S is the sample, A is an aperture that is used for the alignment process, M is the spherical mirror, G is the variable-line-space grating, and D is the CCD detector. The solid line shows the center path of the x-rays after proper alignment. [Fuc09]

It consists of a spherical mirror, a subsequent blazed plane VLS grating, and an uncoated back-illuminated CCD-camera detecting the photons in normal incidence. A schematic drawing is shown in Figure 3.9.

The VLS spectrometer uses the focused synchrotron spot on the sample as source, so no entrance slit is needed. The spot needs to be  $\leq 30 \mu\text{m}$  (dispersive direction) to avoid a reduction of the target energy resolution. The achieved design goal of the spectrometer was to detect all biological relevant edges (O K, N K, C K, S  $L_{2,3}$ ) in one energy window with a resolving power of  $E/\Delta E > 1200$  over the whole energy range. It reaches an efficiency about two orders of magnitude higher than any other state-of-the-art spectrometer. The usable energy range is between 130 and 650 eV. The lower edge is due to the geometry of the optical elements and the upper restriction is caused by the Nickel coating of the spherical mirror and the grating (i.e. all photon energies above Ni edges get absorbed).

The energy calibration for all measurements was done by the alignment of the VLS grating in first order position. Due to the design of the spectrometer it is possible to detect the second and third order of Nitrogen in one energy window. For the first vibrational resonance of  $\text{N}_2$  gas (nominal at 400.88 eV, the energy calibration of the beamline has to be verified by an  $\text{N}_2$  x-ray absorption spectrum) the spread between the elastically scattered peaks (second and third order) has to be 1339.5 channels. This can be tuned by adjusting the grating angle. The right position of the peaks (channels 349.5 and 1689.0) is reached by moving the CCD detector up or down.

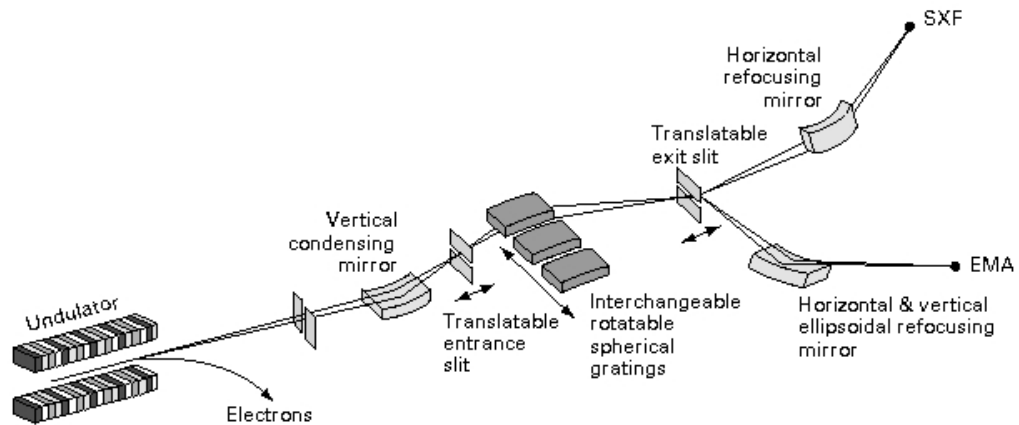


**Figure 3.10:** Schematic drawing of the beamline 8.0 of the Advanced Light source in Berkeley [ALS].

Detailed information about this x-ray spectrometer can be found in [Fuc09] and [Fuc09\_Dr].

### 3.5 The Beamline

The SALS endstation is dedicated to soft x-ray measurements. Such measurements (in particular x-ray emission) require a 3<sup>rd</sup> generation synchrotron light source. All experiments presented in this thesis were performed at beamline 8.0 of the Advanced Light Source (ALS), Lawrence Berkeley National Laboratory in Berkeley, California. Beamline 8.0 of the ALS is designed for high photon flux. This is achieved by using a minimal number of optical elements as shown in Figure 3.10. The beamline operates at photon energies between 80 and 1400 eV using a 5-cm-periodic undulator together with an 1.9 GeV electron beam (of the storage ring). After leaving the undulator the x-ray beam is focused by a condensing mirror on a spherical-grating monochromator with three interchangeable gratings (150, 380, and 925 lines/mm) based on the Rowland-circle-geometry. The resolution of the monochromator is selectable by varying the entrance and exit slits. A typical energy resolution of the beamline is  $< 8000 E/\Delta E$  at a photon flux of  $\sim 10^{11} - 6 \times 10^{15}$  photons/s. In addition to the optical elements shown in Figure 3.10, a bendable mirror placed close to the SALS endstation can be used for refocusing in the vertical direction. With this a spot



size of about 30  $\mu\text{m}$  x 100 $\mu\text{m}$  can be achieved, which is necessary for the energy resolution of the x-ray spectrometer. After this last mirror a gold mesh is installed for measuring the  $I_0$  current, which is proportional to the beam intensity and therefore can be used for normalization purposes.

---

## CHAPTER IV

# Sodium Hydroxide and Sodium Deuterioxide in Aqueous Solution

---

In the recent past, the photon-in-photon-out techniques introduced in chapter 2 were also used for the investigation of liquids and solutions. Especially in the beginning the main focus was on the investigations of liquid water [Wer04, Ode05, Smi04, Fuc08, Tok08]. Especially the local hydrogen bonding configuration was and still is under discussion [Fuc08, Fuc08\_co, Tok08, Pet08]. Our group [Fuc08] and Tokushima et al. [Tok08] presented new high-resolution XES (HRXES) spectra that reveal a fine structure in the  $1b_1$  emission line of liquid water. Furthermore, a surprisingly large isotope effect in the XES spectra of  $H_2O$  and  $D_2O$  (deuterium oxide) as well as a temperature and an excitation-energy dependence was observed. In our model [Fuc08], the spectra are described as a superposition of two individual spectral components, one representing the intact water molecules and the second one relating to ultra-fast molecular dissociation on the timescale of the emission process. The assignment of the latter component representing the dissociated water molecules is supported by its similarity to the (resonantly excited) XES spectrum of the  $OH^-$  ions in an aqueous sodium hydroxide (NaOH) solution, as well as by theoretical considerations [Ode05, Ode09, Ode09\_2]. Based on these experiments, aqueous NaOH as well as sodium deuterioxide (NaOD) solved in  $D_2O$  was investigated in detail in this thesis. This is especially important because NaOH was used as a strong base to change the pH-values of the amino acid solutions presented in chapter 6.

Sodium hydroxide is completely ionic, i.e., it contains sodium cations and hydroxide anions. The anions make NaOH and NaOD strong bases. In the solid state the ions form a crystalline lattice.

Considering the importance of the aqueous hydroxide ion in chemistry and biology, it seems surprising that only a few investigations of its electronic properties exist. In the literature, x-ray absorption studies of aqueous  $OH^-$  ions were performed by Cappa et al. [Cap07]. Furthermore, studies with x-ray diffraction spectroscopy [Meg08, Tia08, Spa99, Sch95] and x-ray photoelectron spectroscopy [Azi08, Win06, Win04] can be found.

In this thesis, XAS, XES, and RIXS studies were performed on aqueous NaOH and NaOD solutions with different concentrations. A RIXS map of solid NaOH is also presented for comparison with the liquid data. The concentrations were chosen to 25wt%, 12.5wt%, and 6.25wt% and were reached by adding H<sub>2</sub>O or D<sub>2</sub>O to a 50 wt% NaOH solution and a 40 wt% NaOD solution, respectively. For the solid sample a NaOH pallet was used and mounted on a sample holder with carbon tape.

## 4.1 Aqueous Solutions of NaOH and NaOD

### 4.1.1 The XAS Spectra – Isotope Effect and Concentration Dependence

Figure 4.1 shows the XAS spectra of NaOH and NaOD which are compared to those of H<sub>2</sub>O and D<sub>2</sub>O. For water and heavy water the typical absorption edges with a pre-edge can be observed. While the pre-edge (at a photon energy of ~534.5 eV) corresponds to the unoccupied 4a<sub>1</sub> molecular orbital, the main edge (~536.5 eV) originates from the 2b<sub>2</sub> orbital. For D<sub>2</sub>O the absorption onset is at slightly higher excitation energy than for H<sub>2</sub>O (blue shift of about 160 meV) [Fuc08, Cav05, Ode05]. This shift of the absorption onset can tentatively be explained by a slight difference in the initial state [Fuc09\_Dr]:

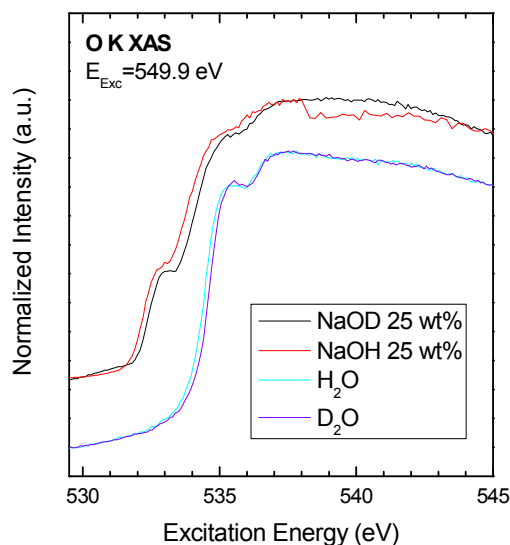


**Figure 4.1:** XAS spectra of aqueous NaOH and NaOD solutions (25 wt%) and H<sub>2</sub>O and D<sub>2</sub>O.

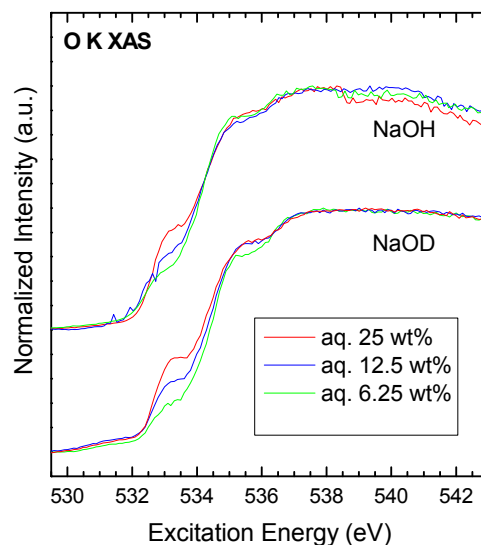


**Figure 4.2:** XAS spectra of aqueous NaOH and NaOD solutions with different weight concentrations (25 wt%, 12.5 wt%, and 6.25 wt%).

At the same temperature the deuterated liquids have a less dynamical hydrogen bond network in comparison to liquids containing hydrogen [Har05] and thus have an energetically lower arrangement in the initial state of the absorption process. A similar isotope effect can be observed of the NaOH and NaOD solutions with 25 wt% in Figure 4.1. Here, the shift between the two species is approximately 230 meV and might also be a result of the dynamic hydrogen bond network. The absorption spectra of NaOH and NaOD reveal an additional feature at  $\sim 533$  eV in comparison to the H<sub>2</sub>O and D<sub>2</sub>O spectra. This pre-pre-edge is exclusively assigned to the OH<sup>-</sup> and OD<sup>-</sup> ions [Cap07]. With the pre-pre-edge, a direct probe of the electronic structure of the hydroxide ions without spectral contributions from water is possible. In the NaOH XAS spectrum an intensity jump at  $\sim 538$  eV is visible which is a measurement artifact.

Please note that the intensities of the pre-edge as well as of the pre-pre-edge appear pronounced in Figure 4.1 in respect to other published data. This is a result of the fluorescence yield saturation effects mentioned in chapter 2.

Figure 4.2 shows the concentration dependence of the aqueous NaOH and NaOD solutions. Here, the pre-pre-edge feature is an indicator for the concentration of the solution. The lower the peak intensity of the pre-pre-edge is, the lower the concentration of the solution and vice versa. A more quantitative evaluation is difficult due to the mentioned saturation effects.

#### 4.1.2 The Non-Resonant O K Edge XES Spectra – Concentration Dependence

The non-resonant O K edge emission spectra the OH<sup>-</sup> and OD<sup>-</sup> ions ( $E_{\text{Exc}} = 549.9$  eV) are dominated by the emission lines of the solvent. The significant features of water and heavy water are visible, consisting of emission from 1b<sub>2</sub>, 3a<sub>1</sub>, and the (split) 1b<sub>1</sub> orbitals [Fuc08, Tok08, Wei09]. As mentioned above, the spectrum of water is a superposition of two different species: the spectrum of undissociated water molecules, which is responsible for the high energy 1b<sub>1</sub> peak, and the spectrum of dissociated water molecules, which is represented by the low energy 1b<sub>1</sub> peak and which is similar to that of OH<sup>-</sup> ions [Fuc08, Ode09, Ode09\_2]. In Figure 4.3 the non-resonant O K edge emission spectra of NaOH and NaOD are shown together with

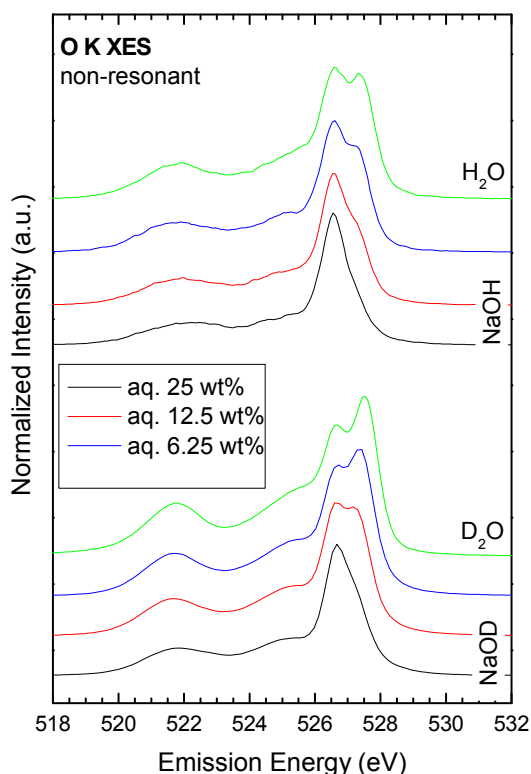


**Figure 4.3:** Non-resonant O K edge XES spectra with  $E_{\text{Exc}}=549.9$  eV. At the top, the solutions of NaOH with different weight concentrations are shown with the spectrum of water for comparison. At the bottom the “D” containing solutions - again with different weight concentrations - can be seen.

those of non-resonant water and heavy water spectra. The highest concentration of 25 wt% means that one  $\text{OH}^-$  ion is surrounded by 6.7 water molecules or one  $\text{OD}^-$  ion is surrounded by 6.2  $\text{D}_2\text{O}$  molecules. For this concentration the high energy  $1b_1$  component merely appears as a shoulder of the (dominant) low energy  $1b_1$  peak. By lowering the concentration (12.5 wt% = 15.5  $\text{H}_2\text{O}$  /  $\text{OH}^-$  or 14.3  $\text{D}_2\text{O}$  /  $\text{OD}^-$ , 6.25 wt% = 33.3  $\text{H}_2\text{O}$  /  $\text{OH}^-$  or 30.8  $\text{D}_2\text{O}$  /  $\text{OD}^-$ ) more  $\text{H}_2\text{O}$  or  $\text{D}_2\text{O}$  molecules surround the ions and the  $1b_1$  high energy “shoulder” increases in intensity. For the 12.5 wt% solution of NaOD the splitting of the peak is already clearly visible. The energy positions of the  $3a_1$ ,  $1b_2$ , and low energy  $1b_1$  peaks match those of pure water or pure heavy water perfectly [Fuc08, Wei09]. The experimental data thus confirms the theory that the high energy  $1b_1$  peak represents the undissociated water molecules.

#### 4.1.3 The RIXS Maps – the Electronic Structure of the Hydroxide and Deuterioxide Ions

All spectra presented in the sections above were taken from RIXS maps. In the following the RIXS maps of the NaOH and NaOD solutions will be discussed.

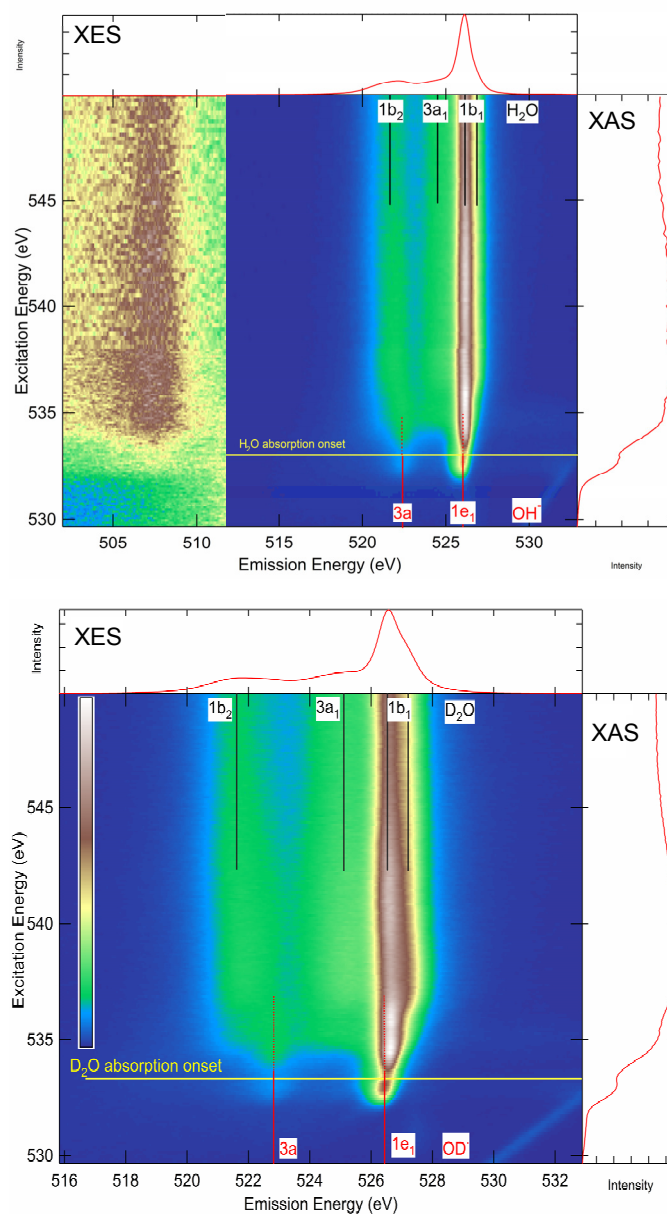


**Figure 4.4: Top:** O K-edge RIXS map of an NaOH solution (25 wt%). The horizontal axis represents the emission energy, the vertical axis shows the excitation energy. The emission intensity is color-coded (in arbitrary units). The absorption onset of H<sub>2</sub>O is shown as yellow horizontal line. The vertical lines give the positions of the OH<sup>-</sup> (red) and H<sub>2</sub>O (black) orbitals. Above the map, a non-resonant spectrum at an excitation energy of 549.9 eV is shown. The right panel corresponds to a partial fluorescence yield absorption spectrum by integrating over all emission energies shown. The left part of the map represents the (magnified) 2a<sub>1</sub> orbital of water. **Bottom:** O K-edge RIXS map of a NaOD solution (25 wt%). The lines represent the same features as in the NaOH map.

---

Since only the ratio between OH<sup>-</sup> (OD<sup>-</sup>) and H<sub>2</sub>O (D<sub>2</sub>O) changes for different weight concentrations, in the following exemplarily the maps with the highest concentration (25 wt%) are discussed. In the following text the maps are shortly called: “NaOH” and “NaOD”. In Figure 4.4 the RIXS maps of NaOH and NaOD with 25 wt% are presented. The spectra at the top of the maps show the non-resonant excited emission spectra ( $E_{\text{Exc}} = 549.9$  eV), which are also shown in Figure 4.3 and the spectra on the right represent the partial fluorescence yield absorption spectra (see Figure 4.1 and 4.2). The maps can be separated into two main parts, namely below and above the absorption onset of the solvent (yellow horizontal lines). For the NaOH RIXS map the water onset is also visible by the 2a<sub>1</sub> emission line of H<sub>2</sub>O. The 2a<sub>1</sub> orbital appears at an emission energy  $\sim 507.5$  eV. The 2a<sub>1</sub> intensity is very weak in comparison to the other water emission lines because of the dominant s-character of this orbital and thus the very small dipole transition matrix element. In the RIXS map the area around the 2a<sub>1</sub> was magnified to make the line visible. The 2a<sub>1</sub> orbital represents exclusively the H<sub>2</sub>O molecules and is not influenced by the hydroxide ions. Therefore, the line is a good indicator for the H<sub>2</sub>O absorption onset. The same 2a<sub>1</sub> line is visible for the NaOD RIXS map but here the emission energy window was chosen differently in Figure 4.4 (bottom) to emphasize the main part from 518 eV to 530 eV.

Below the solvent absorption onset, the emission spectra (i.e., horizontal cuts through the RIXS map) are dominated by two main peaks of the occupied OH<sup>-</sup> or OD<sup>-</sup> ion orbitals, namely the 3a and the 1e<sub>1</sub> orbitals. Above the absorption onset, four peaks are found, similarly to the emission spectrum of water and heavy water as was discussed in the section before. The vertical lines in Figure 4.4 show the energetic position of the emission lines of the different ion (red) and solvent (black) orbitals. As will be discussed in the following, an undisturbed spectrum of the OH<sup>-</sup> and OD<sup>-</sup> ions can be extracted from the RIXS map. For this purpose, an excitation energy between the absorption onset of OH<sup>-</sup> (OD<sup>-</sup>) at 531.6eV (531.9 eV) and H<sub>2</sub>O (D<sub>2</sub>O) at 533 eV (533.3 eV) is chosen. In this region, the emission spectra of the ions are neither influenced by emission from the solvent molecules nor by Raman-shifts of the OH<sup>-</sup>. The emission spectra at these energies are shown in Figure 4.5. As mentioned above two main peaks can be observed. The presence of two lines, as well as their energy separation, agrees well with density functional theory (DFT) calculations of a single (i.e., gas phase) OH<sup>-</sup> or OD<sup>-</sup> ion. The DFT calculations were made with Gaussian03 and the basis set B3LYP/6-31G+(d,p). In Figure 4.5 the 3a orbital is found at an emission energy of 522.6 eV, and the 1e<sub>1</sub> orbital at an emission energy of 526.1 eV, i.e., separated by 3.5 eV. In comparison the calculated energy separation is found to be  $\sim 3.3$  eV for both ions.



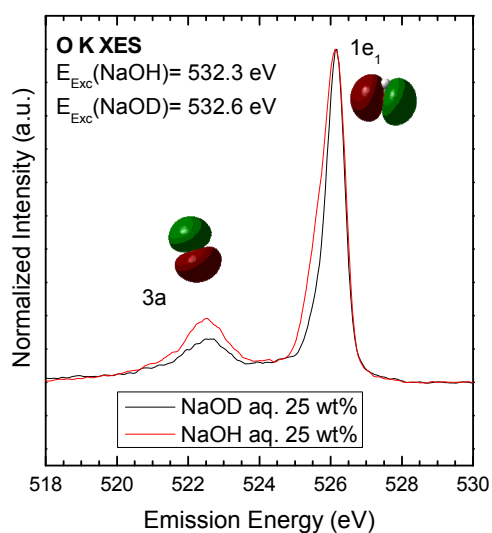


**Figure 4.5:** O K-edge XES spectrum of a NaOH solution (25 wt%) at an excitation energy of 532.3 eV, compared with an O K-edge XES spectrum of a NaOD solution (25 wt%) at an excitation energy of 532.6 eV. The occupied orbitals of the related ions as calculated by density functional theory are shown at the respective emission lines.

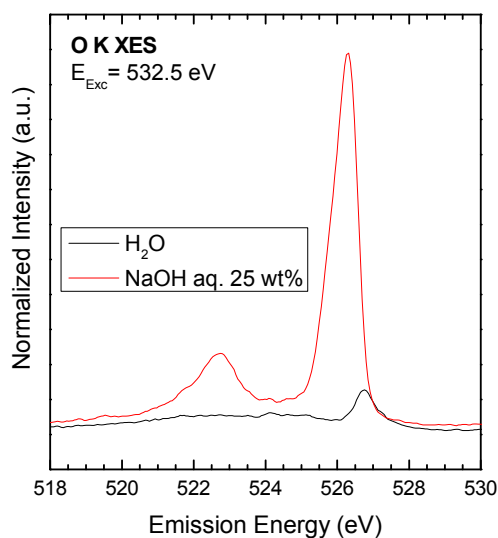


**Figure 4.6:** O K-edge XES spectrum of a NaOH solution (25 wt%) at an excitation energy of 532.5 eV, compared with an O K-edge XES spectrum of H<sub>2</sub>O at the same excitation energy.

Both peaks in the emission spectra show a slight asymmetry on the low photon energy side. This “shoulder” rises with increasing excitation energy. The asymmetry might be the result of different effects. First, the asymmetry could be due to the limited excitation resolution which might result in a contribution from Raman-regime of the solvent. To estimate the intensity of such contributions, the emission spectra of NaOH and H<sub>2</sub>O at an excitation energy of 532.5 eV were compared and are shown in Figure 4.6. The water and NaOH RIXS maps were measured right behind each other and thus the spectra could be normalized on the nitrogen signal of the Si<sub>3</sub>N<sub>4</sub> window membrane for a quantitative comparison. As evident from Figure 4.6, the water Raman component can not be responsible for the asymmetry of the peaks. Other origins of the asymmetry might be different local environments of the individual OH<sup>-</sup> / OD<sup>-</sup> ions with slightly different emission energies or effects due to coupling to vibrational states. The

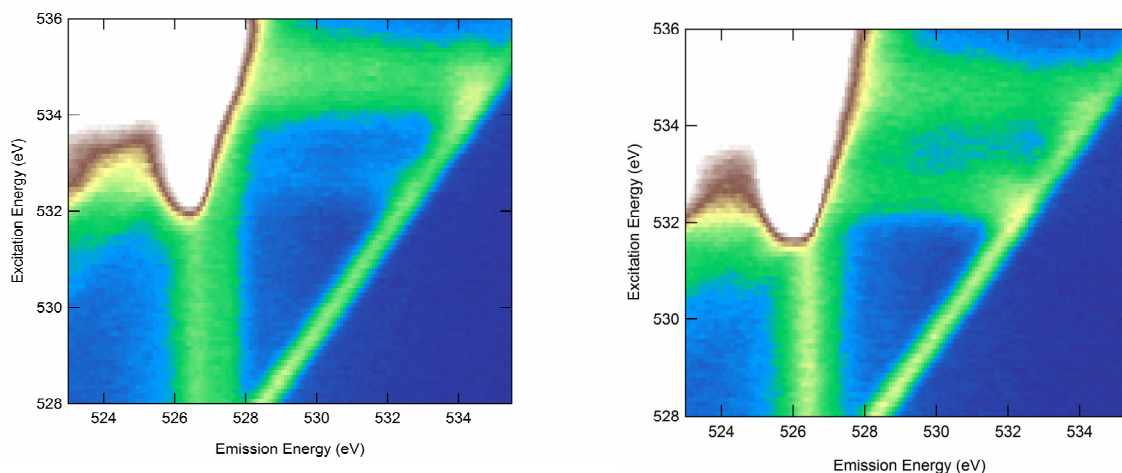


**Figure 4.7:** O K-edge RIXS maps of NaOH solutions (6.25 wt% left and 25 wt% right). The part of interest is zoomed and the color code is modified to reveal the weak features.

most probable explanation for the asymmetry is an ultra-fast dissociation on the same timescale as the RIXS process, similar to the case of  $\text{H}_2\text{O}$  and  $\text{D}_2\text{O}$ . This explanation is supported by the fact that the intensity of the shoulder in the  $\text{OH}^-$  spectrum is higher than in the  $\text{OD}^-$  spectrum. As mentioned before the “shoulder” changes with the excitation energy but the  $\text{OD}^-$  spectrum “shoulder” is always weaker than the corresponding  $\text{OH}^-$  “shoulder”. For the deuteroxide ion the proton dynamics is slower than for the hydroxide ion (nearly a factor of two due to their mass) and thus the possibility for the  $\text{OH}^-$  to dissociate is higher than for the  $\text{OD}^-$ . In fact, first dynamical DFT calculations of NaOH solutions by M. Odellius [Ode\_Pri] also reveal a second peak next to the  $1e_1$  peak at lower energy. This peak is consistent with the shoulder in the experimental data and supports the dissociation model. In such an ultra-fast dissociation process of the  $\text{OH}^-$  ion, the proton moves away and leaves an  $\text{O}^{2-}$  ion behind. This results in the observed spectral intensity at lower emission energy than that of the starting ion. Thus it is most likely that the dissociated component and the asymmetry of the peak is indicative for  $\text{O}^{2-}$ . If one could measure an emission spectrum of a single  $\text{O}^{2-}$  ion, the spectrum would be free of vibrational broadening and thus the spectral features would appear as very sharp lines. In a resonant Auger study of HCl by Björnholm et al. [Bjö97] sharp lines were found for the spectral fraction of the dissociated molecule. They also calculated RIXS spectra of HCl which showed similar sharp features for the dissociated component. However, newer dynamical calculations of different liquids and solutions (e.g., [Ode09] and calculations performed by M. Odellius for the studies in chapter 5) always show a continuous shift of the emission lines as a function of time. Thus the resulting spectrum will reveal broadened features.

A closer look at the RIXS maps reveals additional features that are less obvious. Figure 4.7 shows two “close-up” RIXS maps of the NaOH solutions with 25 wt% and 6.25 wt%. The diagonal line in the maps is the Rayleigh (elastically scattered) peak. The Rayleigh line shows two resonances at excitation energies of 532.5 eV (weak for the 6.25 wt% solution) and of 534.5 eV. These resonances are the result of an enhancement of the particular decay channel due to a resonant population of unoccupied molecular states, i.e., the pre-edge ( $4a_1$  orbital of water) and the pre-pre-edge. At these energies a core exciton is formed which leads to an enhanced elastic peak. For a higher  $\text{OH}^-$  ion concentration the resonance in the pre-pre edge is stronger.

From the resonances additional intensity extends horizontally towards the emission spectrum and is nearly independent of the chosen emission energy. This additional intensity might be due to different effects, i.e., vibrational broadening, electron losses, or a different chemical environment, and thus results in a continuum of energy losses. For the RIXS maps with higher concentration the intensity of this “loss continuum” is (again) higher.

Furthermore, a vertical line at an emission energy of 526.4 eV can be observed, which is due to a non-resonant spectrum excited with higher harmonics/orders of the undulator/monochromator.

## 4.2 Solid NaOH - an Investigation

In Figure 4.8 the RIXS map of solid sodium hydroxide is shown. The emission spectrum at a (non-resonant) excitation energy ( $E_{\text{Exc}} = 549.9$  eV) is shown at the top and on the right side the PFY absorption spectrum is presented, which is integrated over the whole emission energy range (512 eV – 536 eV).

The XAS spectrum in Figure 4.8 is quite different compared to the XAS spectra of the aqueous solutions which is expected due to the difference between the hydration shell environment of the solutions and the ion lattice of solid NaOH. For the solid XAS spectrum a dominant pre-edge feature at  $\sim 533$  eV can be observed which corresponds to the pre-pre-edge feature in the liquid spectra. At first glance the solid state pre-edge feature seems to be broader compared to the pre-pre-edge features in the solution. After subtracting the background (in the case of the solution the background is water) the solid shows a FWHM of 1.6 eV and the solution a FWHM of 1.3 eV.

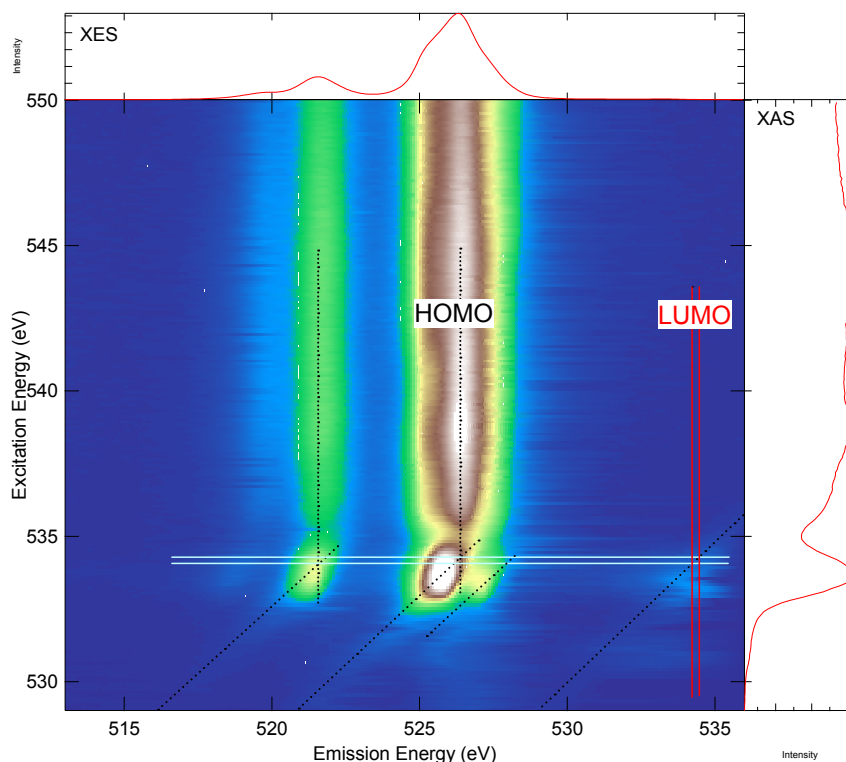


**Figure 4.8:** O K-edge RIXS maps of solid NaOH. Above the map, a non-resonant spectrum at an excitation energy of 549.9 eV is shown. The right panel corresponds to a partial fluorescence yield absorption spectrum by integrating over all emission energies shown. The dotted vertical lines indicate the areas above the Raman regime and the dotted diagonal lines stand for the Raman regime. The crossing points of the horizontal line through the HOMO and the Rayleigh line indicate the HOMO-LUMO distance.

In Figure 4.9 the non-resonant emission spectra of solid NaOH ( $E_{\text{Exc}} = 549.9$  eV), NaOH in solution with 25 wt% ( $E_{\text{Exc}} = 549.9$  eV), and liquid water ( $E_{\text{Exc}} = 550.1$  eV) are shown. For a better comparison the resonant XES spectra (dotted in Figure 5.9) of the solution at an excitation energy of 532.5 eV and the solid at an excitation energy of 533.5 eV are also presented in the graph. As for the XAS spectra, a difference between the solid and the liquid spectra is expected due to the different local environment. The non-resonant spectrum of the solid NaOH reveals two main peaks at 521.6 eV and 526.3 eV. Hereby, the low energy feature is associated with the 3a orbital in the solution and is not suppressed by a water signal in the solid state as can be seen in the non-resonant spectrum of the solution. The high energy feature can be assigned to the  $1e_1$  orbital and shows a red shift of 0.3 eV in respect to the non-resonant XES spectrum of NaOH in solution. For this peak at the high energy side as well as at the low energy side a shoulder can be observed. While the low energy shoulder is very

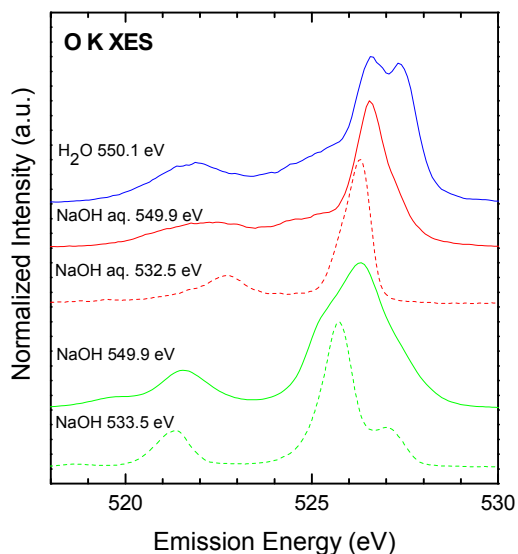


**Figure 4.9:** Non-resonant O K XES spectra of liquid water with  $E_{\text{Exc}} = 550.1$  eV, NaOH solution (25 wt%) with  $E_{\text{Exc}} = 549.9$  eV, and solid NaOH with  $E_{\text{Exc}} = 549.9$  eV. Resonant O K XES spectra (dotted) of the NaOH solution ( $E_{\text{Exc}} = 532.5$  eV) and the solid NaOH ( $E_{\text{Exc}} = 533.5$  eV) are shown for comparison.

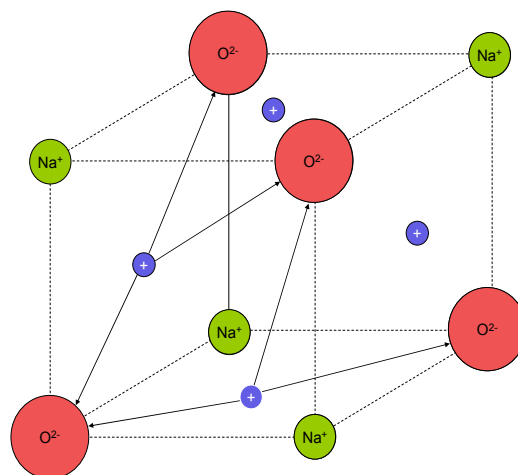


**Figure 4.10:** Model of the NaOH unit cell. The lattice constant is  $5.10 \text{ \AA}$  and the ion diameters are  $2.8 \text{ \AA}$  for the  $\text{O}^{2-}$  ions and  $1.9 \text{ \AA}$  for the  $\text{Na}^+$  ions.

obvious in the non-resonant spectrum it only occurs as a slight asymmetry in the resonant spectrum similar as in the case of the resonant solution XES spectrum. In comparison the high energy shoulder seems to be a separate feature in the resonant region, as can be best seen in the RIXS map in Figure 4.8. The shoulders of the  $1e_1$  emission line might be explained by the following model:

The ion lattice of NaOH has a NaCl structure. Hereby, the next neighbors of a hydroxide ion are sodium ions. In Figure 4.10 the unit cell of NaOH is shown with a lattice constant of  $5.10 \text{ \AA}$  and the ion diameters of  $2.8 \text{ \AA}$  ( $\text{O}^{2-}$ ) and  $1.9 \text{ \AA}$  ( $\text{Na}^+$ ) [Sch95]. Hydroxide ions in NaOH tend to undergo a pronounced self-dissociation, i.e., the  $\text{OH}^-$  can form  $\text{H}_2\text{O}$  as well as  $\text{O}^{2-}$  ions [Sch95, Spa99]. The proton of one hydroxide ion can move nearly freely between the nearest neighbor oxygen ions and the  $\text{OH}^-$  ion can thus dissociate to  $\text{H}_2\text{O}$  and  $\text{O}^{2-}$ , as is indicated by arrows in Figure 4.10. In [Sch95] this probability to find a  $\text{H}^+$  ion in NaOH was calculated. Since x-ray emission spectroscopy is fast enough to measure the different states they should be visible in the detected spectrum. In the case of NaOH three components should be visible, a strong  $\text{OH}^-$  signal, a water signal, and an  $\text{O}^{2-}$  signal. The deprotonated component can be

---

found at the low energy side, which is also in agreement with the observation of a possible dissociation process in the resonant liquid NaOH spectra. The high energy shoulder of the main peak in the non-resonant emission spectrum of solid NaOH would then represent the water component. Hereby, the energy position would be in good agreement with the high energy  $1b_1$  peak of liquid water spectrum, which represents the undissociated water molecules.

To verify this model ground-state calculations as well as calculations including dynamics are necessary which will be performed in near future.

In Figure 4.8 also different black lines are drawn. The diagonal dotted lines (which are parallel to the elastically scattered peak in the right corner) indicate the Raman-like regime of the main peaks. For the “water feature” the Raman shift is not as clearly observable as for the main peaks because it is suppressed by the non-resonant features of the higher harmonics/orders of the undulator/monochromator. The vertical dotted lines show the above Raman regime. At the crossing points of these two lines a horizontal line is drawn. Since the Raman regime ends once the excitation energy is high enough to reach the LUMO, the distance between the crossing point of the high energy peak and the crossing point at the elastically scattered peak can be indicated as the distance between the HOMO and the LUMO. The crossing point for the 3a peak is at an excitation energy of 534 eV. For the high energy features the Raman shift is not as clear as for the 3a peak since it interferes with the highly-excited non-resonant spectrum (see above) and is close to the other strong line. For the NaOH specific HOMO-LUMO distance the crossing point of the main feature is taken (at an excitation energy of 534.3 eV). Thus the resulting HOMO-LUMO distance would be  $8.1 \pm 0.3$  eV. However, in view of the selfdissociation model presented above, it is questionable whether it makes sense to give a clear position for the HOMO-LUMO distance. Because it is difficult to assign the correct position of the  $1e_1$  emission line (HOMO) while there is the  $H_2O$  dissociation feature on the higher energy side of the HOMO.

### 4.3 Summary

In this chapter the XES and XAS spectra and the RIXS maps of NaOH, NaOD solutions with different weight concentrations and solid NaOH were presented.

The XAS spectra of the solutions and the solid state revealed a pre-edge feature that could be exclusively assigned to the  $OH^-$  and  $OD^-$  ions. The intensity of this pre-

edge resonance depends on the ion concentration. Furthermore, the solution spectra are dominated by the solvent, namely H<sub>2</sub>O or D<sub>2</sub>O, where the typical unoccupied molecular orbitals are observed. For the solid NaOH XAS spectrum a similar pre-edge feature could be observed which is slightly broadened in respect to the solution spectra.

The non-resonant XES spectra of the solutions also showed a concentration dependence of the high energy 1b<sub>1</sub> emission line. The high energy 1b<sub>1</sub> peak stands for the undissociated water and thus the peak intensity is an indication for how many water molecules are in the solution. The OH<sup>-</sup> / OD<sup>-</sup> absorption onset is at lower energies than the absorption onset of water / heavy water. Therefore, the presented RIXS maps gave the possibility to reveal the undisturbed OH<sup>-</sup> / OD<sup>-</sup> emission spectrum below the water absorption onset. Two main peaks could be observed which are in good agreement with DFT calculations of the ions. Both peaks show an asymmetry at the low energy side. Here (again) proton dynamics during the core-hole lifetime takes place. The solid state XES spectra revealed a high energy and a low energy shoulder for the 1e<sub>1</sub> peak. With the suggested model of pronounced self-dissociation the high energy shoulder was assigned to the water component and the low energy shoulder to the O<sup>2-</sup> ion component.

Furthermore, an estimation of the HOMO-LUMO distance of solid NaOH could be given by assigning the OH<sup>-</sup> feature to the corresponding HOMO level.

---



## CHAPTER V

# Studies of Amino Acids in a Liquid Environment

---

The first amino acid – asparagine – was discovered in 1806 by the French chemists Vauquelin and Robiquet [Vau1806]. Today, twenty naturally occurring amino acids are known. These standard amino acids are the building blocks for proteins and peptides and thus of all living creatures [Bry03]. Particularly relevant in understanding biological activity is the effect of water on the protein structure and how water molecules arrange around protein molecules under physiological conditions. When studying the electronic structure of amino acids one goal is thus to shed light not only on the electronic structure of amino acids as such, but also on their interaction with water molecules from the hydration shell. Then, in a next step, hydration shell influences on entire proteins can be studied, such that, in the future, it might even be possible to solve the mystery of the salt and solvent effects on the structure of proteins, as described by the Hofmeister series [Col85, Cac97].

An amino acid is a molecule containing both amine and carboxyl functional groups. These functional groups are connected via the same carbon atom ( $\alpha$ -carbon). The general chemical structure of the twenty standard amino acids (also:  $\alpha$ -

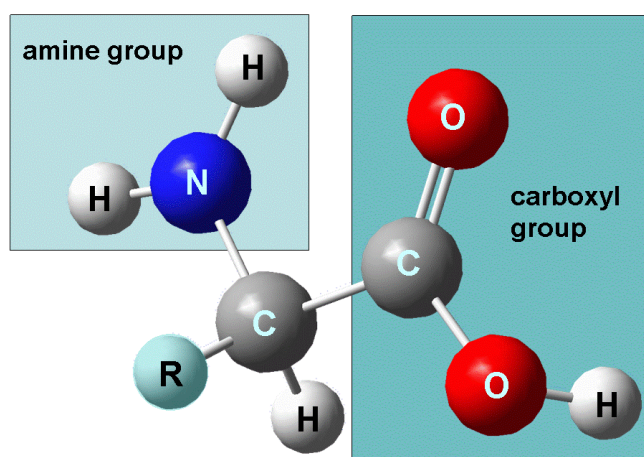


**Figure 5.1:** General chemical structure of an  $\alpha$ -amino acid in its neutral state, containing an amine and a carboxyl functional group, as well as an R group representing an organic side chain.

---

amino acids) is shown in Fig. 5.1. The group labeled R - located next to the  $\alpha$ -carbon - represents an organic side chain. Amino acids can be classified in four groups: weak acid, weak base, hydrophilic, or hydrophobic. To which group an acid belongs is determined by the side chain (R group) [Cre93].

As mentioned above, the standard amino acids contain an amine functional group as well as a carboxyl group and can therefore be acid and base at the same time. For this reason amino acids are very sensitive to pH-value changes. At a certain pH-value, known as the isoelectric point, the number of protonated amine groups with a positive charge is equal to the number of deprotonated carboxyl groups with a negative charge. Overall the molecule is neutral. In this configuration, amino acids are also called *zwitterions*. Note that amino acids can only be in the zwitterionic state as solids and in solution but not in the gas phase [Rem06]. In an (aqueous) solution the configuration of the amino acid depends on the pH-value. For a neutral pH-value the zwitterionic form is dominant; at low pH values, i.e., for an acidic solution, the amino acid is in a cationic form, and for high pH values, i.e., a basic solution, the dominant form is the anion. To understand the pH dependence it is necessary to know the  $pK_a$  value (the acid dissociation constant) given by:

$$pK_a = -\log_{10} K_a \text{ with } K_a = \frac{[A^-][H^+]}{[HA]} \quad (5.1)$$

HA is a generic acid (Brønsted-acid) and  $A^-$  represents the conjugated base of the acid. For amino acids, the separate  $pK_a$  values of the carboxyl group ( $pK_{COOH}$ ) and the amine group ( $pK_{NH_2}$ ) are important. At these values the protonation of the amine fraction or the carboxyl fraction start and the isoelectric point is given by:

$$pH_{iso} = \frac{pK_{COOH} + pK_{NH_2}}{2} \quad (5.2)$$

The various amino acids possess different  $pK_a$  values, but within the given error bars, a value of  $2.1 \pm 0.3$  for the  $pK_{COOH}$  and of  $9.5 \pm 1.5$  for the  $pK_{NH_2}$  can be used [Nel00].

In contrast to their central importance for biological processes, only a limited number of studies dealing with the electronic structure of amino acids exist in literature. For solid state amino acids there are mainly x-ray absorption (XAS) and x-ray photoelectron spectroscopy (PES) investigations [Yag 04, Zub04, Zub04\_2, Bee05, Has98, Nyb00, Nyb03, Zub07, Zub05, Zub06, Boe97, Tan01, Gor03, Kaz02, Zub04\_3, Cop04, Tzv04, Zub05\_2, Löf97, Wu87, Wil09, Ote06, Boz94], glycine x-ray emission spectroscopy (XES) studies [Has00, Nyb00, Nyb03], and a few investigations by ultra-

violet photoelectron spectroscopy (UPS) [Nyb03, Bee05]. Furthermore, the electronic structure of gas phase amino acids was investigated by XAS and PES [Gor03, Ple07, Cou05, Ple07\_2, Pow03, Sla88, Kla76, Can79, Can83]. For amino acids in solution, where the pH-dependence plays an important role, reports in literature are rare, presumably due to the technical challenges of studying liquids and solutions with electron and x-ray spectroscopies, as mentioned in Chapter 3. In the recent past, first XAS studies dealing with solutions and pH-dependence were published by Messer et al. [Mes05, Mes05\_2] and Aziz et al. [Azi08\_2], as well as one XPS study by Nolting et al. [Nol07].

Studying organic molecules in general and amino acids in particular with soft x-ray techniques is a challenge, in particular since they are very sensitive to x-rays. High photon densities, such as those at third-generation synchrotron undulator beamlines, can cause beam damage to the sample within less than a second. Earlier (2004) studies of our group were conducted to derive the various possible ways of beam damage for a variety of amino acids, e.g., via dehydration and decarboxylation [Zub04, Zub04\_2, Zub04\_3]. A recent study by Wilks et al. is in accordance with these results [Wil09]. To avoid beam damage, the experiments have to be carefully planned and optimized to minimize or avoid all radiation induced effects. For example, beam damage of solid amino acids can be determined by a series of spectra taken after increasing exposures to x-rays. Therefore, spectra with one, two, three...up to 20 seconds have to be recorded on the same spot. From such a series the critical exposure time after which beam damages contribute a significant portion to the overall spectrum can be determined. For solutions, beam damage is not as critical as for the solid state, provided the solution can be flowed at a sufficient rate. Experiments using static solutions, in contrast, are invariably prone to a multitude of experimental artifacts and should be considered with great caution. As described in Section 3.2, the solution in our experiments is measured in a flow-through mode and thus is never exposed for more than 1 ms to the beam, thus ensuring that undamaged molecules are being measured at all times.

For amino acids in solution, other experimental challenges need to be overcome. As an example, glycine and lysine showed a high tendency to form a gas bubble behind the window membrane during flow operation. The presence of such a bubble can easily be identified when comparing the data with reference measurements of gaseous N<sub>2</sub> (Fig. 5.2). In general, all measurements of liquids can suffer from this complication, e.g., if a small air bubble is present in the liquid feed-in tubes. Depending on the liquid, the bubble oftentimes simply passes the window membrane during the measurement process, momentarily reducing the RIXS intensity. For amino acids, however, we find that the bubble (from residual air in the feed-in tube or beam-induced) does not move through the cell, but nests right behind the window membrane

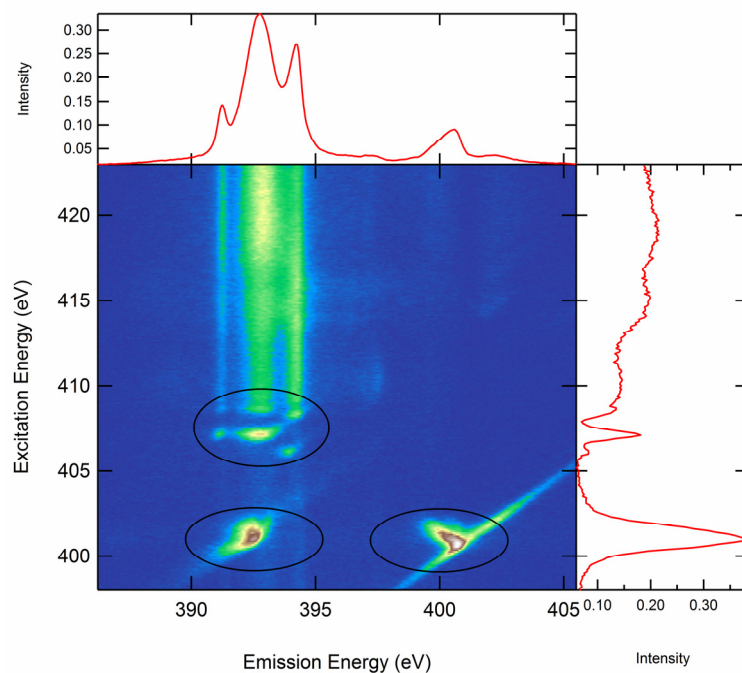


**Figure 5.2:** RIXS map of N<sub>2</sub> gas. Characteristic features are marked with circles.

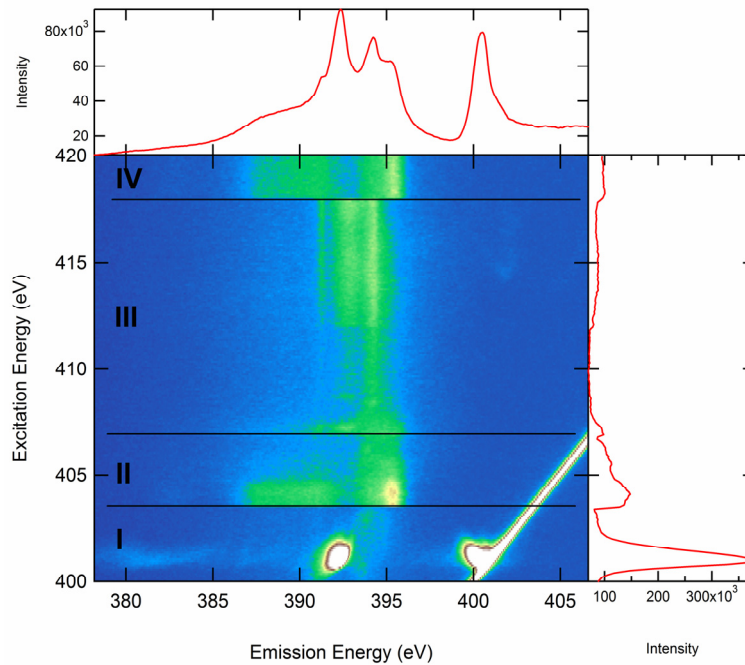


**Figure 5.3:** RIXS map of glycine pH-value 12.61. The four regions indicate the change between gas bubble behind the membrane and the “real” liquid. II and IV corresponds to liquid spectra.

while the liquid is passing “behind” the bubble. This likely occurs for two reasons playing together. First, the membrane is always bulging towards the vacuum and thus forms a cavity suitable for gas bubble trapping. And second, solutions of small amino acids (like glycine and lysine) have a higher surface tension than most other solutions of relevance here [Moo86]. Therefore, it is energetically favorable to form a bubble and attach it to the membrane environment, rather than to dislodge and remove it with the flowing solution.

If a bubble has formed behind the membrane, the XES spectra or the RIXS map show contributions from the gaseous species, for example of N<sub>2</sub> molecules when comparing with the reference map (spectra) shown in Figure 5.2. The RIXS map of N<sub>2</sub> shows its “fingerprint” with some characteristics and very sharp features in the resonant region (in the map indicated with ovals). Furthermore, the XES spectrum of N<sub>2</sub> (at an excitation energy of 423eV, shown above the map in Fig. 5.2) shows clearly separated peaks. Figure 5.3, in contrast, shows a time-dependent (as well as excitation-energy dependent) map of glycine (pH value of 12.61), during the collection of which a bubble temporarily formed behind the window (Region I and III), while other regions (II and IV) show RIXS map information representative of glycine.

To solve the “bubble problem”, further optimization of the membrane and its inner surface are necessary. A first step is to change the membrane design to reduce the bulging and a variation of the flow speed to increase the possibility to remove the bubble. Other possible solutions could be to change the pressure in the cell to reduce bubbles or to include a flow-barrier into the liquid channel to make an artificial swirl behind the membrane.

## 5.1 The Smallest Amino Acid: Glycine

The simplest of all amino acids – glycine – has an R group consisting of a single hydrogen atom. Glycine has the function of a neurotransmitter and is a building block of structural proteins, as in, e.g., fibroin, collagen,  $\alpha$ -keratins, and tropomyosin [Nyb00].

Figure 5.4 shows the chemical structure of glycine in its neutral state, as a zwitterion, as an anion (“deprotonated”), and as a cation (“protonated”). Furthermore, the pK<sub>a</sub> values (pK<sub>NH<sub>2</sub></sub> = 9.77 and pK<sub>COOH</sub> = 2.35) and the pK<sub>iso</sub> (6.06) value are given.

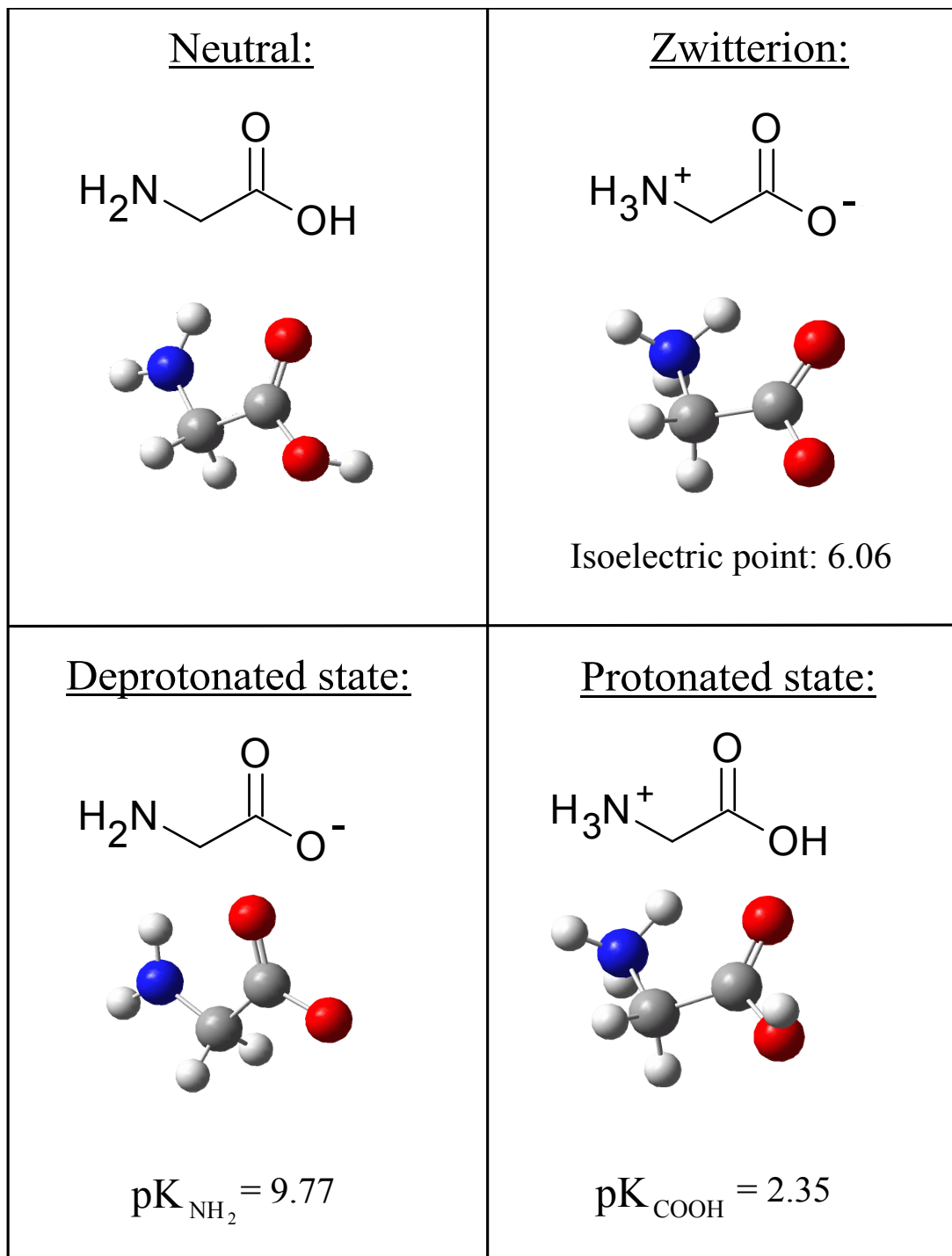


**Figure 5.4:** Top: neutral and zwitterionic state of glycine. Bottom: possible protonated states of glycine. On the left side the anion with the protonated carboxyl fraction (called: deprotonated state) is shown and on the right side the cation with the protonated amine fraction (called: protonated state).

In literature [Nel00], the anion is known as the deprotonated amine fraction ( $pK_{\text{NH}_2}$ ) and the cation as the protonated carboxyl fraction ( $pK_{\text{COOH}}$ ). In this thesis - for simplicity - the anion is referred to as the deprotonated state and the cation as the protonated state.

For the experiments presented in the following, an aqueous solution with half of the saturation concentration of glycine was used (12.5 g / 100 ml). The pH-values were regulated with sodium hydroxide. The pH-value for the zwitterionic state was set to  $6.14 \pm 0.05$  (short pH 6; the isoelectric point is at 6.06) with a pH-meter. For the deprotonated state the pH-value was  $12.61 \pm 0.05$  (short pH 12). A value high above the  $pK_{\text{NH}_2}$  value was chosen to ensure that indeed all amine groups are deprotonated.

For the glycine studies the main focus was on the nitrogen K edge. Glycine molecules possess only one nitrogen atom. Thus every change around this nitrogen atom, like the deprotonation of the amine fractional group, should be visible in the N K x-ray spectra. Low pH-values, which would be needed to generate the protonated state, were not possible to achieve with the current set-up. To measure below the  $pK_{\text{COOH}}$  value would cause a high risk of corrosion of the stainless steel walls of various parts of the liquid cell design. Note that, at the nitrogen edge, it is expected that the spectra of the zwitterionic state and the protonated state are very similar due to the very similar environment of the N atom. This is also true for the oxygen and carbon K edges when comparing the zwitterionic state and the deprotonated state, as will be shown later in this chapter.

### 5.1.1 The Nitrogen K Edge Absorption - a Comparison between Solid State, Solution, and Gas Phase

For solid state and gaseous glycine the unoccupied states have been studied quite in detail [Ple07, Gor03, Zub04, Has98, Zub05, Zub06, Boe97, Kaz02, Zub04\_3, Cop04, Wil09]. Therefore, for the investigation of this amino acid, the absorption spectra are a good starting point.

The comparison of gaseous, aqueous, and solid state glycine N K-edge absorption spectra for a pH-value of approximately 6 is shown in Figure 5.5. The absorption spectrum of the powder sample was measured with total electron yield (TEY) and the aqueous solution with partial fluorescence yield (PFY). Both spectra look similar in shape. This leads to the conclusion of a weak influence of the water molecules on the spectral signature of the N K-edge XAS spectra (which are very

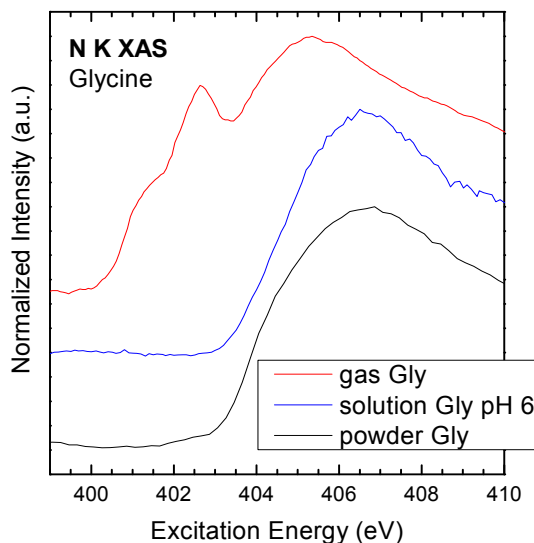


**Figure 5.5:** N K XAS of gas phase glycine (red) [Gor03], a glycine aqueous solution with pH 6 (blue), and a glycine powder sample (black). The gas phase is measured with inner-shell electron energy-loss spectroscopy, the solution with partial fluorescence yield, and the powder sample with total electron yield.

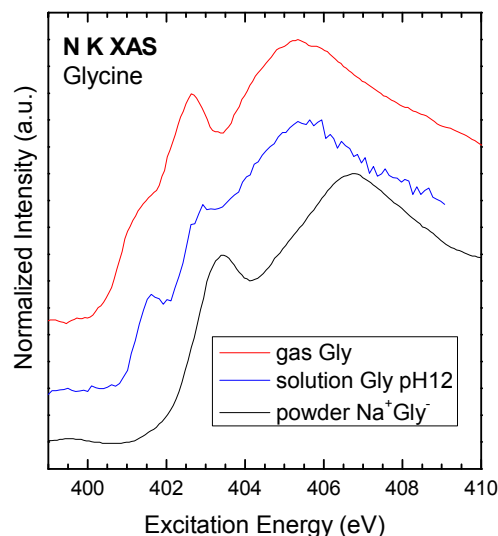


**Figure 5.6:** N K XAS of gaseous glycine (red) [Gor03], aqueous glycine pH 12 (blue), and  $\text{Na}^+\text{Gly}^-$  powder sample (black) [Zub06].

broad). In contrast, the gas phase inner-shell electron energy-loss spectroscopy (ISEELS) spectrum shows two main differences with respect to the solution and the solid spectra [Gor03]. First, a clear red shift of the main peak is visible and, second, two pre-edge features at 401.3 eV and 402.5 eV emerge. It should be noted that in gas phase the amino acid does not form a zwitterion and thus possesses an  $\text{NH}_2$  amine group, while glycine molecules in the solid and the solution both have a protonated amine group  $\text{NH}_3^+$  and therefore a different local structure probed in the N K-edge XAS spectra [Gor03]. The gas phase spectrum should therefore rather be compared with that of a solution at pH 12. As shown in Figure 5.6, they are indeed very similar, supporting this argumentation.

Regarding the red shift observed in Figs. 5.5 and 5.6 (i.e., powder and pH 6 solution vs. gas phase and pH 12 solution), we speculate that it is due to the change of the large charge near the probed N atoms. Fig. 5.6 also shows, as a reference, a spectrum of  $\text{Na}^+\text{Gly}^-$  powder [Zub06]. The  $\text{Na}^+\text{Gly}^-$  powder sample should more closely resemble that of the pH 12 solution, but it is a commercially bought sample and the composition is not well known, i.e., it is not certain the sample contains only



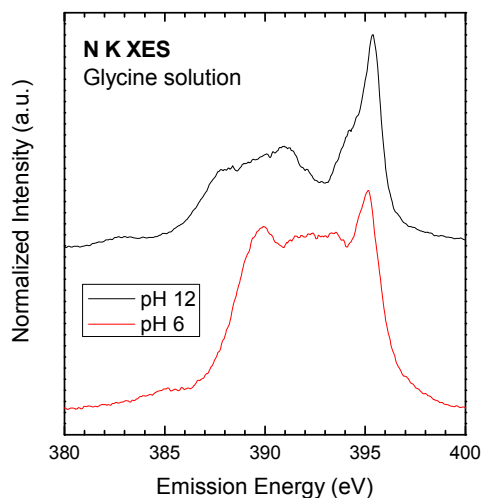


**Figure 5.7:** N K non-resonant excited emission spectra ( $E_{\text{Exc.}}=420$  eV) of glycine solutions with different pH-values (red: pH = 6 and black: pH = 12).

deprotonated amine fractional groups. Furthermore, the here-studied  $\text{Na}^+\text{Gly}^-$  powder is an ionic solid, which is not identical to a deprotonated solute molecule in a solution. Thus, it is not surprising that the spectrum differs from that of the pH 12 solution and of the gas (as well as from the zwitterionic powder sample).

The two pre-edge features in the gas and pH 12 glycine spectra can be assigned to nitrogen  $1s \rightarrow \sigma^*$  transitions and are representative for the deprotonated amine fractional group [Gor03, Mes05]. Note that the here-presented liquid absorption spectra are consistent in shape, energy position, and intensity with the liquid absorption spectra previously published in literature [Mes05]. Since there is a clear difference in the absorption spectra between the protonated and deprotonated amine fractional group the next step is to investigate the non-resonant emission spectra to shed further light on the electronic structure of the glycine solute and the impact of the solvent environment.

### 5.1.2 The Nitrogen K Edge Emission of Glycine – Impact of Different pH-Values

The differences between the zwitterionic and the deprotonated state should also induce significant changes in the non-resonant x-ray emission spectra of glycine. To understand and interpret the emission spectra correctly (in this section the N K edge spectra), proton dynamics during the core-hole lifetime and therewith the possibility of hydrogen dissociation on the femtosecond timescale have to be taken into account, as in the case of water [Fuc08].

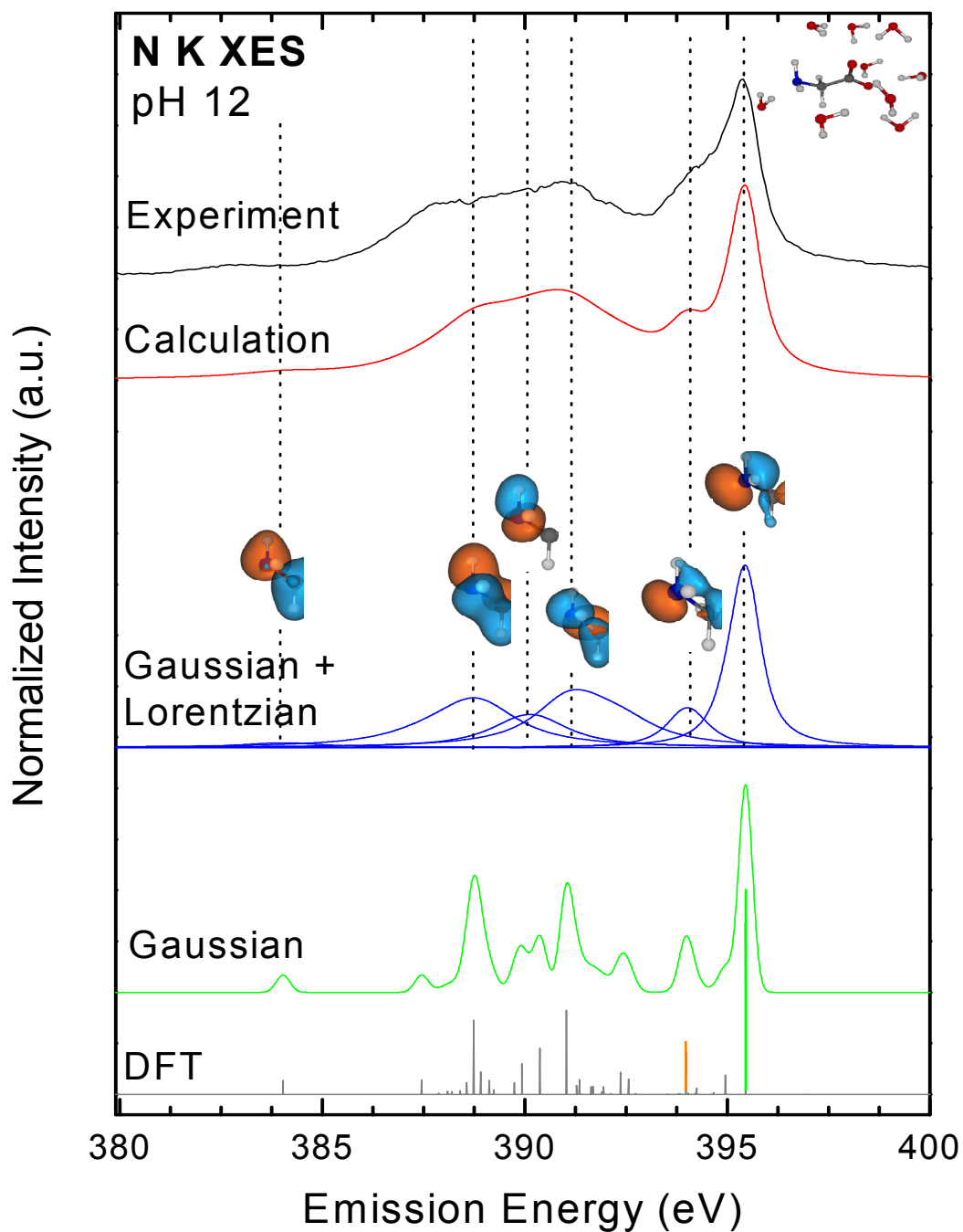


**Figure 5.8:** Bottom: B3LYP calculated positions and intensities of the molecular orbitals for the pH 12 solution. Green spectrum: calculated spectrum broadened by a Gaussian (FWHM 0.4 eV). Blue peaks: broadened by a Gaussian and different Lorentzians. The pictures above show the most prominent orbital corresponding to each group of orbitals. Red spectrum: sum of the calculated blue peaks. Black spectrum: non-res. N K XES of glycine pH12 ( $E_{\text{Exc.}} = 420$  eV).

In Figure 5.7, the non-resonant XES spectra of two different glycine solutions, pH-values of 6 and 12, are shown. The spectra are extracted from the N K RIXS maps at an excitation energy of 420 eV. As can be seen, the spectra are very different.

Density functional theory (DFT) calculations can reveal the orbitals of the molecule and their energies in respect to each other. Therefore, Michael Odelius (Fysikum, Stockholm University, Sweden) performed DFT calculations by using the StoBe-deMon code [Her02] on the level of gradient-corrected exchange and correlation functionals [Per86, Bec88]. All atoms were described with double-zeta valence basis sets including polarization functions [God92], except for the core-excited atom, which is described using a flexible IGLO basis set [Kut90]. The calculations for a single deprotonated (pH12) glycine molecule surrounded by water molecules, i.e., in solution, showed the occupied molecular orbitals, which can refill the N1s core-hole. In order to display the calculation on a common energy scale with the experimental data, a constant offset was added to the energy position of the orbitals, such that the highest calculated orbital fits the position of the corresponding experimental peak at 395.8 eV. The occupied orbitals are shown in forms of lines at the bottom of Figure 5.8 and the solid curve above the lines represents the spectrum of the occupied orbitals after including the experimental broadening by convolving every single orbital with a Gaussian with a full width at half maximum (FWHM) of 0.4 eV. To also include the lifetime broadening, the calculated spectrum was convoluted with suitable Lorentzian functions to account for lifetime, vibrational and other broadenings. The Lorentzian width varies between 0.7 eV (highest energetic peak) and 2.5 eV (lowest energetic peak). Assuming, that the lifetime broadening is dominant this can be understood as follows. The lifetime broadening includes not only the lifetime of the N1s core-hole which would be equal for all peaks but also of the respective valence-hole. To refill a valence-hole the dominating electronic decay process is an Auger process and therefore, the energy gain when refilling the valence hole from a state of higher energy must be high enough to excite the another electron into an unoccupied state. The lower the state the higher is the possibility for a refill and the shorter is the lifetime of the valence-hole. A shorter lifetime of the valence-hole then leads to a larger lifetime broadening. This was also observed for CdS [Wei07]. In Figure 5.8 the peaks for different lifetime broadenings are shown (blue) as well as their sum (red). For the single peaks the molecular orbitals were sorted into groups. For each group of orbitals the one with the strongest spectral intensity is also shown in Figure 5.8. These orbitals can be seen enlarged in the appendix of this thesis.

The intensity variation between the different orbitals is a result of the corresponding dipole matrix elements (equation 2.3) and depends on their symmetry, shape, and overlap with the nitrogen 1s orbital. E.g., the highest occupied molecular orbital (HOMO, green line) at 395.8 eV has a p-type character with a knot-plane at the N atom. The orbital is mainly localized at the nitrogen atom, which leads to the

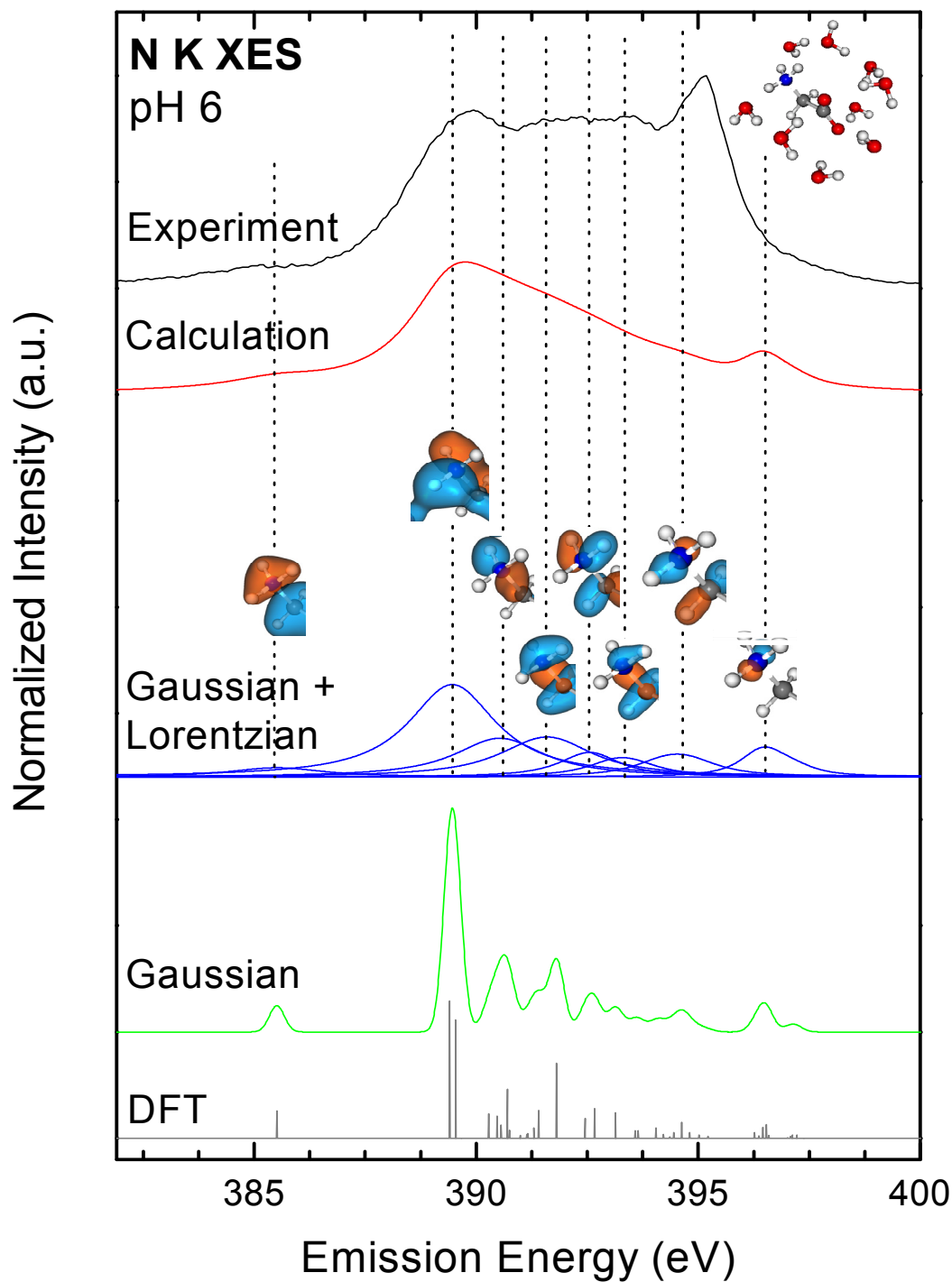


**Figure 5.9:** Bottom: B3LYP calculated positions and intensities of the molecular orbitals for the pH 6 solution. Green spectrum: broadened by a Gaussian (FWHM 0.4 eV). Blue peaks: broadened by a Gaussian and different Lorentzians. The pictures above show the most prominent orbital corresponding to each group of orbitals. Red spectrum: sum of the calculated blue peaks. Black spectrum: non-res. N K XES of glycine pH12 ( $E_{\text{Exc.}} = 420$  eV).

intensity in the spectrum (please note, the molecule belongs to the  $C_s$  group). For the next orbital shown (lower energy, orange line) the orbital has also a p-character but is more delocalized and therefore, the intensity is lower. The molecular orbitals which have only a minimal contribution to the spectrum are mostly orbitals with s-type symmetry. Furthermore, Figure 5.8 shows the experimental data (top spectrum) for the pH 12 solution. The calculated spectrum is in very good agreement with the experiment. The main difference is the missing intensity on the low energy side of the HOMO peak (around 394 eV) and between 385 eV and 387 eV. This can be attributed to the fact that the calculation is an electronic ground state calculation which does not include proton dynamics and final-state effects. Further calculations are needed to verify this model.

For the zwitterionic state (pH 6) the same calculations were performed. The result is shown in Figure 5.9. Again the single lines represent the calculated molecular orbitals and the spectrum above represents the convolution with a Gaussian function (FWHM = 0.4 eV). The lifetime broadenings were chosen the following way: same molecular orbitals at pH 6 have the same broadening width as for pH 12 and for the molecular orbitals which had no contribution to the pH 12 spectrum the widths were chosen similar. Thus the lifetime broadening varies between 1 eV and 2.5 eV. The different lifetime broadened peaks as well as the sum and the corresponding prominent orbitals are also shown in Figure 5.9 (enlarged in the appendix). Even without convoluting the lifetime broadening it is apparent that the calculation looks quite different to the experimental data (top spectrum). The experimental spectrum has the highest intensity for the high energy peak at 395.1 eV which is very weak in the calculated spectrum. Good agreement is achieved at the low energy side of the spectrum (approximately 5 eV lower at 389.7 eV). First preliminary dynamical calculations made by M. Odelius indicate that the non-resonant XES spectrum of the pH 6 solution is very strongly influenced by proton dynamics involving a rapid N-H bond elongation. I.e., during the lifetime of the core-hole a proton of the protonated amine group ( $NH_3^+$ ) moves away from the molecule. Ultimately this dissociation process results in an amine group similar to the one at higher pH value ( $NH_2$ ). In first approximation, the experimental spectrum can then be described by a (weighted) sum of the dissociated spectrum, i.e., with  $NH_2$  group, and the undissociated spectrum, i.e., with  $NH_3^+$  group (similar to the case of water see chapter 5 and [Fuc08]). This model can indeed explain the dominant high energy peak for the experimental data which is prominent for glycine at high pH. This is illustrated in Figure 5.10 where the calculated spectra of pH6 and pH 12 were added (with weighting factors of 1 for the spectrum at pH 6 and 1.2 for the spectrum at pH 12) and compared with the experimental spectrum of the zwitterion. As can be seen, the sum is in agreement with the dominant peaks at 389.7 eV and 395.1 eV. However, it shows a much lower intensity between 392 eV to 394 eV. This might be due to the rather simple model but also (speculatively) point to a

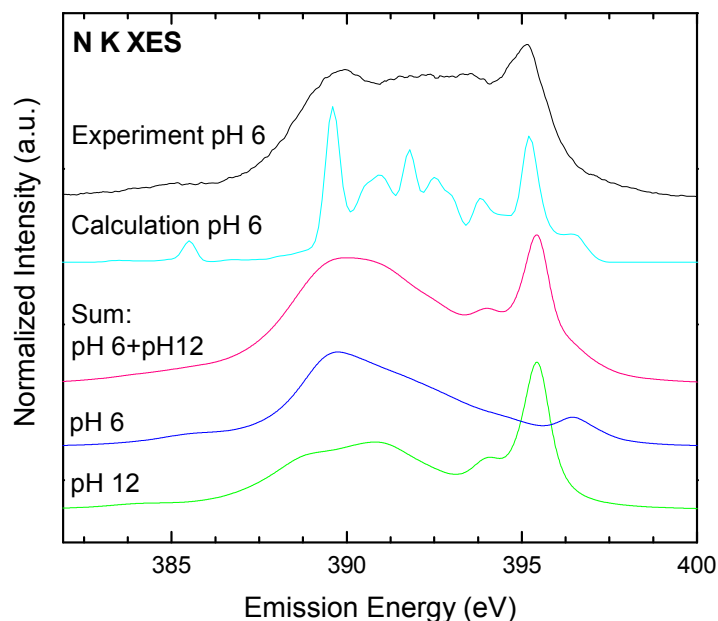


**Figure 5.10:** Comparison of the non-res. N K XES spectrum (pH 6) with the calculated pH 6 spectrum (incl. proton dynamics) and the sum (pH 6+1.2\* pH 12) of the calculated spectra for pH 6 and pH 12.

third component ( $\text{NH}^-$ ). Figure 5.10 also shows the first calculated emission spectrum of a glycine pH 6 solution including dynamical effects. The calculation includes the experimental broadening and the lifetime broadening of the core-hole but no additional broadenings. The calculation still looks different as compared to the experiment but clearly points out the evidence of proton dynamics.

### 5.1.3 The Nitrogen K RIXS Map of the pH 6 Solution

The left side of Figure 5.11 shows 12 resonant XES spectra of the glycine solution with a pH-value of 6. Excitation energies vary from 404.7 eV (bottom spectrum) up to 411.6 eV (top spectrum) which is also indicated by the elastically scattered peak at the respective photon energies. The shown spectra represent horizontal cuts through the map. The only visible difference in the spectra is a decrease of the intensity of the peak at an emission energy of 395 eV for the spectrum excited with a photon energy of 404.7 eV. The dissociation of the amine group which was described in the section above, in form of the high energy peak is noticeable in every spectrum. The N K RIXS map corresponding to the single spectra on the left can be seen in the middle of Figure 5.11. The inset on top of the map represents a non-resonant XES spectrum with an

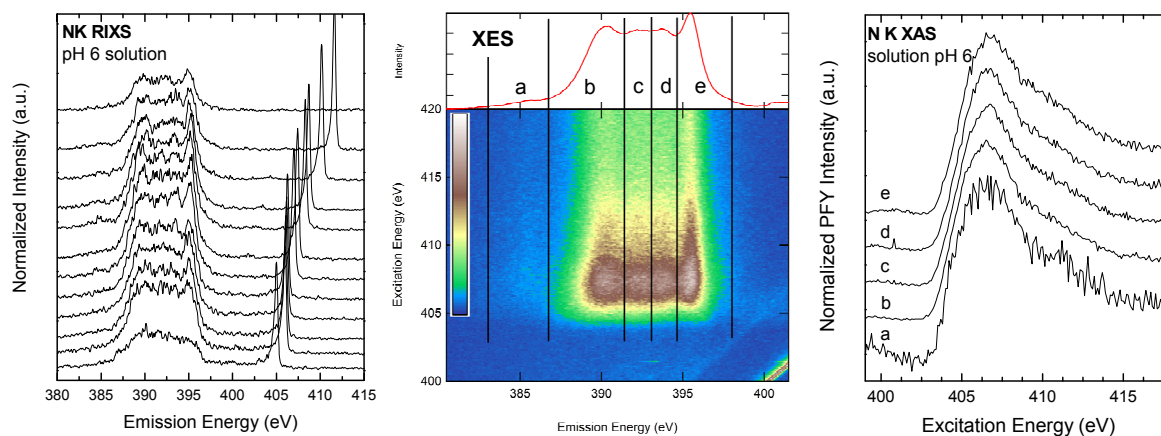


**Figure 5.11:** In the middle the N K RIXS map of the pH 6 solution is shown. On top of the map a non-resonant XES spectrum ( $E_{\text{Exc}} = 420$  eV) is shown. On the left side resonant spectra are shown representing horizontal cuts through the map for excitation energies between 404.7 eV and 411.6 eV. The right side represents the different decay channel-selective partial fluorescence yield XAS spectra for the regions chosen in the RIXS map (black lines).

excitation energy of 420 eV. The black vertical lines separate the energy regions for the decay channel-selective partial fluorescence yield absorption spectra shown on the right of Figure 5.11. In RIXS maps it can often be observed that resonantly enhanced features use the fluorescence yield from other decay channels leading to intensity variations with excitation energy for the different decay channels. The noise for the area **a** is much higher than for the other areas because the represented occupied molecular orbital has an s-character and is therefore weaker. All decay channel-selective PFY XAS spectra in Figure 5.11 (right) look very similar.

#### 5.1.4 A Glance at the Carbon K and the Oxygen K Edge of Glycine

When comparing different pH-values (pH 6 and pH 12) most changes are expected at the nitrogen K edge. In comparison, the carbon K edge and the oxygen K edge are expected to be much more similar for the two pH-values. Here, the structure of  $\text{COO}^-$  is the same for both cases and for the oxygen edge there should only be a spectral change by switching to low pH-values at which the carboxyl group gets protonated.

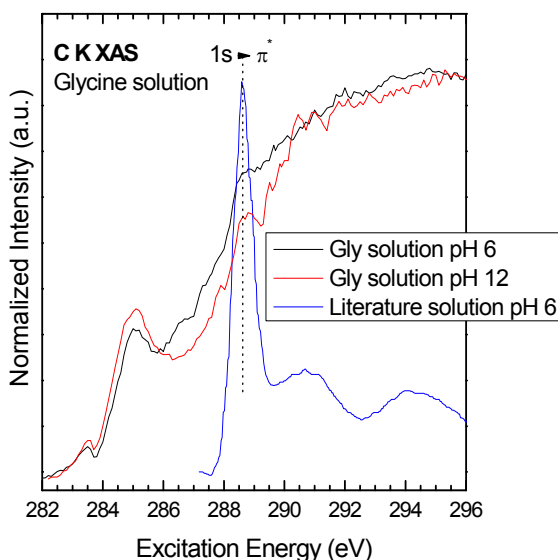


**Figure 5.12:** C K XAS of glycine solutions for pH 6 (black) and pH 12 (red). The blue spectrum was taken from literature [Mes05] and reveals the typically XAS spectrum for glycine at the C K edge with the sharp  $C1s \rightarrow \pi^*$  transition.

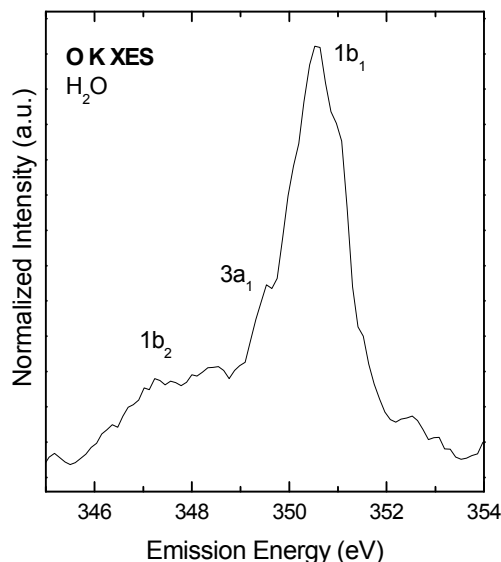


**Figure 5.13:** O K edge of the glycine pH 6 solution. The spectrum looks similar to a spectrum of  $H_2O$  since the water molecules are dominant at the O K edge.

### The Carbon K edge of Glycine

The carbon K edge for pH 6 and pH 12 was measured with XAS and the result is presented in Figure 5.12. The spectral features in the spectra of the different pH-values (red and black line) are similar but are quite different to the spectrum found in literature [Mes05]. The strong resonance at 288.6 eV can be assigned to the  $C 1s \rightarrow \pi_{C=O}^*$  transition [Mes05], which is supported by different calculations and previous measurements of solid and gaseous glycine. The broad resonances at higher energies are due to transitions to a variety of different  $\sigma^*$  states [Mes05]. At approximately 290 eV a feature is formed by transitions on the amine carbon whereas, all other features at higher excitation energies have significant contribution from the carboxyl carbon as well as from the amine carbon [Gor03, Mes05].

The resonance at 288.6 eV is present in the pH 6 and pH 12 measurements presented here but very weak (dotted line). The experimental data also shows features which are not visible in spectrum taken from literature. This might



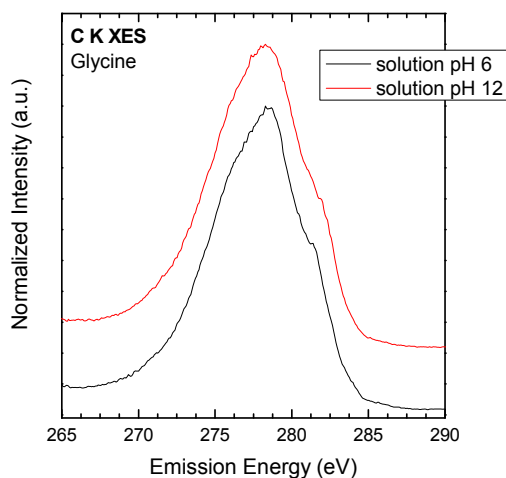


**Figure 5.14:** Non-resonant C K XES spectra of glycine solution pH 6 and pH12 ( $E_{\text{Exc}} = 297$  eV).

(again) be a hint for a gas bubble behind the window membrane. However, this could be excluded by checking the spectral region of the oxygen edge which is measured with the new VLS spectrometer in parallel to the carbon edge. A gas bubble behind the window membrane is usually indicated by the missing of the splitting of the  $1b_1$  orbital (high energetic peak in the water XES spectrum) which is the most characteristic feature of the spectrum of liquid water. As can be seen in Figure 5.13 the oxygen edge of the carbon spectrum shows similar features than a typical liquid water spectrum with the molecular orbitals  $1b_2$ ,  $3a_1$ , and the splitted  $1b_1$  [Fuc08, Wei09, Ode09, Ode09\_2] but the splitting is not as clear due to possible deposits on the window membrane.

These deposits would be another possible explanation. In this case, the carbon signal of the solution might still be visible but the spectrum would be dominated by the “dirt” background spectrum. The deposit could be on the vacuum side of the window membrane and might be result of contamination over time of storage or more likely be from a layer of organic material deposited on the liquid side of the window membrane. For the latter the XAS and XES spectra are expected to be similar to amorphous carbon due to the extended exposure to x-rays which is true for the XES spectra shown in Figure 5.14 [Abr08]. In future experiments care has to be taken to avoid contributions from any deposits on the window membrane. This can be done by control measurements with pure water before and after the actual measurement. For pure water there should be no signal at the carbon edge.

Due to the strong amorphous carbon like contributions in the spectra it is impossible to shed light on the electronic structure of the carbon edge of glycine. In the carbon XES spectra one would expected to be able to distinguish between the amine carbon and the carboxyl carbon during by resonant excitation of the respective

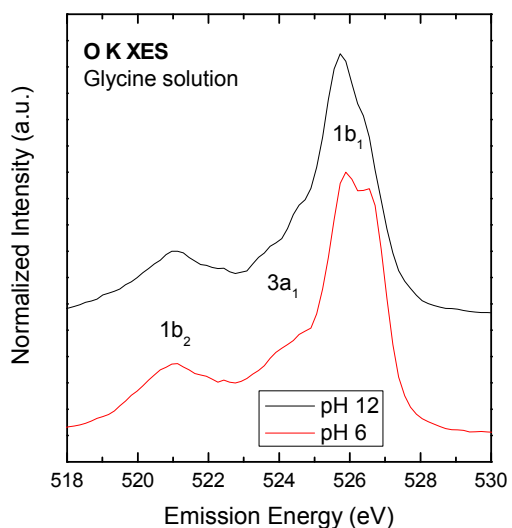


**Figure 5.15:** Non-resonant O K XES spectra of glycine solution with pH 6 and pH 12 ( $E_{\text{Exc}}=549.9$  eV).

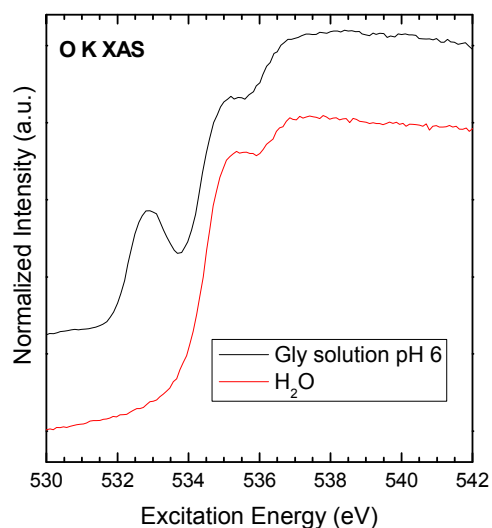


**Figure 5.16:** Comparison of O K XAS spectra of glycine solution pH 6 and of liquid water. The glycine spectrum shows an additional feature at 532.8 eV.

N 1s levels. Indeed, XPS spectra [Wu87, Boz94] show a splitting between these core levels of 2 eV.

### The Oxygen K Edge

Glycine has the highest solubility for H<sub>2</sub>O (24.99 g in 100 g solvent) while e.g. for hexane the solubility is only  $1.21 \times 10^{-5}$  g / 100 g [Fen75]. Therefore, water is the solvent of choice which complicates the interpretation of the oxygen K edge because the measured spectrum is always a sum of the spectra of the solvent and of the solute.

As can be seen in Figure 5.15, water is the dominant contribution in the absorption spectra which exhibits the typical pre-edge of water at  $\sim 535$  eV [Fuc08\_PRL, Cav05, Ode05]. In the pH 6 solution an additional feature at 532.8 eV (pre-pre-edge) can be found which was also observed for gas phase and solid state glycine at the oxygen edge [Gor03, Mes05]. The pre-pre-edge can be assigned to the  $O1s \rightarrow \pi_{C=O}^*$  transition [Mes05]. Since glycine is expected to have the same local environment for pH 6 and pH 12 at the carboxyl group ( $\text{COO}^-$ ) the XAS spectrum of the pH 12 solution is supposed to reveal the same pre-pre-edge as for the pH 6 solution.

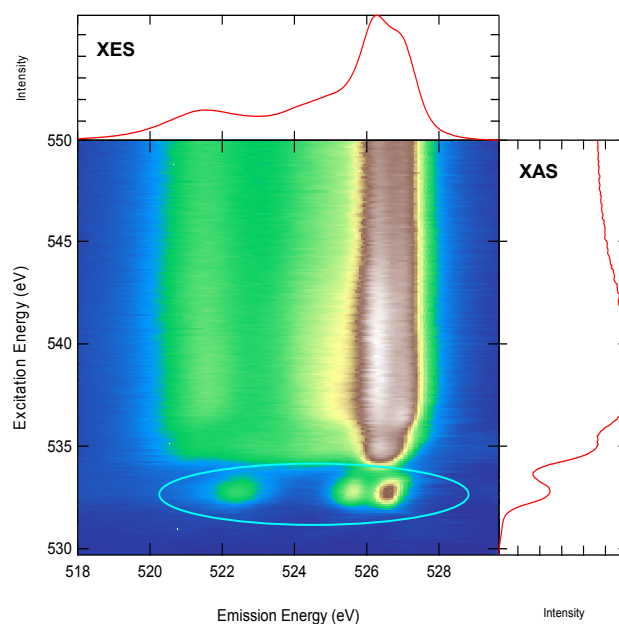


**Figure 5.17:** O K edge RIXS map of a glycine solution at a pH value of 6. The top panel shows the non-resonant emission spectrum ( $E_{\text{Exc}}=549.9$  eV) and the panel on the right the PFY absorption spectrum. The area circled in the map shows the glycine specific emission features. Right: resonant O K XES spectrum ( $E_{\text{Exc}}=532.8$  eV) of the same solution. The corresponding molecular orbitals are shown above the emission peaks.

The non-resonant XES spectra are also dominated by the solvent (Figure 5.16). For the pH 6 solution the spectrum shows the occupied molecular orbitals of water with the typical splitting of the  $1b_1$  peak. Figure 5.16 also shows the non-resonant XES spectrum of the pH 12 solution. Since the pH-value was reached by adding NaOH to the zwitterionic glycine solution, the XES spectrum of pH 12 looks very similar to a non-resonant NaOH spectrum with high concentration (see chapter 4).

The O K RIXS map of a glycine solution with a pH value of 6 is shown in Figure 5.17. The non-resonant emission spectrum on top of the map is the one shown in Figure 5.16, the absorption spectrum (on the right hand side in Fig. 5.17) was presented in Figure 5.15. When exciting into the pre-pre-edge and thus into the  $O1s \rightarrow \pi_{C=O}^*$  transition below the water absorption onset ( $\sim 534$  eV) the emission spectra can exclusively be attributed to the oxygen atoms of the glycine molecule. The corresponding region is marked in the map. A resonant XES spectrum at an excitation energy of 532.8 eV is shown in Figure 5.18 (top). Furthermore, in Figure 5.18 calculations at the O K edge of glycine with pH 6 are presented. At the bottom the occupied molecular orbitals are shown and the solid green line above represents the spectrum of the occupied orbitals after including the experimental broadening by convolving with a Gaussian (FWHM = 0.4 eV). Broadenings due to valence hole lifetime and other effects (e.g. vibrations) were described by a Lorentzian (assuming

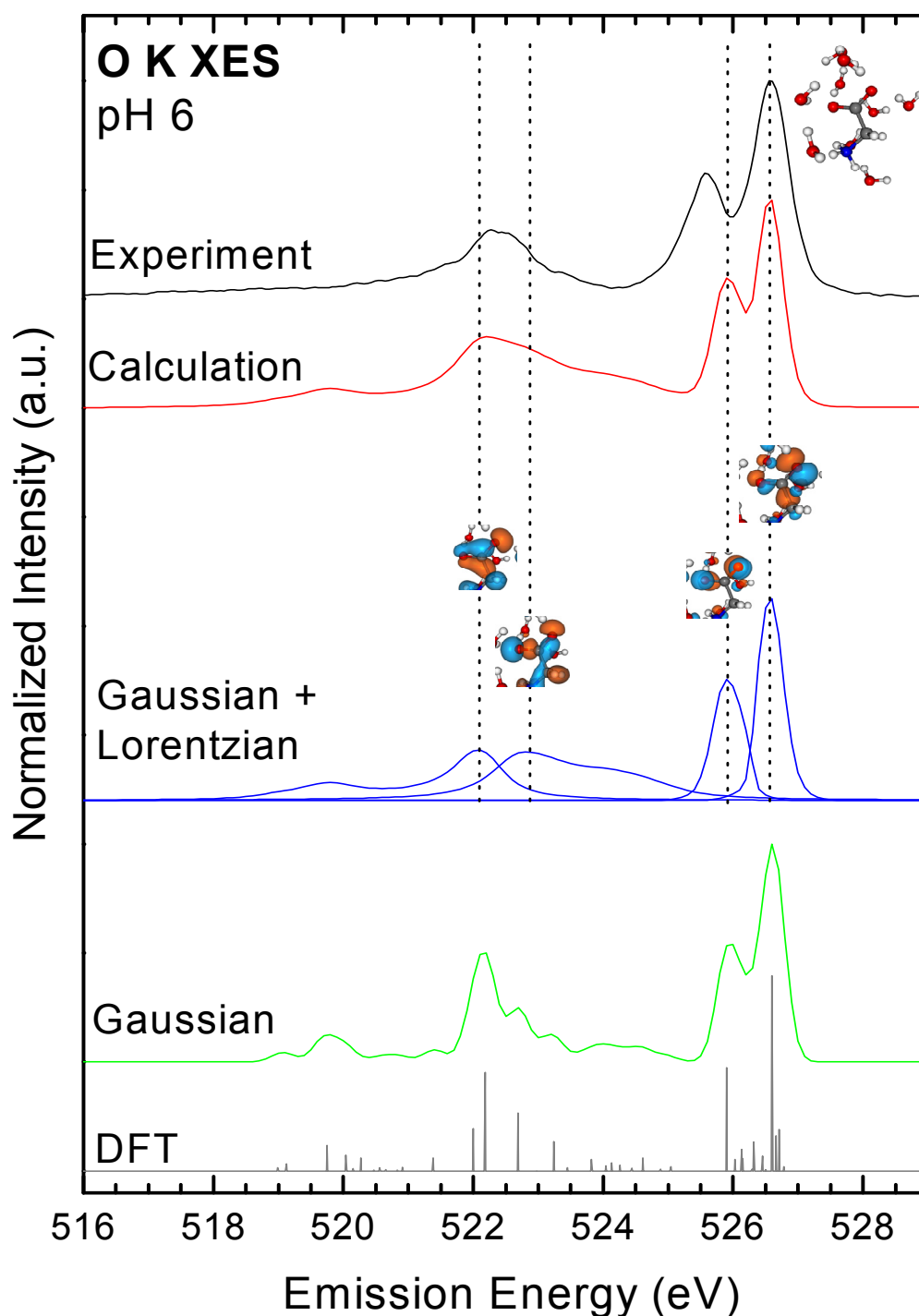


**Figure 5.18:** Bottom: DFT calculated positions and intensities of the molecular orbitals for the pH 6 solution. Green spectrum: broadened by a Gaussian (FWHM 0.4 eV). Blue peaks: broadened by a Gaussian and different Lorentzians. The pictures above show the most prominent orbital corresponding to each group of orbitals. Red spectrum: sum of the calculated blue peaks. Black spectrum: res. O K XES of glycine pH6 ( $E_{\text{Exc.}} = 532.8$  eV).

that the valence hole lifetime is the dominating effect). Their widths vary between 0.1 eV for the highest energetic peak and 0.7 eV for the lowest energetic peak.

The calculated wave functions of the four orbitals leading to the strongest spectral intensity are also shown in Figure 5.18 (enlarged shown in the appendix). The two molecular orbitals with the highest emission energies (526.5 eV and 525.5 eV) are the oxygen lone-pair orbitals which have a strong p-type character. For the orbital at 526.5 eV the knot-plane of the orbital is lying in the symmetry-plane of the molecule. The knot-plane of orbital corresponding to the peak at 525.5 eV is turned by 90° and thus perpendicular to the symmetry-plane. The molecular orbitals at 522.7 eV and 522.2 eV are  $\sigma_{C-O}$  bonding states with a small wave function amplitude around the O 1s orbital and thus the intensities of the peaks corresponding to these orbitals are weaker.

The main difference between calculated and experimental spectrum is the energy distance between the two high energy lines which is much smaller in the calculated spectrum. Two possible reasons for this discrepancy are: First, the calculation is again only a ground-state calculation and thus dynamical effects and final-state effects are not taken into account. Second, the experimental spectrum is a resonant emission spectrum (the non-resonant spectra are dominated by the water signal) while the calculated spectra are for non-resonant excitation. In the resonant XES spectra different additional effects can influence the spectra, e.g., contributions from the Raman-regime of the solvent and energy shifts in the resonant region.

### 5.1.5 Summary

In this section XES and XAS spectra of glycine solutions at the three relevant edges were presented. It is the first time resonant XES data of this molecule is available and with the help of the novel instrumentation presented in chapter 3 (namely the high-resolution, high-transmission x-ray spectrometer and the new liquid flow-through cell) it was possible to measure complete RIXS maps.

By varying the pH-value of the solution, the influence of the deprotonation of the amine group on the spectra was observed in the XES and XAS spectra at the nitrogen edge. Furthermore, the spectra were discussed in detail together with DFT calculations. It can be found that the XES spectra of the pH 12 solution are in very good agreement with the calculations not taking dynamic effects into account whereas for the pH 6 solution pronounced differences between this type of calculation and the experiment were found. First preliminary calculations taking dynamic effects into account showed that at pH 6 proton dynamics play a prominent role and the spectrum can be seen as a combination between dissociated amine groups (pH 12) and undissociated amine groups (pH6).

---

The carbon edge spectra are dominated by deposits on the window. For the deposits a similarity to amorphous carbon could be found. For this edge further investigations are needed.

At the oxygen edge the XES as well as the XAS spectra are dominated by the used solvent for excitation energies above the respective absorption edge of the solvent. The absorption spectra show a glycine specific pre-pre-edge feature. By exciting into this “pre-pre-edge”, the resonant XES spectra reveal the occupied orbitals for glycine. With the help of DFT ground-state calculations an assignment of the spectral lines to molecular orbitals is possible.

## 5.2 An Amino Acid with Two Amine Groups: Lysine

Lysine is one of the essential amino acids. Together with histidine and arginine, it is one of the base-amino acids which means that it possesses an alkaline group that is protonated in the neutral state. Compared to glycine that has a hydrogen atom as R-group, lysine has an n-butythamine side chain which is a stronger base than the  $\alpha$ -amine group. With the  $\alpha$ -amine group and the n-butythamine side chain lysine thus consists of two amine fractional groups.

Figure 5.19 shows the chemical structure of lysine in the zwitterionic state, with two deprotonated amine groups and with two protonated amine groups. Finally, lysine is also shown as cation with all fractional groups (including the carboxyl group) protonated. Furthermore, the  $pK_a$  and  $pK_{iso}$  values are given. For lysine there are not only  $pK_{NH_2}$  and  $pK_{COOH}$  values but as well a value for the side chain ( $pK_{side}$ ).

As for glycine (at pH 6), a half-saturated aqueous solution (15 g / 100 ml) of lysine was used for the measurements. Since lysine is a base in aqueous solution the pH-values were not only regulated with sodium hydroxide but also with hydrochloric acid to achieve the lower pH-values. The pH-value for the zwitterionic state was set to 9.59 (short pH 9; the isoelectric point is at a pH of 9.74). For the double-deprotonated state the pH-value was 13.28 (short pH 13), and the double-protonated state was set to a pH-value of 5.15 (short pH 5). The focus of the lysine studies was on the nitrogen edge, and thus on the pH-induced local changes of both amine fractional groups. Note, that at a pH of 9 the deprotonation and thus the zwitterionic state is not accomplished at the  $\alpha$ -amine group but at the side chain amine group.

Lysine also shows the tendency to hold gas bubbles right behind the window membrane (see discussion above). Therefore, the maps are partly (especially before the

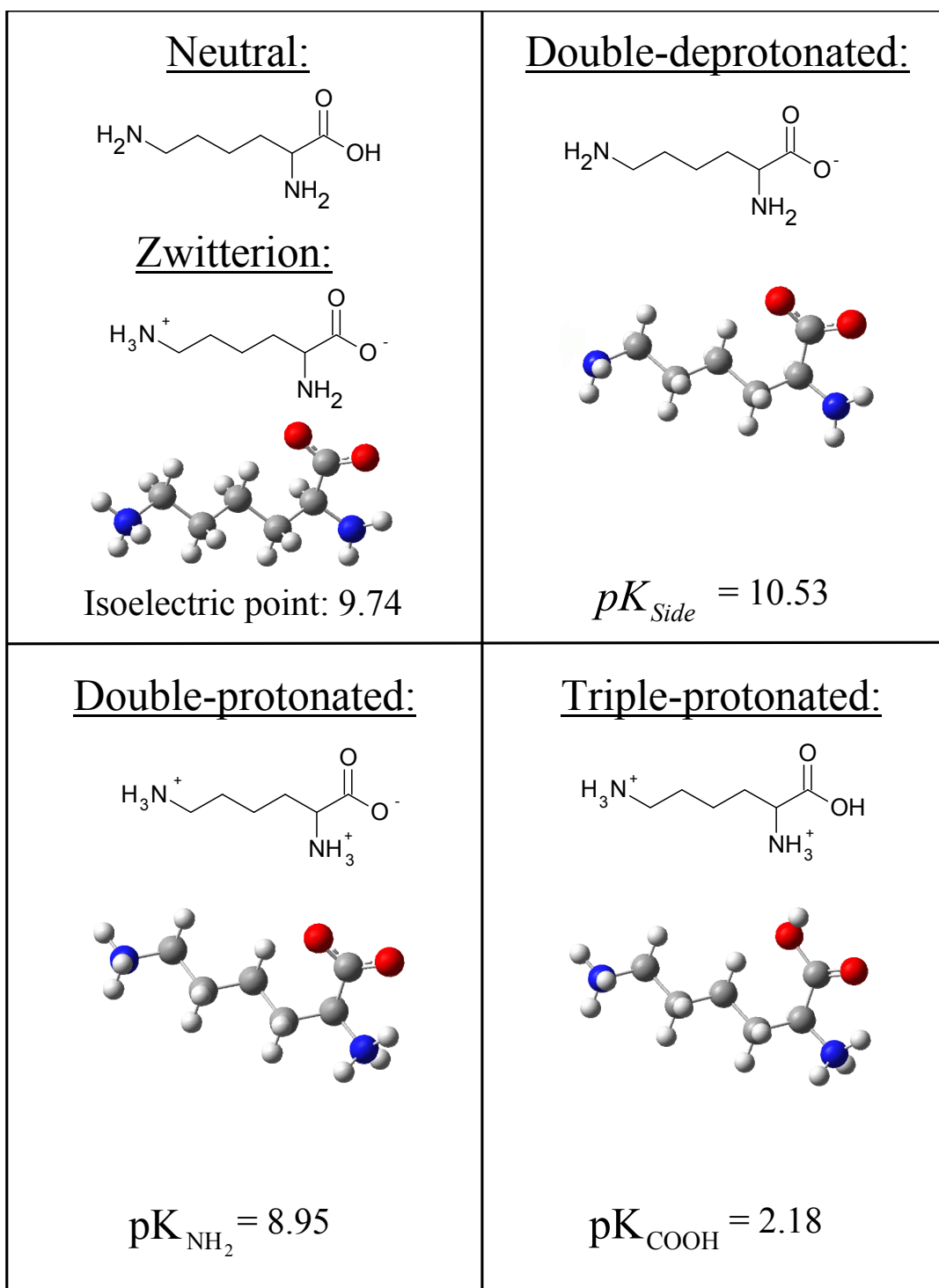


**Figure 5.19:** Top left: neutral and zwitterionic state of lysine. Top right: double-deprotonated state of lysine. Bottom left: double-protonated state of lysine. Bottom right: triple-protonated state (carboxyl group is protonated).

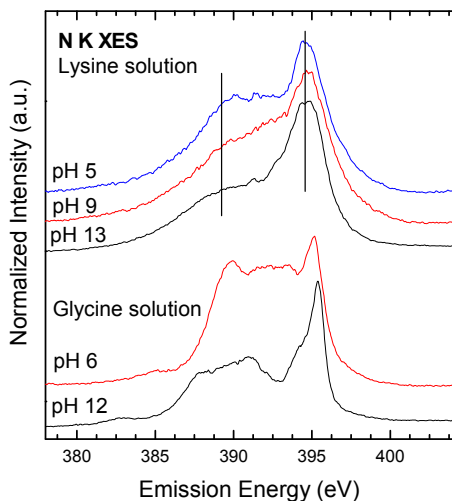


**Figure 5.20:** Non-resonant N K XES spectra of three lysine solutions with different pH concentrations (pH 5, pH 9, and pH 13) and glycine with pH-value 6 and pH-value 12.

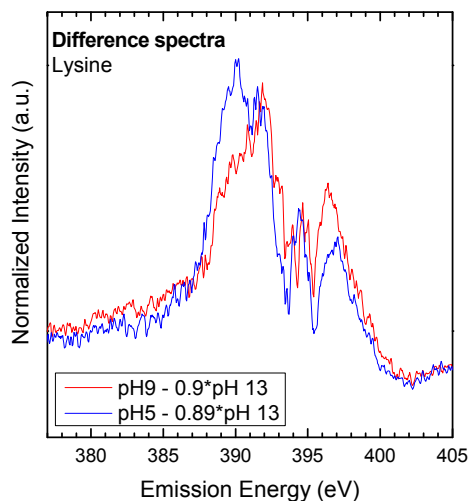


**Figure 5.21:** Differences of the spectra in Figure 5.20. The double-deprotonated state (pH 13) was subtracted from the other states with similar weight factors.

absorption onset and at the absorption edge) disturbed by spectral features of the air in the bubbles (mainly  $N_2$  and  $O_2$  gas). As a result only the non-resonant N K edge emission spectra are presented in the following. These spectra were verified with the oxygen signal appearing in the same energy window of the spectrometer. Since the oxygen signal reveals the typical emission lines of liquid water the N K edge spectra are real solution spectra.

### The Nitrogen K Edge – a Comparison of Different pH-Values

Messer et al. [Mes05\_2] found that the XAS spectrum of lysine in the liquid zwitterionic state can be explained as a mixture of the protonated and deprotonated XAS spectra of glycine. At pH 10, the XAS spectrum of lysine shows the two pre-edge features representing the  $NH_2$  fraction and the broad resonance at approximately 406 eV for the  $NH_3^+$ . This assignment is based on the fact that in the zwitterionic state a deprotonated amine group exists in addition to the protonated amine group. This result leads to the speculation that the absorption spectra are dominated by the “fingerprints” of the  $NH_2$  and  $NH_3^+$  fractions. Thus a XAS spectrum of a lysine solution at pH 5 at which both amine groups are protonated, should look similar to those of a glycine solution at pH 6 for which the amine group is also protonated. The spectra of lysine at



pH 13 at which both amine groups are deprotonated should look similar to the XAS spectra of glycine at pH 12.

In Figure 5.20, non-resonant XES spectra of lysine solutions with the three different pH-values are presented together with the two different pH-values of glycine for comparison. All three spectra of lysine are dominated by a sharp peak at  $\sim 395$  eV and a broad shoulder between 385 eV to 393 eV. The main difference between the different pH-values is the ratio between these two features: The lower the pH-value, the higher is the spectral weight of the broad shoulder between 385 eV and 393 eV. Since the lysine solution with pH 13 consists of two deprotonated amine groups, the feature at 395 eV most likely can be associated with the deprotonated state (similar to glycine). As in the case of glycine the weight of this peak decreases with decreasing pH-value. In Figure 5.21 the differences of the spectra shown in Figure 5.20 are presented. Here the pH 13 spectrum was subtracted from the pH 9 and the pH 5 spectrum with similar weight factors ( $1 \cdot \text{pH } 9 - 0.9 \cdot \text{pH } 13$  and  $1 \cdot \text{pH } 5 - 0.89 \cdot \text{pH } 13$ ). The weight factors were chosen so that the difference spectrum was never negative. The differences show the increase of the low energy area as a function of pH-value. Based on the differences between the spectra at different pH-values and the results on glycine discussed above, the spectra can now be qualitatively explained as follows. The peak at 395 eV is mainly related (and thus indicative) to deprotonated amine groups ( $\text{NH}_2$ ), while it is weaker for protonated amine groups ( $\text{NH}_3^+$ ). However, due to proton dynamics during the core-hole lifetime as it was observed for glycine it is expected that the peak at 395 eV is still visible even for protonated amine groups. Thus, the experimental spectrum at the lowest pH is the sum of the dissociated amine groups ( $\text{NH}_2$ ) and the undissociated  $\text{NH}_3^+$  groups. The larger broadening width of the lysine spectra peaks in comparison to the glycine peaks (see Figure 5.20) might be due to the two amine groups with a slightly different chemical environment.

The findings above lead to the following picture: Deprotonated amine groups have a characteristic emission feature at approx. 395 eV. This feature is also visible for emission spectra with no deprotonated amine groups because of ultra-fast dissociation processes. Between 385 eV and 393 eV the emission spectra are dominated by the protonated ( $\text{NH}_3^+$ ) amine groups. The higher the intensity in this area the more protonated amine groups are in the solution. Thus XES is a good tool to indicate the different amine groups in an amino acid. Provided that for one amino acid the spectra with all amine groups protonated and with all amine groups deprotonated are available, it is possible to determine the relative fraction of protonated/deprotonated amine groups for different pH-values by describing the emission spectrum as a superposition of the spectra of the two “extreme” cases.

Furthermore, it will be interesting, whether it will be possible to distinguish between the two different amino group nitrogen atoms in future resonant XES

---

investigations. Especially in the zwitterionic state, they have a different local environment and should be separable in the spectra. In XPS measurements the splitting of these core-levels was found to be 2 eV in a solid state sample [Boz94]. For pH 13 and pH 5 this separation is expected to be much smaller because the amine groups have the same structure. Furthermore, the RIXS maps at the oxygen K edge might give additional experimental input. Finally, calculations might shed more light on the influence of proton dynamics on the spectra of lysine and allow a more quantitative evaluation.

### 5.3 Summary and Outlook

In this chapter the focus of the investigations was on the electronic and chemical properties of two different amino acids. Glycine is the simplest amino acid and contains only one amine group while lysine has two amine groups. In the neutral state amino acids function as a base and acid at the same time. Thus they are called zwitterions and are very sensitive to pH changes. The pH-dependency of amino acid solutions was demonstrated for the nitrogen K edge XAS and XES spectra. By changing the pH-value the local environment at the nitrogen atom changes ( $\text{NH}_2 \leftrightarrow \text{NH}_3^+$ ), which has a direct influence on the spectra. Furthermore, for lower pH-values (protonated amine groups) the XES spectra are influenced by strong proton dynamics.

During the core-hole lifetime a proton of the protonated amine group dissociates from the molecule and the remaining amine group has the structure of the deprotonated group. First DFT calculations confirm this dissociation model of amino acids. Qualitatively the high energy peak in the N K XES spectra can be attributed to the deprotonated amine group and the low energy area to the protonated amine group. As the comparison between glycine and lysine shows, the exact shape of the spectra depends on the chemical environment of the amine groups.

The oxygen K RIXS maps are dominated by the signal from the solvent ( $\text{H}_2\text{O}$  and aqueous NaOH solution). Still, the XAS spectra show a pre-pre-edge feature 532.8 eV which can exclusively be related with the amino acid oxygen atoms. By exciting into this unoccupied state of glycine the O K RIXS map reveals the occupied orbitals of glycine with high wave function amplitude around the O 1s core-levels. First DFT calculations are in good agreement with the experimental data and show that the two high energetic peaks can be seen as the oxygen lone-pair orbitals lying parallel and perpendicular to the symmetry-plane of the glycine molecule. The peaks at lower energy can be described as  $\sigma_{\text{C-O}}$  bonding states.

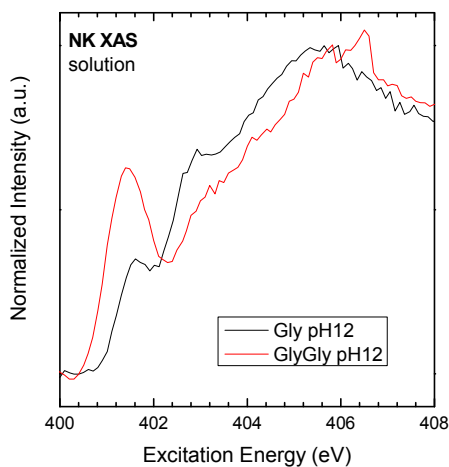


**Figure 5.22:** First XAS spectrum of the peptide diglycine in aqueous solution with a pH-value of 12 in comparison with the glycine solution with a pH-value of 12.

For future measurements it is very important to take special care of the bubble problem discussed above. With this problem solved a complete set of RIXS maps at all relevant edges will give the full electronic information of the respective amino acid. Further DFT calculations (at all edges) will help to understand the spectra and reveal proton dynamical effects. The parameter window should also be extended to low pH-values to investigate the protonation change at the oxygen edge and to complete the picture at the nitrogen edge. With the new silicon-free membranes described in chapter 3 amino acids with sulfur groups (e.g., cysteine) can now be part of the investigations.

On step ahead of the amino acids is the investigation of peptides and proteins. They consist of different amino acids and are named depending on the number of amino acids in the molecule ( $\leq 100$  amino acids: peptide and  $> 100$  amino acids: protein). The smallest peptide diglycine is a good starting point for the investigations. Diglycine is a combination of two glycine molecules where a water molecule is removed at the peptide bond. First XAS measurements show an enormous change in the N K spectra in comparison to a single glycine molecule (see Figure 5.22). Further measurements of diglycine, especially the RIXS map are expected to give detailed information about the peptide/protein bonds and their influence on the electronic and chemical properties of peptides/proteins.

---

## CHAPTER VI

# Simple Alcohols and Acids

---

In this chapter the focus is on measurements of the simplest alcohol (methanol) and the simplest carboxylic acid (acidic acid). Both liquids play a role in our daily life and are also part of biological processes.

### 6.1 Methanol

Methanol is the simplest alcohol and can be synthesized from the simplest alkane methane by replacing one hydrogen by a hydroxide group. The chemical structure of methanol is shown in Figure 6.1. The properties of methanol are important for different technical applications. At room temperature, methanol is a polar liquid and due to its low freezing point ( $-97^{\circ}\text{C}$ ) it is often used as anti-freeze, e.g., in cars or pipelines. In addition, it is a very common solvent. During the last decades it became more and more important for the automotive industry and can be used as motor fuel or as component of biodiesel.

While the geometry of liquid methanol was under debate the last 50 years [Tau52, Pau67, Tor89, Hau87, Jor81, Han03, Mor02, Pag03, Sar93, Mon81, Tan84] little is known about its electronic properties. The structural discussion was about the

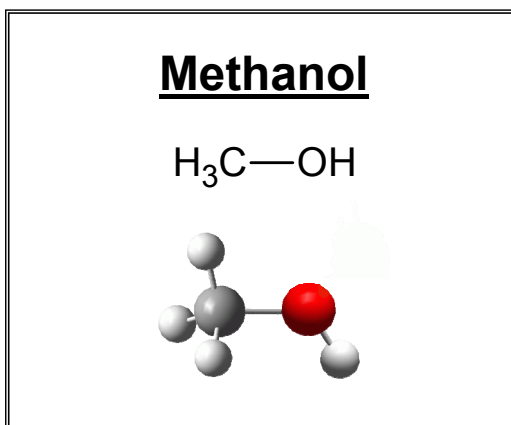


Figure 6.1: Chemical structure of methanol.

---

hydrogen bonding network in liquid methanol. Hereby two different scenarios were suggested. In the first model it was proposed that the molecules build hydrogen bonded one-dimensional chains [Tau52, Tor89]. In contrast, the second model proposed that the molecules form cyclic (hydrogen-bonded) hexamer structures [Pau67]. In both cases the molecules cluster and the hydrogen bond is formed at the hydroxide group. In the case of a ring structure every hydrogen atom of the hydroxide group should be involved to form the hydrogen bonds. In literature this discussion is supported by theoretical [Tsu99, Hau87, Jor81, Han03, Mor02, Pag03] and experimental studies [Sar93, Mon81, Tan84, Nar84, Mag82, Yam99]. Most experiments used neutron diffraction or x-ray scattering. The application of XAS and XES to liquid samples gave new input to the discussion about the microscopic structure of methanol [Guo03, Kas05]. Based on their data and DFT calculations Guo et al. [Guo03, Kas05] proposed a model containing a mixture of chain and ring structures.

For this thesis pure liquid methanol was used to measure RIXS maps of the C K and the O K edge.

### 6.1.1 The O K Edge of Methanol

In Figure 6.2 the O K edge RIXS map of liquid methanol is shown. A non-resonant emission spectrum at an excitation energy of 549.4 eV is shown on top of the map. On the right side the partial (514.5 eV – 533 eV) fluorescence yield absorption spectrum is presented.

The absorption spectrum reveals three weak features at 534.5 eV, 535.8 eV, and 537 eV (indicated by the black dotted horizontal lines). These peaks are in good agreement with other experimental data of liquid methanol [Guo03, Kas05]. Furthermore, the peak positions agree with theoretical studies of gas phase methanol [Tam08, Hu06, Hui91] where the first resonance at about 534 eV is assigned to the  $O1s \rightarrow \sigma_{O-H}^*$  transition with some contributions of the p orbital at the C atom [Wil05]. The next two features are assigned to the  $3p_a'$  and the  $\sigma_{C-O}^*$  resonances [Tam08]. In the calculated spectra the peaks are present for the hydrogen bond ring configuration as well as for the chains. For the rings all molecules are equivalent and thus the absorption features are at the same photon energy for each molecule. For the chains the local environment of each molecule is different which leads to shifted peak positions in the absorption spectra for each molecule [Tam08]. Thus, the experimental spectra are a mixture of the two components leading to the weak features observed. Furthermore, saturation effects might be a reason for the weakness of the pre-edge features.

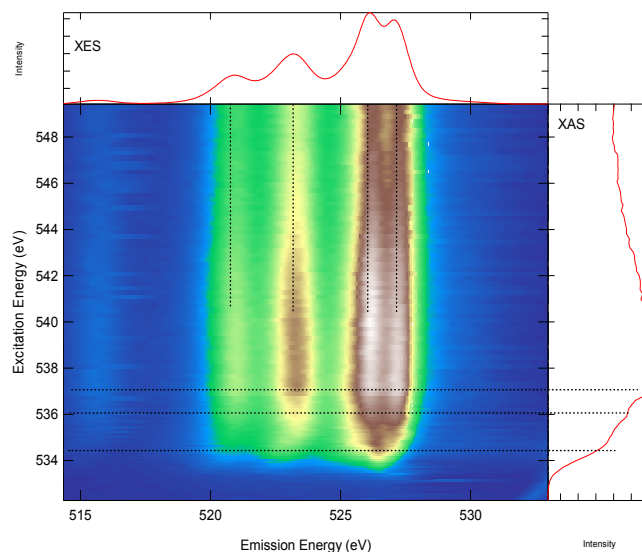


**Figure 6.2:** O K edge RIXS map of liquid methanol. The top panel shows the non-resonant emission spectrum ( $E_{\text{Exc}}=549.4$  eV) and the panel on the right the PFY absorption spectrum. The dotted horizontal and vertical lines represent the absorption and emission features.

The (non-resonant) x-ray emission spectrum at 549.4 eV on top of the RIXS map in Figure 6.2 shows four main features, namely the  $5a'$ , the  $1a''$  and  $6a'$  (which appear as one line), the  $7a'$  and  $2a''$  emission lines [Kas05]. Guo et al. and Kashtanov et al. described the x-ray emission spectra as a superposition of ring and chain components [Guo03, Kas05]. The high-resolution spectra in this thesis reveal a clear splitting of the high energy feature (525.9 eV and 527.1 eV) which might be interpreted as the different bonding species described in [Guo03, Kas05]. Hereby, the high energetic component (527.1 eV) would represent the chain structure and the low energetic (525.9 eV) the ring structure. The two other features at 523.2 eV and 520.8 eV would be a superposition of chain and ring structure. At an excitation energy of 534.5 eV (first resonance feature, marked with horizontal dotted line) the RIXS map reveals only one peak which - following the model of Guo and Kashtanov - would stand for the ring structure. The shift of the emission features between first and second dotted horizontal line of the map can again be attributed to Raman effects.

The model of Guo et al. [Kas05] seems quite unlikely based on their own DFT XES calculations of gas phase methanol. These calculations (Figure 6.3) reveal two clearly separated peaks (in the spectra 525.9 eV and 527.1 eV) without any hydrogen-bond interaction and are in very good agreement with our non-resonant XES spectrum as can be seen in Figure 6.3. The model of Guo et al. is based on their calculation of a very limited “liquid” system, i.e. an (isolated) chain and an (isolated) ring. These calculations lead to only one (much broader) high-energy feature instead of the  $7a'$  and  $2a''$  lines. For chains they find a different energy position of this feature as for rings

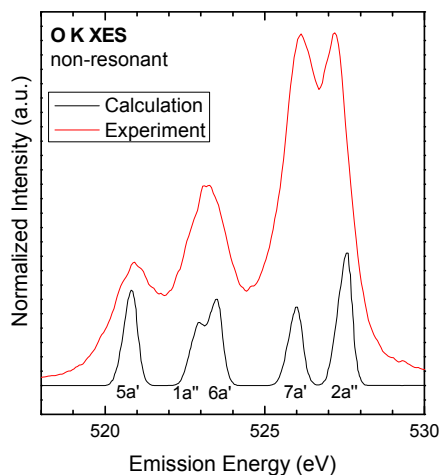


**Figure 6.3:** Comparison between the non-resonant OK XES spectrum of liquid methanol ( $E_{\text{Exc}} = 549.4$  eV) and DFT calculations made by Kashtanov et al. [KAS05]. The nomenclature of the molecular orbitals is given in the spectrum.

which they identify with the two lines in the experimental spectra. While the data of Guo et al. might be explained by these calculated spectra, our high resolutions spectra are much better explained by their gas phase calculations. As will be shown below, also our C K XES rather supports a simpler model in which the spectra can mainly be explained by an interaction free system (gas phase) and the influence of hydrogen bonding has to be searched in the finer details and based on more comprehensive calculations.

### 6.1.2 The C K Edge of Methanol

The x-ray absorption spectrum of the carbon K edge of liquid methanol is shown in Figure 6.4 as the right panel of the RIXS map. It is a partial fluorescence yield spectrum (emission energies between 286.4 eV and 299.4 eV were integrated). The spectrum reveals three main features; one at 287.8 eV, one at 289.1 eV, and the third one at 290.1 eV (horizontal dotted lines). The absorption spectrum presented here is in good agreement with gas phase measurements of methanol [Tam08] as well as measurements of liquid methanol [Kas05]. Hereby, the first absorption feature (287.8 eV) is assigned to a  $\text{C}1s \rightarrow \sigma_{\text{O-H}}^*$  transition and the second feature (289.1 eV) contains a combination of  $\text{C}1s \rightarrow \sigma_{\text{C-H}}^*$  and  $\text{C}1s \rightarrow 3p_a''$  resonances. The two features shift for the ring structure with respect to the molecule [Tam08]. Furthermore, the absorption spectrum of liquid methanol is dominated by saturation effects which weaken the “contrast” in the spectrum.

The (non-resonant) x-ray emission spectrum (299.4 eV) of liquid methanol at the C K edge is presented on top of the RIXS map in Figure 6.4. Where former publications of Kashtanov et al. [Kas05] only showed a broad emission line at



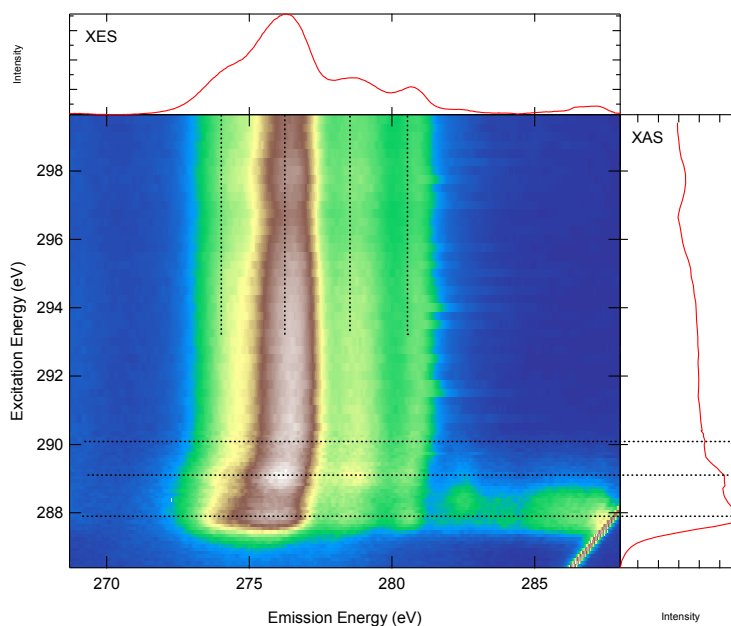


**Figure 6.4:** C K edge RIXS map of liquid methanol. The top panel shows the non-resonant emission spectrum ( $E_{\text{Exc}}=299.4$  eV) and the panel on the right the PFY absorption spectrum. The dotted horizontal and vertical lines represent the absorption and emission features.

approx. 276.5 eV with a shoulder at  $\sim 280$  eV the high-resolution XES spectra in this thesis reveal more details. Here, four main emission lines ( $5a'$ ,  $1a'' + 6a'$ ,  $7a'$ , and  $2a''$ ) are clearly visible at emission energies of 274.1 eV, 276.2 eV, 278.7 eV, and 280.8 eV. These peaks are again in very good agreement with the gas phase calculations presented in [Kas05] as can be seen in Figure 6.5 where calculation and experiment are compared. The split peak at 276 eV in the calculation appears as one broad line in the experiment (276.2 eV).

The C K XES and the O K XES calculations show the same molecular orbitals ( $5a'$ ,  $1a''$ ,  $6a'$ ,  $7a'$ , and  $2a''$ ) which can be seen in Figure 6.6 together with the experimental spectra. In this graph, the O K and C K emission spectra are plotted on a common energy scale by setting the energy of the  $2a''$  orbital to a value of 0 eV. Both spectra show the same orbitals, as expected but with different intensities. These different intensities are a result of the localization of the orbital in the molecule. For example the  $2a''$  emission line dominates the O K spectrum but is much weaker in the C K spectrum, i.e., the wavefunction of this orbital is more located around the oxygen atom. In comparison, the wavefunctions of the  $1a''$  and  $6a'$  orbitals seem more located at the carbon than at the oxygen. The wave functions of the  $5a'$  and the  $7a'$  seem to be delocalized for both atoms. Note, that in the experimental spectrum the  $7a'$  line is

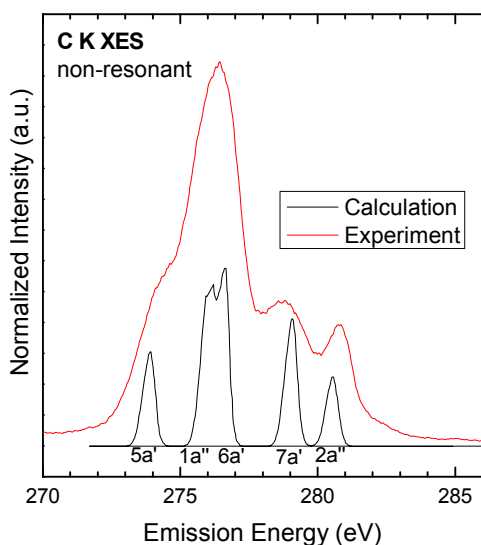


**Figure 6.5:** Comparison between the non-resonant C K XES spectrum of liquid methanol ( $E_{\text{Exc}}=299.4$  eV) and DFT calculations made by Kashtanov et al. [Kas05]. The nomenclature of the molecular orbitals is given in the spectrum.

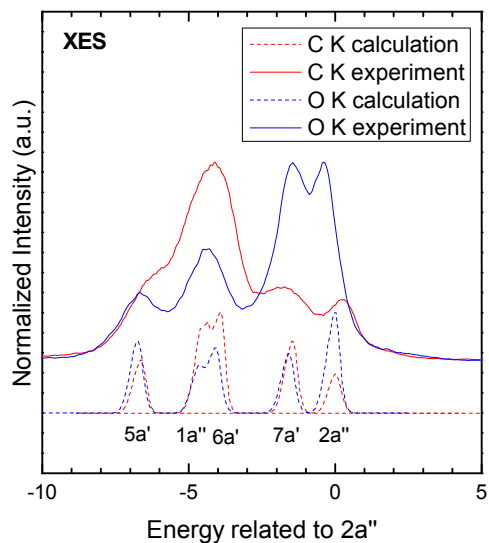


**Figure 6.6:** Comparison between the experimental and calculated O K and C K XES spectra.

much broader in the C K spectrum than in the O K spectrum and thus appears to be weaker.

The RIXS map in Figure 6.4 shows a clear shift of the emission lines in the excitation energy region from 286 eV to 290 eV. This can not alone be due to a Raman-shift because the spectrum does not shift parallel to the elastic peak (see Figure 6.4). The map reveals even more effects, e.g., in the zoomed area shown in Figure 6.7. This area represents the region at the absorption resonances and close to the elastically scattered peak. As can be seen there are strong resonant features at the elastically scattered peak and discrete losses over an excitation energy range of  $\sim 1.5$  eV can be found. The strong resonant feature at the elastically scattered peak represents a core exciton. With a core exciton also a local change in the environment can be found and thus other losses are favored. This is the reason why the losses in this map can only be found in the extended area shown in Figure 6.7. Possible reasons for the losses could be e.g. vibrational broadening or a change of the overall system due to ultra-fast electron hopping. To verify the reasons this map area as well as the whole RIXS map will be subject of further investigations. Also DFT calculations for the liquid state will

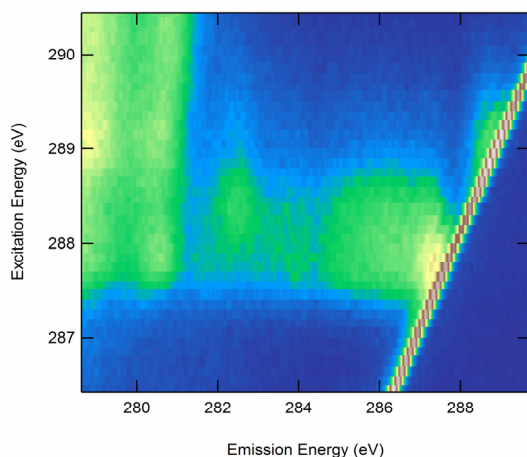


**Figure 6.7:** Extended area of the C K edge RIXS map. Discrete losses of the elastic peak are visible (see text).

be performed to shed light on the origins of the effects observed in the RIXS map.

## 6.2 Acetic Acid

Acetic acid is the simplest carboxylic acid where the hydroxide group of methanol is replaced with a carboxylic group ( $\text{CH}_3\text{COOH}$ ). Its chemical structure is shown in Figure 6.8. As an aqueous solution it is often simply called vinegar, since acetic acid gives vinegar its characteristic smell. Pure acetic acid (also called: ice-vinegar) has a freezing point below room temperature ( $16^\circ\text{C}$ ) and is a water-free acid

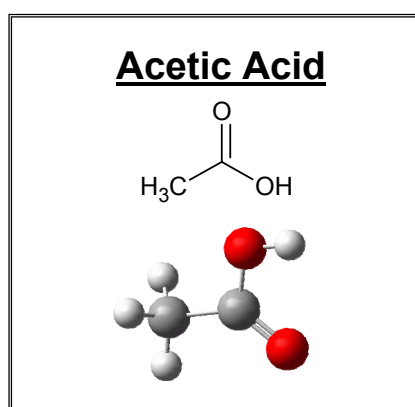


**Figure 6.8:** Chemical structure of acetic acid.

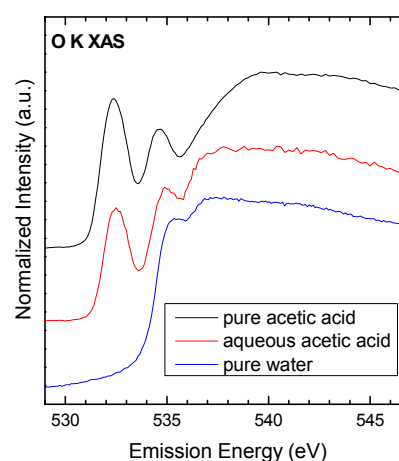


**Figure 6.9:** O K XAS spectra of pure acetic acid, aqueous acetic acid and pure water.

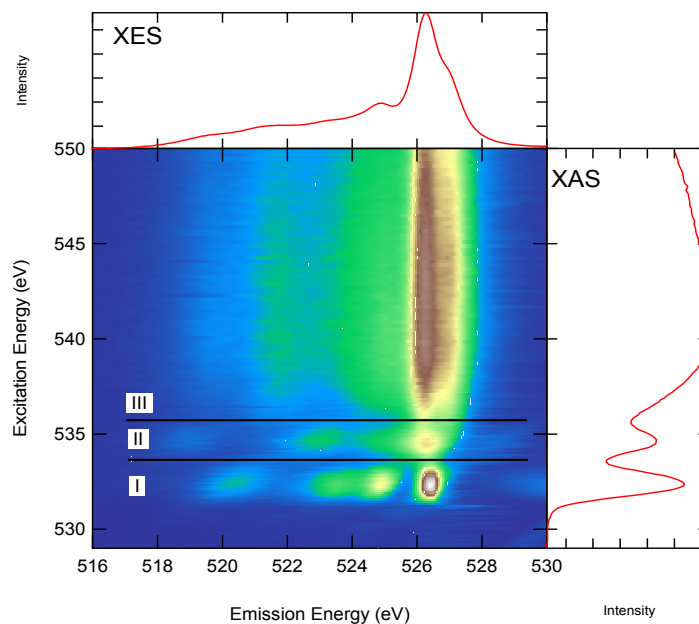


**Figure 6.10:** O K edge RIXS map of pure liquid acetic acid. The top panel shows the non-resonant emission spectrum ( $E_{\text{Exc}}=549.8$  eV) and the panel on the right the PFY absorption spectrum. The horizontal lines represent the regions where it is possible to distinguish between the two different chemical species of oxygen atoms.

but very hygroscopic. Acetic acid can be produced with methanol carbonylation, i.e., methanol reacts with carbon monoxide with the help of a catalyst. Furthermore, it is produced in the human body as a result of alcohol oxidation.

In respect to the electronic structure for acetic acid – as for methanol – little is known. A few studies of gas phase acetic acid with electron energy loss spectroscopy [Duf08, Rob88, Urq02] and XPS [Bri91, Bri91\_2] were published. In the recent past Tokushima et al. [Tok09] presented the first O K XES and XAS studies of liquid acetic acid.

The O K and C K RIXS map measurements for this thesis were recorded with nearly pure (99.7%) acetic acid. The aqueous acetic acid solution was reached by mixing pure acetic acid with the same amount of ultra-pure water. In the following the first is called “pure acetic acid” and the second “aqueous acetic acid”.

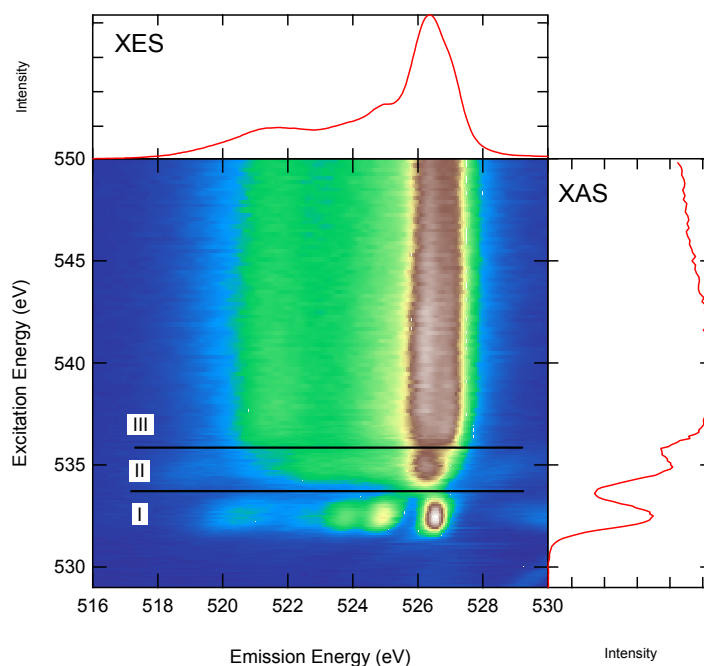


**Figure 6.11:** O K edge RIXS map of aqueous acetic acid. The top panel shows the non-resonant emission spectrum ( $E_{\text{Exc}}=549.8$  eV) and the panel on the right the PFY absorption spectrum. The horizontal lines represent the regions where it is possible to distinguish between the two different chemical species of oxygen atoms.

### 6.2.1 The O K Edge of Acetic Acid– a RIXS Map Study

Recently the first XAS and XES spectra at the oxygen K edge for liquid acetic acid were published by Tokushima et al. [Tok09]. They revealed a strong excitation energy dependence in the XES spectra through site-selective excitation of the two oxygen atoms in the carboxyl group. Therefore, the absorption spectra are a good starting point to find the energies locally exciting the different O atoms in the molecule. In Figure 6.9 the O K XAS spectra of pure acetic acid, aqueous acetic acid, and pure water are shown. The pure acetic acid spectrum shows two resonant features at 532.3 eV and 534.5 eV. The spectrum of the aqueous acetic acid is very similar to the one of pure acetic acid but the two resonances have both a small blue shift (for the first resonance (532.3 eV): 0.1 eV and for the second resonance (534.5 eV): 0.4 eV). Due to the comparison with gas phase acetic acid [Rob88, Duf08] as well as with liquids with only the C=O (acetone  $\text{OC}(\text{CH}_3)_2$ ) or the hydroxide ( $\text{H}_2\text{O}$ ) component Tokushima et al. [Tok09] were able to assign the two resonant features to certain transitions and thus to the two different oxygen atoms. The strong resonance at 532.3 eV represents the O1s

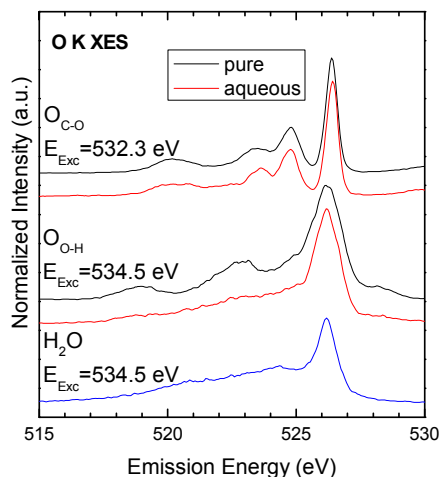


**Figure 6.12:** O K XES spectra for  $E_{\text{Exc}}=532.3$  eV and 534.5 eV. The excitation energies stand for the different O components of the acid. The black spectrum present the pure acetic acid and the red spectrum the aqueous acetic acid. The blue spectrum is liquid water at an  $E_{\text{Exc}}=534.5$  eV for comparison.

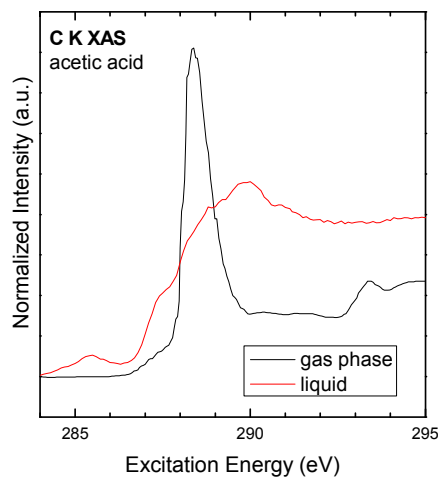


**Figure 6.13:** C K XAS spectra of pure acetic acid. The black spectrum represents the gas phase measured with (ISEELS) [Rob88] and the red spectrum is the liquid phase.

$\rightarrow \pi^*$  transition at the C=O component. The mentioned resonance is present in the acetone absorption spectra but not in liquid water. The second resonance can be assigned to the O1s  $\rightarrow \pi^*$  transition of the hydroxide component but also to the O1s  $\rightarrow 3p$  transition of the C=O component. However, the contribution of the C=O component is negligible for the acetic acid spectra [Rob88, Tok09]. Furthermore, in Figure 6.8 the influence of the water is visible for the aqueous acetic acid solution. This can be seen by the shape of the aqueous acetic acid spectrum in the region of the pre-edge and main edge of liquid water. Since the two resonances could be assigned to the two different oxygen atoms it should be possible to distinguish the two chemical components in the XES spectra by selective excitation into the pre-edges.

In Figure 6.10 the O K edge RIXS map of pure acetic acid is shown. As can be seen, the map is separated into three different excitation energy regions corresponding to the edges in the XAS spectrum. Hence, we can select a chemical site by tuning the excitation energy. For region I (excitation energy from 529 eV to 533.7 eV) a very narrow peak (FWHM 0.43 eV) at an emission energy of  $\sim 526.3$  eV can be observed (also see Figure 6.12) which can – together with the other emission features – be assigned to the oxygen atom belonging to the C=O component. The region II (excitation energy from 533.7 eV to 535.7 eV) reveals a different emission spectrum in

terms of peak separation, structure and width in respect to region I. Hereby, a broader peak at  $\sim 526.2$  eV can be observed. Since this area is assigned to the oxygen atom of the hydroxide group, the broadening of the peak might be explained by core-hole induced dynamics and thus the probed site with the lighter mass atom shows larger peak broadenings [Tok09]. For excitation energies above 535.7 eV (region III) the resulting spectra are a combination of both components. Measurements as well as DFT calculations by Tokushima et al. [Tok09] are in very good agreement with the results for pure acetic acid presented in this thesis.

The O K RIXS map of aqueous acetic acid is presented in Figure 6.11. In comparison to the RIXS map of pure acetic acid the presence of the liquid water is noticeable. In the non-resonant region the emission lines of water ( $1b_2$ ,  $3a_1$ , and  $1b_1$ ) can be observed (see chapter 4) and in region II the influence of water broadens the main peak which is related to the  $O_{O-H}$  atom in pure acidic acid. The XES spectra taken with excitation energies in region I and II of pure acetic acid and aqueous acetic acid are shown for comparison in Figure 6.12. For the spectra at an excitation energy of 532.3 eV (pre-pre-edge) the influence of the water is negligible because the excitation is far below the water absorption onset ( $\sim 534$  eV). At this energy, the features can be assigned to the oxygen atom of the  $C=O$  component (see above). In comparison the XES spectra excited into the hydroxide component ( $E_{Exc} = 534.5$  eV) show a clear water influence. The orbital structure of pure acetic acid is not observable anymore and the spectrum is dominated by one main peak. This peak shows a similar structure as the main peak in a water XES spectrum with the same excitation energy (also shown in Figure 6.12). Thus it is a clear indication that at the  $O_{O-H}$  atom an interaction between the acetic acid and the water molecules take place.

## 6.2.2 The C K Edge of Acidic Acid

While for the O K edge of liquid acetic acid first XES and XAS measurements were performed only gas phase XAS spectra are available for the carbon K edge [Rob88, Duf08]. For the C K edge it is again possible to distinguish between two chemical species of carbon atoms; one belonging to the methyl group ( $CH_3$ ) and the other to the carboxyl group ( $COOH$ ). In Figure 6.13 a gas phase spectrum of acetic acid measured with inner-shell electron energy loss spectroscopy (ISEELS) [Rob88] is shown together with an XAS spectrum of pure liquid acetic acid. The gas phase absorption spectrum reveals a very dominant sharp resonance at 288.7 eV which can be assigned to the  $C1s \rightarrow 3p/\sigma_{C-H}^*$  transition of the  $CH_3$  component and the  $C1s \rightarrow \pi^*$

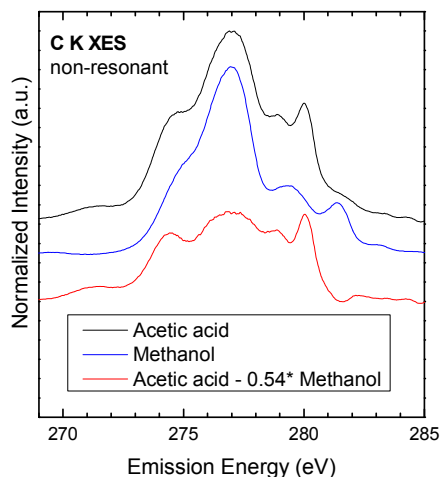


**Figure 6.14:** Non-resonant C K XES spectra ( $E_{\text{Exc}} = 294.9$  eV) of pure acetic acid, pure methanol, and the difference spectrum (acetic acid – 0.54\* methanol).

transition of the C=O component. At excitation energies below this resonance, a weak feature can be observed at  $\sim 287.4$  eV which exclusively belongs to the CH<sub>3</sub> component. The gas phase spectrum above 290 eV is nearly flat and only two very weak features can be seen at 290.56 eV and 291.64 eV [Duf08]. In comparison to the gas phase spectrum, the liquid spectrum looks totally different as can be seen in Figure 6.12. But even with the totally different shape of the liquid XAS spectrum the two first gas features can be seen in the liquid phase. Hereby, the feature at  $\sim 287.4$  eV is much more dominant in the liquid phase as in comparison to the gas phase. This might be due to saturation effects of the fluorescence yield mode where the first feature would be amplified in respect to the other features. Furthermore, weak depositions on the membrane can lead to a change in the spectrum. A hint therefore, could be the feature at  $\sim 285.5$  eV in the liquid spectrum. A further explanation for the differences in the spectra is the difference between single molecules (gas phase) and the hydrogen bond network (liquid). Even so the hydrogen bonds take place at the oxygen and one would expect that the carbon spectrum is not influenced by the hydrogen bond network. But it seems that while building the hydrogen bonds also a change in the carbon environment of the carboxyl carbon takes place and as a result the absorption spectrum reveals a different structure. But to verify the influence of the hydrogen bond network on the carbon atom two steps have to be made. First, with further measurements the saturation effects and the depositions on the membrane have to be ruled out and second, measurements, e.g., different alcohol solutions, are necessary as well as calculations for liquid absorption spectra.



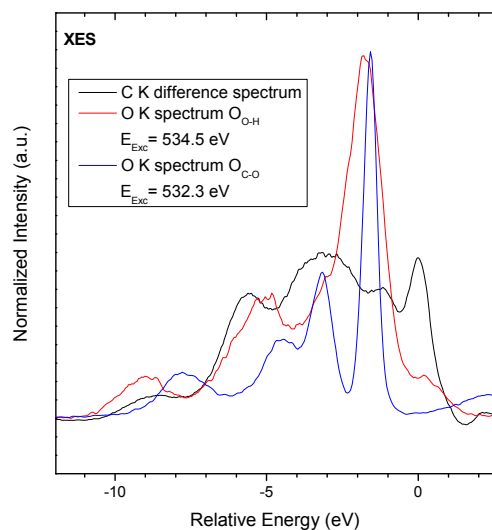


**Figure 6.15:** Comparison between C K XES difference spectrum and resonant O K XES spectra of acetic acid.

Since acetic acid contains two differently bound C atoms it might be possible to observe the two chemically different species in the XES spectra in a similar way as for the oxygen edge. In Figure 6.14 the non-resonant spectrum of acetic acid is shown in comparison to the one of methanol. Some similar features in the spectra can be found. In the simplest approximation, assuming that the CH<sub>3</sub> group in methanol is similar to the one in acetic acid and rather independent of the carboxylic group, the spectrum of acetic acid can be understood as superposition of the separate spectra of the two C atoms. Based on this assumption, the non-resonant methanol C K XES spectrum was subtracted from the acetic acid non-resonant XES spectrum with a weight factor of 0.54 as can be seen in Figure 6.14. This difference spectrum represents the independent COOH group. The subtraction has to be done because there is no chemical which consists of only one carboxyle group and without a C-C bonding. For the difference spectrum shown in Figure 6.15 the molecular orbitals of the carbon of the carboxyle group should have the same or similar molecular orbitals than for the oxygen. In Figure 6.15 the difference spectrum was compared with both resonant oxygen spectra of Figure 6.12. The orbitals are in good agreement for oxygen and carbon.

In further measurements it is planned to measure a RIXS map of gas phase acetic acid to shed more light on the role of the hydrogen bonding environment. Furthermore DFT calculation will also help to get a better understanding of the C K edge of liquid acetic acid.

---

## 6.3 Summary

In this chapter XES, XAS, and RIXS studies of the smallest alcohol (methanol) and smallest acid (acetic acid) at the oxygen and the carbon edge were presented.

The methanol XES spectra for the carbon K edge as well as for the oxygen K edge are in very good agreement with DFT calculations of gas phase methanol. This suggests that previous explanations of the data [Guo03,Kas05], which explained the spectra by a superposition of two different hydrogen bond configurations are unlikely. The presented high-resolution spectra reveal for the first time a clearer structure at the C K edge.

The acetic acid is a good example that x-ray spectroscopies are ideal tools to distinguish between different chemical species of the same element. For the O K edge the C=O component and the hydroxide component can be separated in the XAS spectrum and thus also in the XES spectra. The regions in the resonant excitation areas belong to the C=O or the hydroxide component and in the non-resonant region the spectra are a superposition of both components. Furthermore, for the aqueous acetic acid solution a clear influence of water environment was observed. In this thesis first XAS and XES spectra for the C K edge are presented. The XAS spectra are very different compared to the gas phase spectra. This might be due to hydrogen bond network effects or saturation effects. For non-resonant XES, spectra of acetic acid and methanol were subtracted with a certain weight factor (acetic acid – 0.54\*methanol) to reveal the emission spectra of the carboxyl component.

Both CH<sub>3</sub> containing liquids, methanol and acetic acid, will be the basis of further investigations and especially DFT calculations are needed for a more detailed understanding. Then it might be possible to reveal, e.g., the role of the very sharp feature in the O K edge spectra of acetic acid with a FWHM close to the experimental resolution.

## Summary

---

This thesis was dedicated to the studies of the electronic and chemical properties of liquids and solutions using soft x-ray spectroscopies. The used photon-in-photon-out methods namely x-ray absorption spectroscopy (XAS), x-ray emission spectroscopy (XES), and resonant inelastic x-ray scattering (RIXS) appeared to be an excellent choice for these studies.

In the framework of this thesis, the necessary experimental setup for using the above mentioned experimental techniques on liquids was developed. Hereby, a new flow-through liquid cell was introduced which simplifies the studies of liquids and solutions. The cell design is very flexible and thus can be modified for gases and liquid/solid interfaces. With this cell it is possible to study the samples under well-controlled conditions (temperature and flow rate). The novel flow-through liquid cell is part of the new SALSA synchrotron endstation including an electron analyzer and a novel high-resolution, high-transmission soft x-ray spectrometer. The latter makes it possible to measure two-dimensional RIXS maps in a very short time, which include the full excitation and emission information in one plot.

Making use of the new instrumentation, a variety of different liquids and solutions were investigated. As first system, aqueous solutions of sodium hydroxide (NaOH) and sodium deuterioxide (NaOD) were investigated. In the XAS as well as in the XES spectra a pronounced concentration dependence was found. At non-resonant energies, the spectra are dominated by the solvent and thus look similar to water. Making use of the pre-pre-edge in the absorption spectra which can exclusively be attributed to  $\text{OH}^- / \text{OD}^-$  it was possible to extract the resonant emission spectra of the ions which show an indication for proton dynamics during the core-hole lifetime. For the solid state NaOH XES spectra it was possible to reveal a high energetic shoulder and a low energetic shoulder at the high energy emission feature. These shoulders can be assigned to self-dissociation processes where  $\text{OH}^-$  forms  $\text{O}^{2-}$  ions and  $\text{H}_2\text{O}$ . The study of NaOH was also of interest for the studies of the amino acids, which were in the focus of the next part, since the pH-values of the respective solutions were controlled by NaOH.

In the next part of this thesis, amino acid solutions were investigated. Amino acids are the building blocks of peptides and proteins and thus important for life science. The investigated representatives were glycine, the simplest amino acid, and lysine, an amino acid with two amine groups. Both amino acids react on pH-value

---

changes at the amine group where the local environment at the nitrogen atom changes ( $\text{NH}_2 \leftrightarrow \text{NH}_3^+$ ). A strong change of the spectra induced by this protonation/deprotonation could be found. Furthermore, for low pH-values (protonated amine groups) the amine groups are influenced by strong proton dynamics. First DFT calculations confirm the dissociation model of the amino acids. Qualitatively the high energy peak in the N K XES spectra can be attributed to the deprotonated amine group and the low energy area for the protonated amine group.

Besides amino acids, alcohols and acids are important in biological processes. Therefore, the smallest alcohol (methanol) and the smallest carboxylic acid (acetic acid) were under investigation. For the liquid methanol XES spectra a very good agreement with DFT calculations of gas phase methanol could be found. This observation suggests that the influence of the environment (hydrogen bonding) on the spectra is small. The achieved spectra are in good agreement with DFT calculations found in literature. It was possible to selectively excite the two non-equivalent oxygen atoms in acetic acid and to reveal the carboxyl specific C K XES. The carbon XAS spectra showed strong differences compared to gas phase measurements which might be a hint for the influence of the hydrogen bond network.

The investigation of the electronic and chemical properties of liquids and solutions is a very young field of research and the results presented in this thesis show that it is a very interesting topic. The presented results can be seen as the fundamental frame work for all following studies. With the understanding of basic, i.e., simple, systems as shown in this work it will be possible to understand complex biological systems in their native environment, e.g., peptides and proteins, which are the building blocks of life.

# Zusammenfassung

---

Die hier vorgelegte Doktorarbeit wurde der Untersuchung der elektronischen und chemischen Eigenschaften von Flüssigkeiten und Lösungen mittels weicher Röntgenstrahlen gewidmet. Die verwendeten Photonen-rein-Photonen-raus Methoden, namentlich Röntgenabsorptionsspektroskopie (XAS), Röntgenemissionsspektroskopie (XES) und resonante inelastische Röntgenstreuung (RIXS) stellten sich als exzellente Methoden heraus, diese Systeme zu untersuchen.

Im Rahmen dieser Arbeit wurde eine experimentelle Anlage gebaut, welche notwendig ist um die genannten Messmethoden zur Untersuchung von Flüssigkeiten zu nutzen. Zentraler Teil dieser Anlage ist eine neuartige Durchflussnasszelle, die die Handhabung der Messungen im Vergleich zu älteren Nasszellen vereinfacht. Dabei ist sie variabel genug, um sie zur Messung von Gasen oder Flüssig-Fest-Grenzflächen anzupassen. Mit der Zelle ist es möglich, die zu untersuchenden Flüssigkeiten unter gut kontrollierten Bedingungen (Temperatur und Durchfluss) zu untersuchen. Die Durchflussnasszelle ist Teil einer neuen Synchrotronendstation (SALSA). Für die Messungen stehen dabei ein Elektronenanalysator und ein neuartiges hochauflösendes, hocheffizientes Weichröntgenspektrometer zur Verfügung. Mit diesem Spektrometer ist es möglich, zweidimensionale RIXS Karten in sehr kurzer Zeit (wenige Minuten) aufzunehmen, welche die vollständige Information von Röntgenabsorption und Röntgenemission beinhalten.

Mit Hilfe der neu entwickelten Instrumentierung war es möglich, eine Reihe unterschiedlicher Flüssigkeiten und Lösungen zu untersuchen. Als erstes System wurden wässrige NaOH bzw. NaOD Lösungen erforscht. Die nicht-resonanten Emissionsspektren sind stark von dem genutzten Lösungsmittel dominiert und haben daher Ähnlichkeit mit den Spektren von Wasser und schwerem Wasser. Es war möglich, eine Abhängigkeit der Spektren von der Ionenkonzentration festzustellen. Trotz der Ähnlichkeit der Spektren zu Wasserspektren war es aufgrund eines  $\text{OH}^- / \text{OD}^-$  spezifischen Charakteristikums an der Absorptionskante möglich, resonante Spektren von  $\text{OH}^- / \text{OD}^-$  ohne Beitrag des Spektrums von Wasser zu erhalten. Diese Spektren zeigten Anzeichen für Protonendynamik auf der Zeitskala der Rumpflochlebensdauer ( $\sim 3$  fs). Für die Emissionsspektren von NaOH im festen Zustand konnten an der hochenergetischen Hauptlinie eine niederenergetische und hochenergetische Schulter festgestellt werden. Diese Schultern sind das Ergebnis des Eigendissoziationsprozesses von  $\text{OH}^-$  Ionen, bei welchem  $\text{O}^{2-}$  Ionen und  $\text{H}_2\text{O}$  gebildet werden. Weiterhin waren die Untersuchungen an

---

Natronlauge von Interesse für die folgenden Aminosäurenmessungen, da Natronlauge genutzt wurde, um die gewünschten pH-Wert Änderungen zu erreichen.

Die zweite Gruppe von Flüssigkeiten, die in dieser Arbeit untersucht wurde, sind Aminosäuren. Aminosäuren sind die Bausteine für Peptide und Proteine und damit sehr wichtig für alle Biowissenschaften. Als Vertreter der Aminosäuren wurden Glycin – die kleinste Aminosäure, und Lysin – eine Aminosäure mit zwei Amingruppen – untersucht. Beide Aminosäuren reagieren sensibel auf Änderungen des pH-Wertes mit einer Deprotonierung/Protonierung der Amingruppe ( $\text{NH}_2 \leftrightarrow \text{NH}_3^+$ ). In den experimentellen Spektren konnte ein deutlicher Einfluss dieser Prozesse gefunden werden. Die gemessenen Spektren der protonierten Aminosäuren zeigen deutliche Anzeichen für Dissoziationsprozesse. Erste DFT Rechnungen bestätigten diese Anzeichen und unterstützen das Dissoziationsmodell der Aminosäuren. Qualitativ lässt sich sagen, dass sich die hochenergetische Linie in den N K XES Spektren auf die unprotonierten Amingruppen bezieht und der niederenergetische Bereich im Spektrum den protonierten Gruppen zugeordnet werden kann.

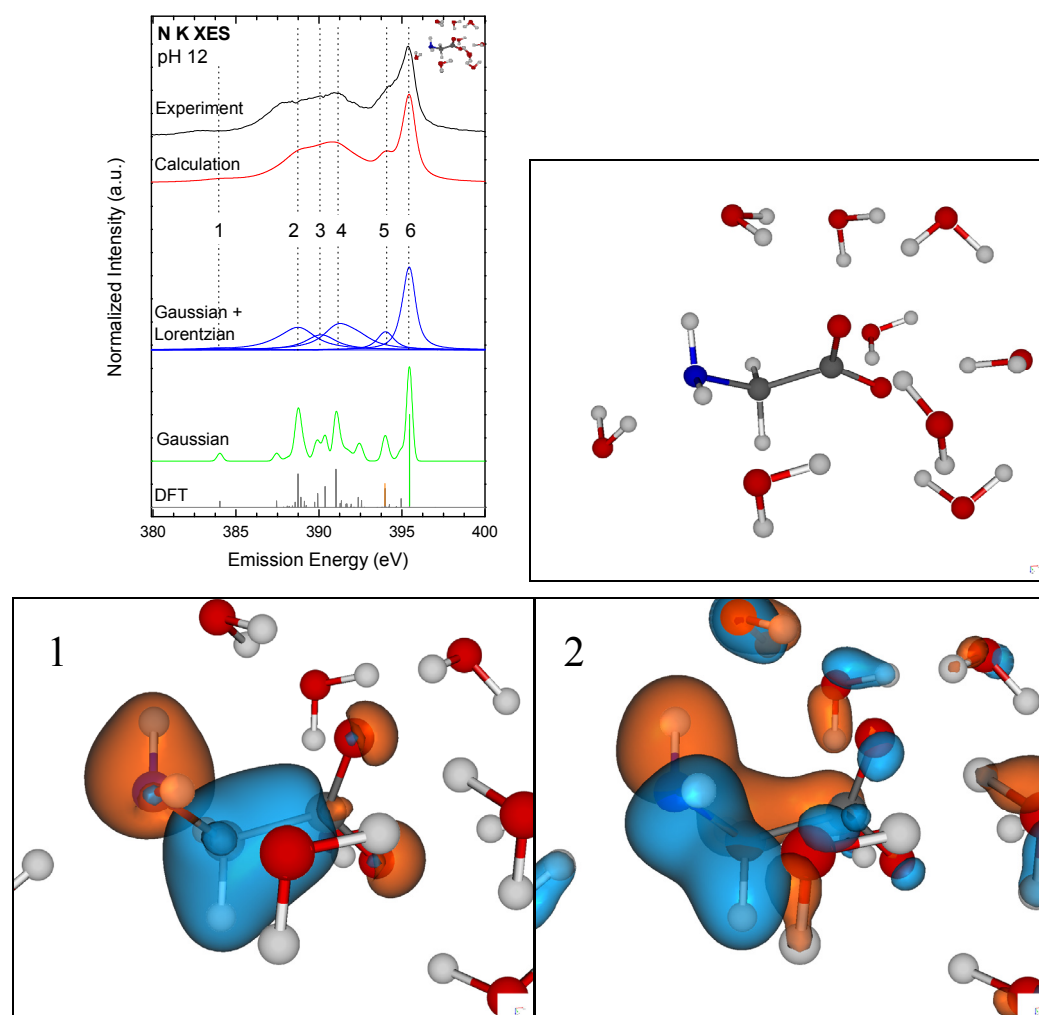
Neben Aminosäuren sind auch Alkohole und organische Säuren von Bedeutung für biologische Prozesse. Daher wurden als Vertreter aus diesen Gruppen der einfachste Alkohol (Methanol) und die einfachste Säure (Essigsäure) untersucht. Die O K und C K XES Spektren von flüssigem Methanol stimmen hervorragend mit Gasphasen DFT Rechnungen überein. Dies lässt den Schluss zu, dass der Einfluss der Umgebung (Wasserstoffbrückenbindungen) auf die Spektren gering ist. Durch resonante Anregung in geeignete unbesetzte Orbitale war es möglich, die zwei unterschiedlichen Sauerstoffatome der Essigsäure zu unterscheiden und auch einen Anhaltspunkt für die Carboxylgruppen-spezifischen C K XES Spektren zu bekommen. An der Kohlenstoffkante zeigten die XAS Spektren große Unterschiede zu Gasphasenmessungen, was ein Hinweis auf den Einfluss der Wasserstoffbrückenbindungen ist.

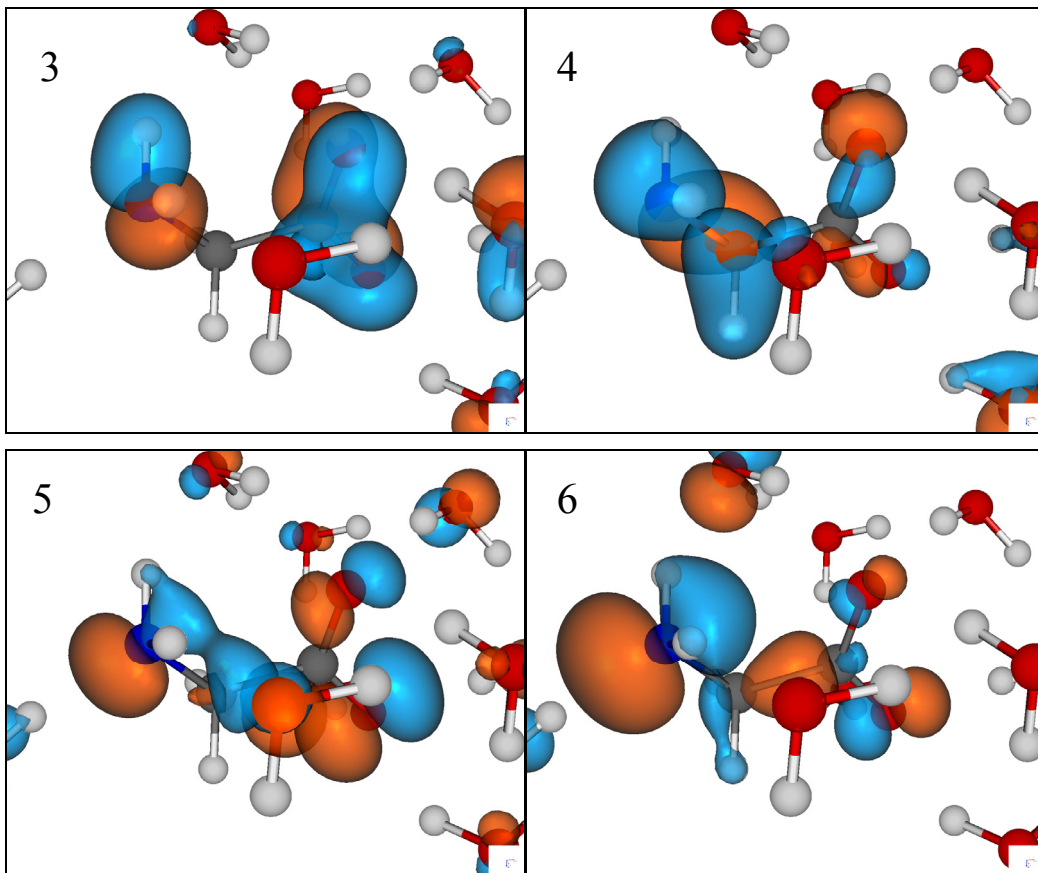
Die Untersuchung der elektronischen und chemischen Eigenschaften von Flüssigkeiten und Lösungen ist immer noch ein sehr junges Forschungsgebiet. Die Ergebnisse dieser Doktorarbeit zeigen, welches interessantes Forschungsgebiet dies ist. Die vorgestellten Ergebnisse können als die grundlegende Basis für alle weiteren Untersuchungen in diesem Forschungsfeld angesehen werden. Mit dem Verständnis einfacher Systeme wird es möglich sein in Zukunft auch komplexe organische Verbindungen in ihrer natürlichen Umgebung zu untersuchen. Ein Beispiel hierfür wären die Peptide und Proteine, welche die Bausteine jedes Lebens bilden.

# Appendix

**A.** Molecular orbitals of a deprotonated glycine solution (pH12) shown in Figure 5.8 related to N K XES.

First the molecule in aqueous solution without orbitals is presented and the following molecular orbitals are shown from low (number 1) to higher (number 6) emission energies corresponding to the energies in Figure 5.8.

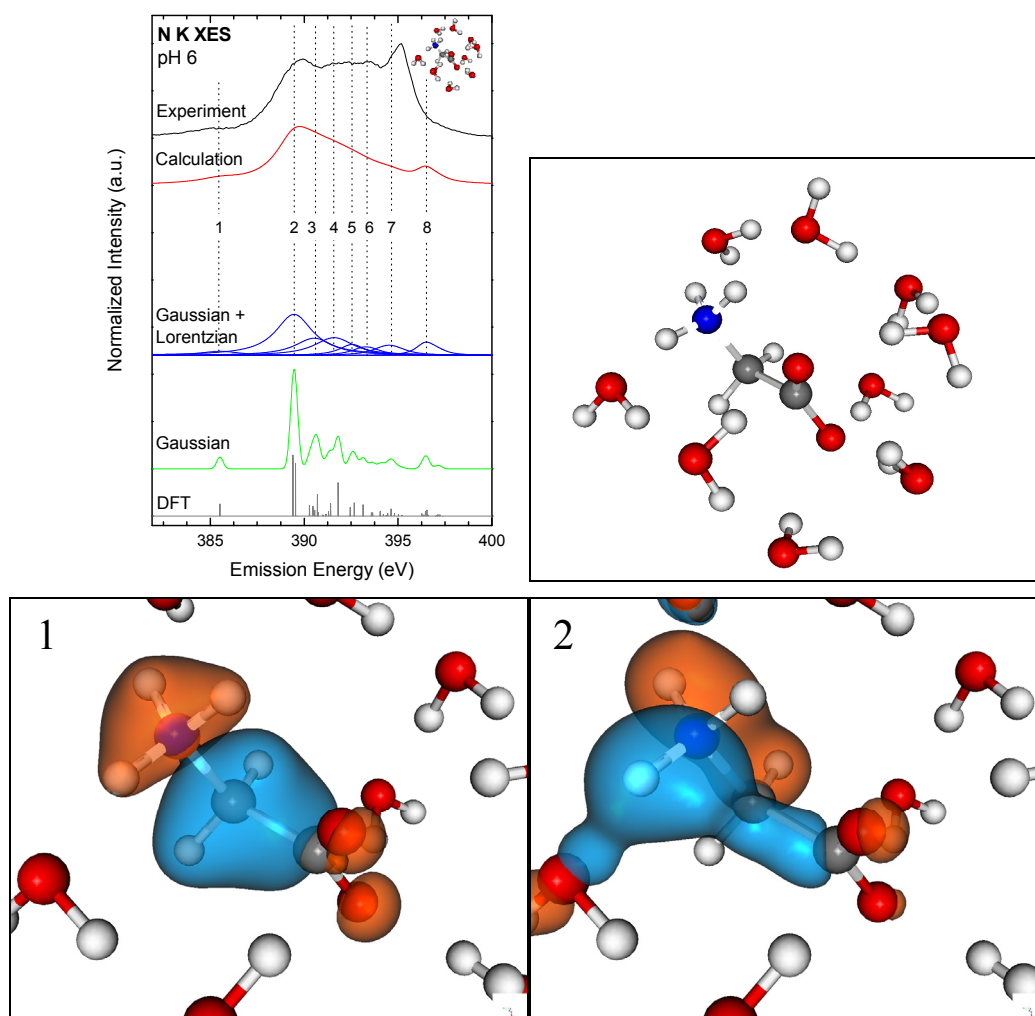


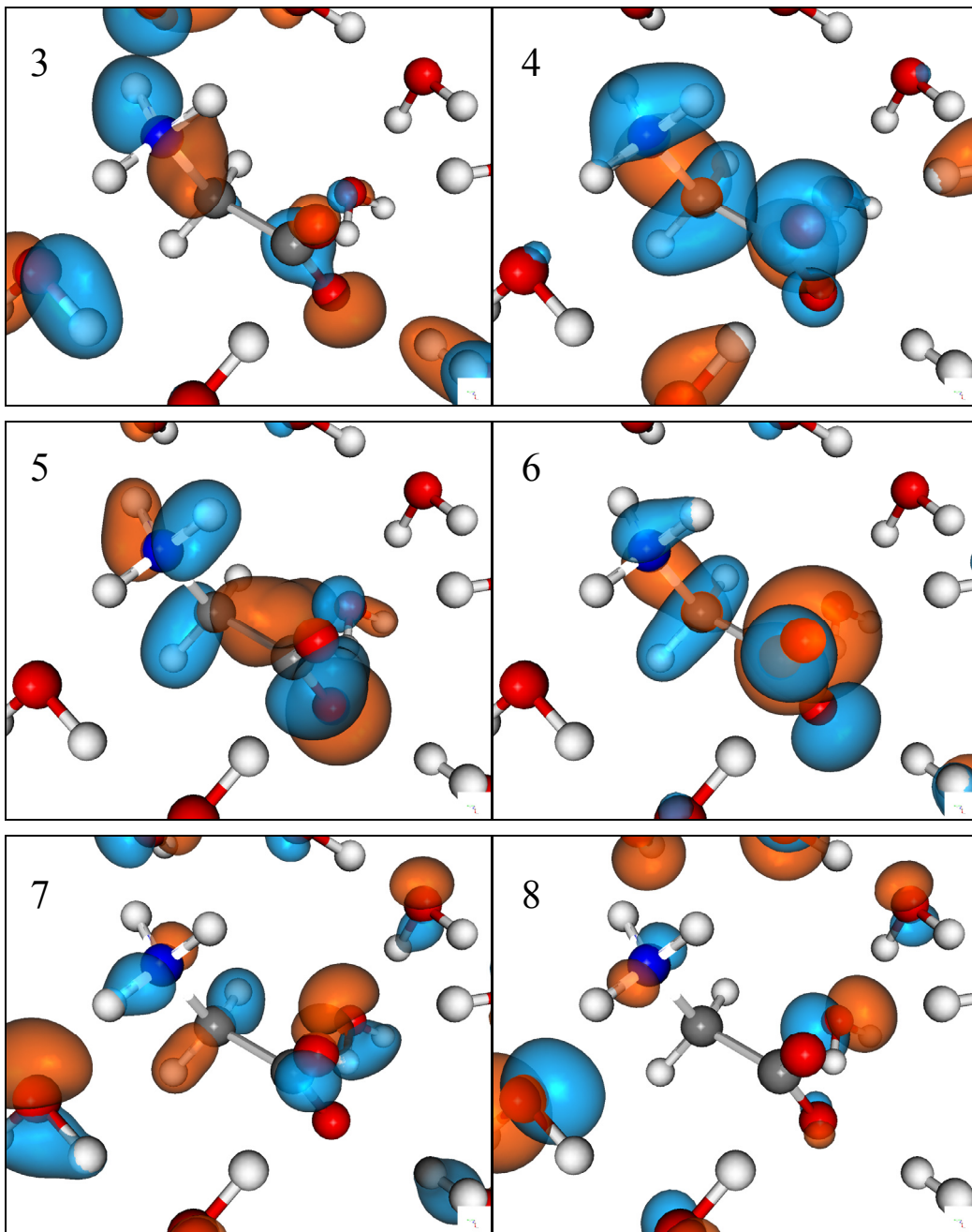




**B.** Molecular orbitals of a protonated glycine solution (pH6) shown in Figure 5.9 related to N K XES.

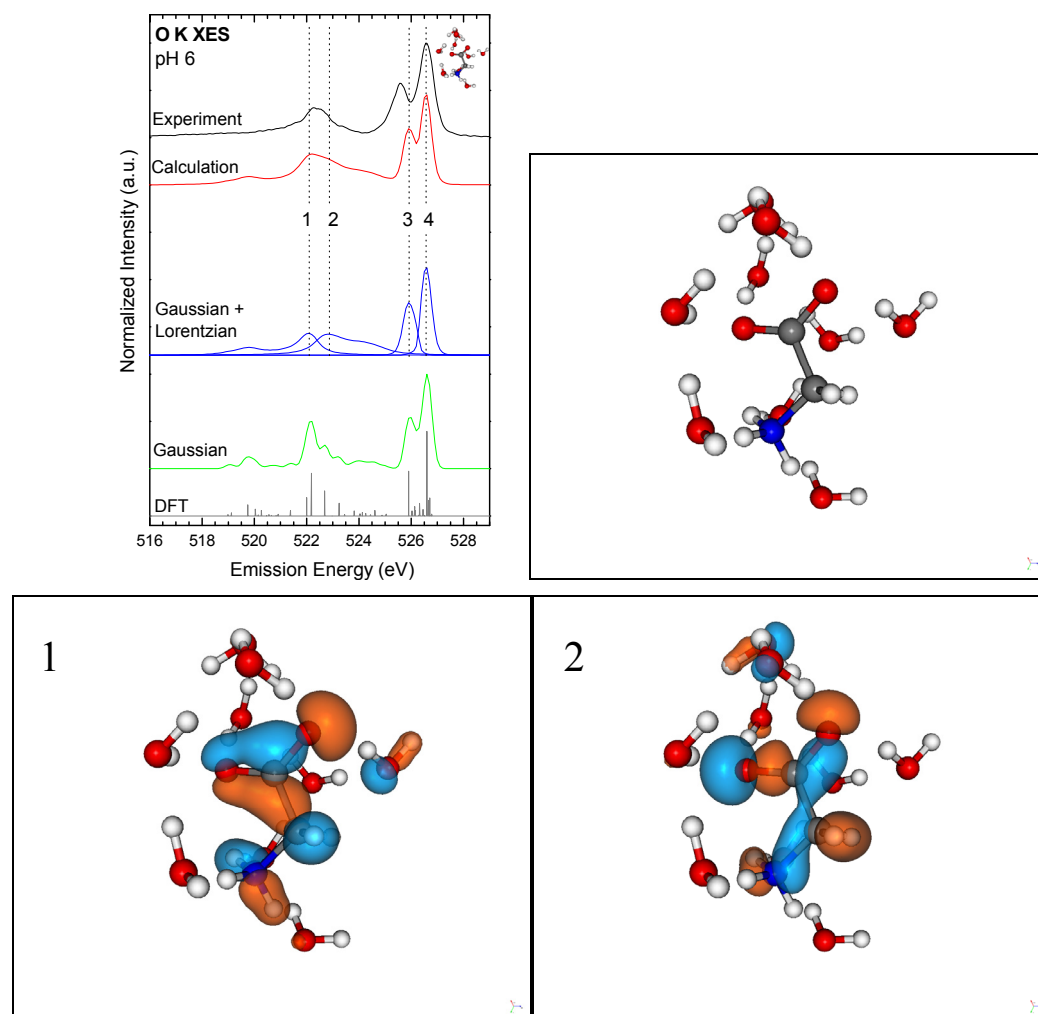
First the molecule in aqueous solution without orbitals is presented and the following molecular orbitals are shown from low (number 1) to higher (number 8) emission energies corresponding to the energies in Figure 5.9.

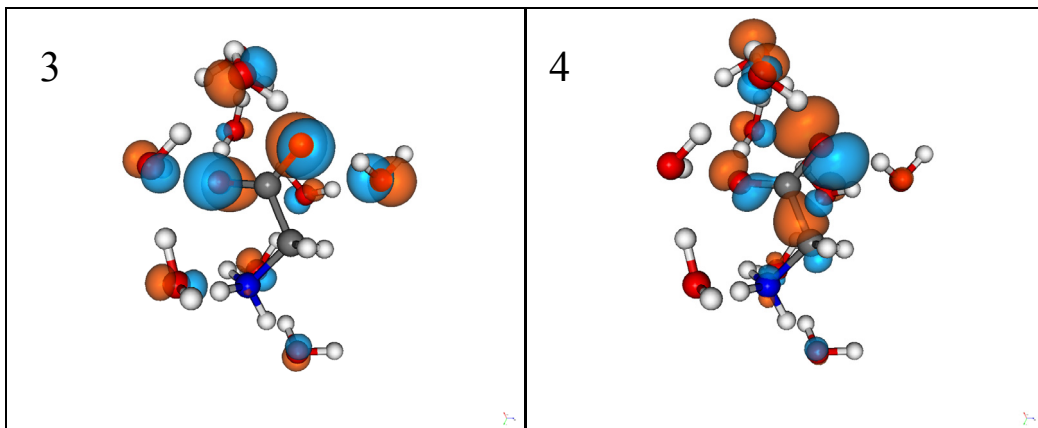




C. Molecular orbitals of a protonated glycine solution (pH6) shown in Figure 5.18 related to O K XES.

First the molecule in aqueous solution without orbitals is presented and the following molecular orbitals are shown from low (number 1) to higher (number 4) emission energies corresponding to the energies in Figure 5.18.





# Bibliography

---

- [Abd00] H. Abdoul-Carime, P. C. Dugal, and L. Sanche, *Desorption induced by electronic transitions (DIET) of neutral fragments from chemisorbed biological molecular systems*, Surf. Sci. **451**, 102 (2000).
- [Ada76] S. M. Adams, E. E. Budzinski, and H. C. Box, *Primary oxidation and reduction products in x-irradiated aspartic-acid*, J. Chem. Phys. **65**, 998 (1976).
- [ALS] [http://www-als.lbl.gov/als/als\\_users\\_bl/8.0.1-Overview.pdf](http://www-als.lbl.gov/als/als_users_bl/8.0.1-Overview.pdf)
- [Azi08] E. F. Aziz, N. Ottosson, M. Faubel, I. V. Hertel, and B. Winter, *Interaction between liquid water and hydroxide revealed by core-hole de-excitation*, Nature **455**, 89 (2008).
- [Azi08\_2] E. F. Aziz, N. Ottosson, S. Eisebitt, W. Eberhardt, B. Jagoda-Cwiklik, R. Vácha, P. Jungwirth, and B. Winter, *Cation-Specific Interactions with Carboxylate in Amino Acid and Acetate Aqueous Solutions: -ray Absorption and ab initio Calculations*, J. Phys. Chem. B **112**, 12567 (2008).
- [Bär05] M. Bär, S. Lehmann, M. Rusu, A. Grimm, I. Kötschau, I. Lauermann, P. Pistor, S. Sokoll, Th. Schedel-Niedrig, M.C. Lux-Steiner, Ch.-H. Fischer, L. Weinhardt, C. Heske, and Ch. Jung, *Cd<sup>2+</sup>/NH<sub>3</sub> – Treatment Induced Formation of a CdSe Surface Layer on CuGaSe<sub>2</sub> Thin Film Solar Cell Absorbers*, Appl. Phys. Lett. **86**, 222107 (2005).
- [Bär05\_2] M. Bär, L. Weinhardt, C. Heske, H.-J. Muffler, M. Ch. Lux-Steiner, E. Umbach, and Ch.-H. Fischer, *Cd<sup>2+</sup>/NH<sub>3</sub>-treatment of Cu(In,Ga)(S,Se)<sub>2</sub> thin film solar cell absorbers – a model for the performance-enhancing processes in the partial electrolyte*, Prog. Photovolt. **13**, 571-577 (2005).
- [Bär05\_3] M. Bär, U. Bloeck, H.-J. Muffler, M. Ch. Lux-Steiner, Ch.-H. Fischer, M. Giersig, T. P. Niesen, and F. Karg, *Cd<sup>2+</sup>/NH<sub>3</sub>-treatment of Cu(In,Ga)(S,Se)<sub>2</sub>: Impact on the properties of ZnO layers deposited by the ion layer gas reaction method*, J. Appl. Phys. **97**, 014905 (2005).

- 
- [Bär06] M. Bär, L. Weinhardt, C. Heske, H.-J. Muffler, E. Umbach, M. Ch. Lux-Steiner, Th. P. Niesen, F. Karg, and Ch.-H. Fischer, *Chemical insights into the Cd<sup>2+</sup>/NH<sub>3</sub>-treatment – an approach to explain the formation of Cd-compounds on Cu(In,Ga)(S,Se)<sub>2</sub> absorbers*, Solar Energy Materials and Solar Cells **90**, 3151-3157 (2006).
- [Bar82] U. von Barth and G. Grossmann, *Dynamical effects in x-ray-spectra and the final-state rule*, Phys. Rev. B: Condens.Matter Mater. Phys. **25**, 5150 (1982).
- [Bec88] A. D. Becke, *Density-functional exchange-energy approximation with correct asymptotic-behavior*, Phys. Rev. A **38**, 3098 (1988).
- [Bee05] M. M. Beerbom, R. Gargagliano, and R. Schlaf, *Determination of the electronic structure of self-assembled L-cysteine/Au interfaces using photoemission spectroscopy*, Langmuir **21**, 3551 (2005).
- [Ben82] A. Benninghoven, W. Lange, M. Jirikowsky, and D. Holtkamp, *Investigations on the mechanism of secondary ion formation from organic compounds - amino-acids*, Surf. Sci. **123**, L721 (1982).
- [Ben98] P. Bennich, T. Wiell, O. Karis, M. Weinelt, N. Wassdahl, A. Nilsson, M. Nyberg, L. G. M. Pettersson, J. Stöhr, M. Samant, *Nature of the surface chemical bond in N<sub>2</sub> on Ni(100) studied by x-ray-emission spectroscopy and ab initio calculations*, Phys. Rev. B **57**, 9274 (1998).
- [Bez08] F. Benzanilla, *Ion Channels: From Conductance to Structure*, Neuron **60**, 456 (2008).
- [Bjö92] O. Björneholm, A. Nilsson, A. Sandell, B. Hernnas, and N. Martensson, *Determination of time scales for charge-transfer screening in physisorbed molecules*, Phys. Rev. Lett. **68**, 1892 (1992).
- [Bjö97] O. Björneholm, S. Sundin, S. Svensson, R. R. T. Marinho, A. N. deBrito, F. Gel'mukhanov, and H. Agren, *Femtosecond dissociation of core-excited HCL monitored by frequency detuning*, Phys. Rev. Lett. **79**, 3150 (1997).

- [Blu09] M. Blum, L. Weinhardt, O. Fuchs, M. Bär, Y. Zhang, M. Weigand, S. Krause, S. Pookpanratana, T. Hofmann, W. Yang, J. D. Denlinger, E. Umbach, and C. Heske, *SALSA – a soft x-ray spectroscopy endstation with a novel flow-through liquid cell*, Rev. Sci. Instrum., in print (2009).
- [Boe97] J. Boese, A. Osanna, C. Jacobsen, and J. Kirz, *Carbon edge XANES spectroscopy of amino acids and peptides*, J. Electron Spectrosc. Relat. Phenom. **85**, 9 (1997).
- [Box71] H. C. Box and E. E. Budzinsk, *Oxidation and reduction of amino acids by ionizing radiation*, J. Chem. Phys. **55**, 2446 (1971).
- [Box72] H. C. Box, *Radiation damage mechanisms as revealed through electron spin resonance spectroscopy*, Annu. Rev. Nucl. Part. Sci. **22**, 355 (1972).
- [Box74] H. C. Box, E. Budzinsk, and H. G. Freund, *Effects of ionizing-radiation on tyrosine*, J. Chem. Phys. **61**, 2222 (1974).
- [Boz94] M. J. Bozack, Y. Zhou, and S. D. Worley, *Structural modifications in the amino-acid lysine induced by soft-x-ray irradiation*, J. Chem. Phys. **100**, 8392 (1994).
- [Bri91] A. N. deBrito, M. P. Keane, N. Correia, S. Svensson, U. Gelius, and B. J. Lindberg, *Experimental and theoretical XPS study of model molecules for poly(methyl methacrylate)*, Surf. Interface Anal. **17**, 94 (1991).
- [Bri91\_2] A. N. deBrito, N. Correia, S. Svensson, and H. Agren, *A theoretical-study of x-ray photoelectron-spectra of model molecules for polymethylmethacrylate*, J. Chem. Phys. **95**, 2965 (1991).
- [Bri99] A. N. deBrito, R. Feifel, A. Mocellin, A. B. Machado, S. Sundin, I. Hjelte, S. L. Sorensen, and O. Björneholm, *Femtosecond dissociation dynamics of core-excited molecular water*, Chem. Phys. Lett. **309**, 377 (1999).
- [Bry03] J. D. Bryngelson and E. M. Billings, *From interatomic interactions to protein structure*, Lecture Notes in Physics **480**, 320 (2003).
- [Bur00] W. P. Burmeister, *Structural changes in a cryo-cooled protein crystal owing to radiation damage*, Acta Crystallographica Section D-Biological Crystallography **56**, 328 (2000).

- 
- [Cac97] M. G. Cacace, E. M. Landau, and J. J. Ramsden, *The Hofmeister series: salt and solvent effects on interfacial phenomena*, Q. Rev. Biophys. **30**, 241 (1997).
- [Cal98] T. A. Callcott, *Soft X-ray Fluorescence Spectroscopy*, In: experimental methods in the physical science **32**, Academic Press (1998).
- [Can79] P. H. Cannington and N. S. Ham, *Photoelectron-Spectra Of Amino-Acids -Survey*, J. Electron Spectrosc. Relat. Phenom. **15**, 79 (1979).
- [Can83] P. H. Cannington and N. S. Ham, *He(I) And He(II) photoelectron-spectra of glycine and related molecules*, J. Electron Spectrosc. Relat. Phenom. **32**, 139 (1983).
- [Cap07] C. D. Cappa, J. D. Smith, B. M. Messer, R. C. Cohen, and R. J. Saykally, *Nature of the Aqueous Hydroxide Ion Probed by X-ray Absorption Spectroscopy*, J. Phys. Chem. A **111**, 4776 (2007).
- [Cav05] M. Cavalleri, M. Odellius, D. Nordlund, A. Nilsson, and L. G. M. Pettersson, *Half or full core hole in density functional theory X-ray absorption spectrum calculations of water?*, Phys. Chem. Chem. Phys. **7**, 2854 (2005).
- [Che02] V. Cherezov, K. M. Riedl, and M. Caffrey, *Too hot to handle? Synchrotron X-ray damage of lipid membranes and mesophases*, J. Synchrotron Radiat. **9**, 333 (2002).
- [Che96] A. C. Cheng and M. Caffrey, *Free radical mediated x-ray damage of model membranes*, Biophys. J. **70**, 2212 (1996).
- [Cof02] T. Coffey, S. G. Urquhart, and H. Ade, *Characterization of the effects of soft X-ray irradiation on polymers*, J. Electron Spectrosc. Relat. Phenom. **122**, 65 (2002).
- [Col85] K. D. Collins and M. W. Washabaugh, *The Hofmeister effect and the behavior of water at interfaces*, Q. Rev. Biophys. **18**, 323 (1985).
- [Coo04] G. Cooper, M. Gordon, D. Tulumello, C. Turci, K. Kaznatcheev, and A. R. Hitchcock, *Inner shell excitation of glycine, glycyl-glycine, alanine and phenylalanine*, J. Electron Spectrosc. Relat. Phenom. **137-40**, 795 (2004).



- [Cou05] L. H. Coutinho, M. G. P. Homem, R. L. Cavasso, R. R. T. Marinho, A. F. Lago, G. G. B. de Souza, and A. N. de Brito, *Photoabsorption and photoionization studies of the amino acid proline in the VUV region*, Brazilian J. Phys. **35**, 940 (2005).
- [Cre93] T. H. Creighton, *Proteins: Structure and molecular properties*, W. H. Freeman, San Francisco (1993).
- [CXRO] [http://henke.lbl.gov/optical\\_constants/filter2.html](http://henke.lbl.gov/optical_constants/filter2.html)
- [Dir27] P. A. M. Dirac, *The Quantum Theory of Emission and Absorption of Radiation*, Proceedings of the Royal Society of London. Series A **114**, 243 (1927).
- [Dud04] L.C. Duda, T. Schmitt, A. Augustsson, and J. Nordgren, *Resonant soft X-ray emission of solids and liquids*, J. Alloys Compd. **362**, 116 (2004).
- [Duf08] D. Dufлот, J.-P. Flament, A. Giuliani, J. Heinesch, and M.-J. Hubin-Franskin, *Electronic excitation of gaseous acetic acid studied by K-shell electron energy loss spectroscopy and ab initio calculations*, Int. J. Mass Spectro. **277**, 70 (2008).
- [Ebe83] W. Eberhardt, T. K. Sham, R. Carr, S. Krummacher, M. Strongin, S. L. Weng, and D. Wesner, *Site-specific fragmentation of small molecules following soft-x-ray excitation*, Phys. Rev. Lett. **50**, 1038 (1983).
- [Eis00] S. Eisebitt and W. Eberhardt, *Band structure information and resonant inelastic soft X-ray scattering in broad band solids*, J. Electron Spectrosc. Relat. Phenom. **110**, 335 (2000).
- [Enn06] A. Ennaoui, M. Bär, J. Klaer, T. Kropp, R. Sáez-Araoz, and M. Ch. Lux-Steiner, *Highly-efficient CD-free CuInS<sub>2</sub> Thin-film Solar Cells and Mini-modules with Zn(S,O) Buffer Layers Prepared by an Alternative Chemical Bath Process*, Prog. Photovolt.: Res. and Appl. **14**, 499 (2006).
- [Fen75] J. H. Fendler, F. Nome, and J. Nagyvary, *Compartmentalization of Amino Acids in Surfactant Aggregates*, J. Mol. Evol. **6**, 215 (1975).
- [Fer50] E. Fermi, *Nuclear Physics*, University of Chicago Press (1950).

- 
- [Feu00] P. Feulner, R. Romberg, S. P. Frigo, R. Weimar, M. Gsell, A. Ogurtsov, and D. Menzel, *Recent progress in the investigation of core hole-induced photon stimulated desorption from adsorbates: excitation site-dependent bond breaking, and charge rearrangement*, Surf. Sci. **451**, 41 (2000).
- [Fir03] M. Friedrich, G. Gavrilu, C. Himcinschi, T. U. Kampen, A. Y. Kobitski, H. Mendez, G. Salvan, I. Cerrillo, J. Mendez, N. Nicoara, A. M. Baro, and D. R. T. Zahn, *Optical properties and molecular orientation in organic thin films*, J. Phys.: Condens. Matter **15**, S2699 (2003).
- [For07] J. Forsberg, L.-C. Duda, A. Olsson, T. Schmitt, J. Andersson, J. Nordgren, J. Hedberg, C. Leygraf, T. Aastrup, D. Wallinder, and J.-H. Guo, *System for in situ studies of atmospheric corrosion of metal films using soft x-ray spectroscopy and quartz crystal microbalance*, Rev. Sci. Instr. **78**, 083110 (2007).
- [For86] S. Forsén, *Nobel Prizes in Chemistry 1986 – Presentation Speech*, From: Nobel Lectures, Chemistry 1981 – 1990, World Scientific Publishing Co., Singapore (1992).
- [Fri02] M. Friedrich, T. Wagner, G. Salvan, S. Park, T. U. Kampen, and D. R. T. Zahn, *Optical constants of 3,4,9,10-perylenetetracarboxylic dianhydride films on silicon and gallium arsenide studied by spectroscopic ellipsometry*, Appl. Phys. A: Mater. Sci. Process. **75**, 501 (2002).
- [Fuc\_PT] O. Fuchs, L. Weinhardt, A. Fischer, M. Weigand, M. Blum, M. Bär, S. Pookpanratana, J. Denlinger, C. Heske, and E. Umbach, *Symmetry resolved resonant x-ray emission study of an ordered PTCDA multilayer on Ag(111)*, in preparation (2009).
- [Fuc08] O. Fuchs, M. Zharnikov, L. Weinhardt, M. Blum, M. Weigand, Y. Zubavichus, M. Bär, F. Maier, J. D. Denlinger, C. Heske, M. Grunze, and E. Umbach, *Isotope and temperature effects in liquid water probed by x-ray absorption and resonant x-ray emission spectroscopy*, Phys. Rev. Lett. **100**, 027801 (2008).
- [Fuc08\_2] O. Fuchs, F. Maier, L. Weinhardt, M. Weigand, M. Blum, M. Zharnikov, J. D. Denlinger, M. Grunze, C. Heske, and E. Umbach, *A liquid flow cell to study the electronic structure of liquids with soft x-rays*, Nucl. Instrum. Methods Phys. Res., Sect. A **585**, 172 (2008).

- [Fuc08\_co] O. Fuchs, M. Zharnikov, L. Weinhardt, M. Blum, M. Weigand, Y. Zubavichus, M. Bär, F. Maier, J. D. Denlinger, C. Heske, M. Grunze, and E. Umbach, *Comment on "Isotope and temperature effects in liquid water probed by x-ray absorption and resonant x-ray emission spectroscopy" - Fuchs et al. reply*, Phys. Rev. Lett. **100**, 249802 (2008).
- [Fuc09] O. Fuchs, M. Blum, M. Weigand, E. Umbach, L. Weinhardt, M. Bär, C. Heske, J. D. Denlinger, Y.-D. Chuang, W. McKinney, Z. Hussain, E. Gullikson, M. Jones, P. Batson, and R. Follath, *High-resolution, high-transmission soft x-ray spectrometer for the study of biological samples*, Rev. Sci. Instrum. **80**, 063103 (2009).
- [Fuc09\_Dr] O. Fuchs, *Soft x-ray spectroscopy of organic molecules and liquids*, Doktorarbeit, Würzburg (2009).
- [God92] N. Godbout, D.R. Salahub, J. Andzelm, and E. Wimmer, *Optimization of Gaussian-type basis-sets for local spin-density functional calculations .I. boron through neon, optimization techniques and validation*, Can. J. Chem. **70**, 560 (1992).
- [Gor03] M. L. Gordon, G. Cooper, C. Morin, T. Araki, C. C. Turci, K. Kaznatcheev, and A. P. Hitchcock, *Inner-shell excitation spectroscopy of the peptide bond: Comparison of the C 1s, N 1s, and O 1s spectra of glycine, glycyl-glycine, and glycyl-glycyl-glycine*, J. Phys. Chem. A **107**, 6144 (2003).
- [Guo02] J.-H. Guo, Y. Luo, A. Augustsson, J.-E. Rubensson, C. Sâthe, H. Ågren, H. Siegbahn, and J. Nordgren, *X-ray emission spectroscopy of hydrogen bonding and electronic structure of liquid water*, Phys. Rev. Lett. **89**, 137402 (2002).
- [Guo03] J.-H. Guo, Y. Luo, A. Augustsson, S. Kashtanov, J.-E. Rubensson, D. K. Shuh, H. Ågren, and J. Nordgren, *Molecular Structure of Alcohol-Water Mixtures*, Phys. Rev. Lett. **91**, 157401 (2003).
- [Gus07] J. B. Gustafsson, H. M. Zhang, E. Moons, and L. S. O. Johansson, *Electron spectroscopy studies of PTCDA on Ag/Si(111)-root 3x root 3*, Phys. Rev. B: Condens. Matter Mater. Phys. **75**, 155413 (2007).
- [Han03] J.-W. Handgraaf, T. S. van Erp, and E. J. Meijer, *Ab initio molecular dynamics study of liquid methanol*, Chem. Phys. Lett. **367**, 617 (2003).

- 
- [Har05] R. T. Hart, C. J. Benmore, J. Neufeind, S. Kohara, B. Tomberli, and P. A. Egelsta, *Temperature dependence of isotopic quantum effects in water*, Phys. Rev. Lett. **94**, 047801 (2005).
- [Has00] J. Hasselström, O. Karis, M. Nyberg, L. G. M. Pettersson, M. Weinelt, N. Wassdahl, and A. Nilsson, *The bonding and electronic structure changes upon adsorption of important functional groups: Glycine on copper*, J. Phys. Chem. B **104**, 11480 (2000).
- [Has98] J. Hasselström, O. Karis, M. Weinelt, N. Wassdahl, A. Nilsson, M. Nyberg, L. G. M. Pettersson, M. G. Samant, and J. Stöhr, *The adsorption structure of glycine adsorbed on Cu(110); comparison with formate and acetate/Cu(110)*, Surf. Sci. **407**, 221 (1998).
- [Hau87] M. Haughney, M. Ferrario, and I. R. McDonald, J. Phys. Chem. **91**, 4934 (1987).
- [Hei01] K. Heister, M. Zharnikov, M. Grunze, L. S. O. Johansson, and A. Ulman, *Characterization of X-ray induced damage in alkanethiolate monolayers by high-resolution photoelectron spectroscopy*, Langmuir **17**, 8 (2001).
- [Her02] K. Hermann, L. G. M. Pettersson, M. E. Casida, C. Daul, A. Goursot, A. Koester, E. Proynov, A. St-Amant, D. R. Salahub, V. Carravetta, A. Duarte, N. Godbout, J. Guan, C. Jamorski, M. Leboeuf, V. Malkin, O. Malkina, M. Nyberg, L. Pedocchi, F. Sim, L. Triguero, and A. Vela, *STOBE Software* (2002).
- [Hes03] C. Heske, U. Groh, O. Fuchs, L. Weinhardt, E. Umbach, T. Schedel-Niedrig, C. H. Fischer, M. C. Lux-Steiner, S. Zweigart, T. P. Niesen, F. Karg, J. D. Denlinger, B. Rude, C. Andrus, and F. Powell, *Monitoring chemical reactions at a liquid-solid interface: Water on CuIn(S,Se)(2) thin film solar cell absorbers*, J. Chem. Phys. **119**, 10467 (2003).
- [Hil92] B. Hille, *Ionic Channels of Excitable Membranes*, Sinauer, Sunderland, Massachusetts (1992).
- [Hu06] Y. J. Hu, B. Fu, and E. R. Bernstein, *Infrared plus vacuum ultraviolet spectroscopy of neutral and ionic methanol monomers and clusters: New experimental results*, J. Chem. Phys. **125**, 154306 (2006).

- [Hui91] F. Huisken, A. Kulcke, C. Laush, and J. M. Lisy, *Dissociation of small methanol clusters after excitation of the O-H stretch vibration at 2.7 MU*, J. Chem Phys. **95**, 3924 (1991).
- [Isa73] M. Isaacson, D. Johnson, and A. V. Crewe, *Electron-beam excitation and damage of biological molecules - its implications for specimen damage in electron microscopy*, Radiat. Res. **55**, 205 (1973).
- [Jor81] W. L. Jorgensen, *Quantum and statistical mechanical studies of liquids .11. transferable intermolecular potential functions – application to liquid methanol including internal rotation*, J. Am. Chem. Soc. **103**, 134 (1981).
- [Kas05] S. Kashtanov, A. Augustsson, J.-E. Rubensson, J. Nordgren, H. Ågren, J.-H. Guo, and Y. Luo, *Chemical and electronic structures of liquid methanol from x-ray emission spectroscopy and density functional theory*, Phys. Rev. B **71**, 104205 (2005).
- [Kaz02] K. Kaznatcheyev, A. Osanna, C. Jacobsen, O. Plashkevych, O. Vahtras, and H. Ågren, *Innershell absorption spectroscopy of amino acids*, J. Phys. Chem. A **106**, 3153 (2002).
- [Kem01] E. S. Kempner, *Effects of high-energy electrons and gamma rays directly on protein molecules*, J. Pharm. Sci. **90**, 1637 (2001).
- [Kla76] L. Klasinc, *Application of photoelectron-spectroscopy to biologically-active molecules and their constituent parts .3. amino-acids*, J. Electron Spectrosc. Relat. Phenom. **8**, 161 (1976).
- [Kra25] H. Kramers and W. Heisenberg, *Über die Streuung von Strahlung durch Atome*, Z. Phys. A **31**, 681 (1925).
- [Kra79] M. O. Krause, *Atomic radiative and radiationless yields for K-shells and L-shells*, J. Phys. Chem. Ref. Data **8** (2), 307 (1979).
- [Kuk97] T. Mayer-Kuckuk, *Atomphysik*, Teubner, Stuttgart (1997).
- [Kut90] W. Kutzelnigg, U. Fleischer, and M. Schindler, *NMR-Basic Principles and Progress*, Springer Verlag, Heidelberg (1990).
- [Lin74] S. D. Lin, *Electron radiation-damage of thin-films of glycine, diglycine, and aromatic amino-acids*, Radiat. Res. **59**, 521 (1974).

- 
- [Löf97] P. Löfgren, A. Krozer, J. Lausmaa, and B. Kasemo, *Glycine on Pt(111): a TDS and XPS study*, Surf. Sci. **370**, 277 (1997).
- [Ma92] Y. J. Ma, N. Wassdahl, P. Skytt, J. Guo, J. Nordgren, P. D. Johnson, J. E. Rubensson, T. Boske, W. Eberhardt, and S. D. Kevan, *Soft x-ray resonant inelastic-scattering at the C K edge of diamond*, Phys. Rev. Lett. **69**, 2598 (1992).
- [Ma94] Y. J. Ma, *X-ray absorption, emission, and resonant inelastic scattering in solids*, Phys. Rev. B: Condens. Matter Mater. Phys. **49**, 5799 (1994).
- [Ma95] Y. J. Ma, K. E. Miyano, P. L. Cowan, Y. Aglitzkiy, and B. A. Karlin, *Anisotropy of Si kappa-beta Emission – Interference of Fluorescence X-ray*, Phys. Rev. Lett **74**, 478 (1995).
- [Ma96] Y. J. Ma, *X-ray resonant inelastic scattering*, J. Electron Spectrosc. Relat. Phenom. **79**, 131 (1996).
- [Mag82] M. Magini, G. Paschina, and G. Piccaluga, *On the structure of methyl-alcohol at room-temperature*, J. Chem. Phys. **77**, 2051 (1982).
- [McC58] G. McCormick and W. Gordy, *Electron spin resonance studies of radiation damage to peptides*, J. Phys. Chem. **62**, 783 (1958).
- [Meg08] T. Megyes, S. Bálint, T. Grósz, T. Radnai, and I. Bakó, *The structure of aqueous sodium hydroxide solutions: A combined solution x-ray diffraction and simulation study*, J. Chem. Phys **128**, 044501 (2008).
- [Mei89] A. Meisel, G. Leonhardt, and R. Szargan, *X-ray Spectra and Chemical Binding*, Springer Verlag, Berlin (1989).
- [Mes05] B. M. Messer, C. D. Cappa, J. D. Smith, K. R. Wilson, M. K. Gilles, R. C. Cohen, and R. J. Saykally, *pH Dependence of the Electronic Structure of Glycine*, J. Phys. Chem. B **109**, 5375 (2005).
- [Mes05\_2] B. M. Messer, C. D. Cappa, J. D. Smith, W. S. Drisdell, C. P. Schwartz, R. C. Cohen, and R. J. Saykally, *Local Hydration Environments of Amino Acids and Dipeptides Studied by X-ray Spectroscopy of Liquid Microjets*, J. Phys. Chem. B **109**, 21640 (2005).

- [Min98] T. Minami and K. Nasu, *Dissipation of core-hole momentum by phonons in soft x-ray radiation processes from valence band to core level of wide-gap insulators*, Phys. Rev. B: Condens. Matter. Phys. **57**, 12084 (1998).
- [Mon81] D. G. Montague, I. P. Gibson, and J.C. Dore, *Structural studies of liquid alcohols by neutron-diffraction .I. deuterated methyl-alcohol CD<sub>3</sub>OD*, Mol. Phys. **44**, 1355 (1981).
- [Moo86] W. J. Moore and D. O. Hummel, *Physikalische Chemie*, de Gruyter, Berlin (1986).
- [Mor02] A. Morrone and M. E. Tuckerman, *Ab initio molecular dynamics study of proton mobility in liquid methanol*, J. Chem. Phys. **117**, 4403 (2002).
- [Nar84] A. H. Narten and A. Habenschuss, *Hydrogen-bonding in liquid methanol and ethanol determined by x-ray -diffraction*, J. Chem. Phys. **80**, 3387 (1984).
- [Nil95] A. Nilsson and N. Martensson, *Initial and final state rule in X-ray spectroscopies of absorbates*, Physica B **208 & 209**, 19 (1995).
- [Nil97] A. Nilsson, M. Weinelt, T. Wiell, P. Bennich, O. Karis, N. Wassdahl, J. Stöhr, M. Samant, *An atom-specific look at the surface chemical bond*, Phys. Rev. Lett. **87**, 2847 (1997).
- [Nol07] D. Nolting, E. F. Aziz, N. Ottosson, M. Faubel, I. V. Hertel, and B. Winter, *pH-Induced Protonation of Lysine in Aqueous Solution Causes Chemical Shifts in X-ray Photoelectron Spectroscopy*, J. Am. Chem. Soc. **129**, 14068 (2007).
- [Nyb00] M. Nyberg, J. Hasselström, O. Karis, N. Wassdahl, M. Weinelt, A. Nilsson, and L. G. M. Pettersson, *The electronic structure and surface chemistry of glycine adsorbed on Cu(110)*, J. Chem. Phys. **112**, 5420 (2000).
- [Nyb03] M. Nyberg, M. Odellius, A. Nilsson, and L. G. M. Pettersson, *Hydrogen bonding between adsorbed deprotonated glycine molecules on Cu(110)*, J. Chem. Phys. **119**, 12577 (2003).
- [Ode\_Pri] M. Odellius, private communication

- 
- [Ode05] M. Odelius, H. Ogasawara, D. Nordlund, O. Fuchs, L. Weinhardt, F. Maier, E. Umbach, C. Heske, Y. Zubavichus, M. Grunze, J. D. Denlinger, L. G. M. Pettersson, and A. Nilsson, *Ultrafast core-hole-induced dynamics in water probed by x-ray emission spectroscopy*, Phys. Rev. Lett. **94**, 227401 (2005).
- [Ode09] M. Odelius, *Molecular dynamics simulations of the fine structure on oxygen K-edge x-ray emission spectra of liquid water and ice*, Phys. Rev. B **79**, 144204 (2009).
- [Ode09\_2] M. Odelius, *Information Content in O[1s] K-edge X-ray Emission Spectroscopy of Liquid Water*, J. Phys. Chem. A **113**, 8176 (2009).
- [Ote06] E. Otero and S. G. Urquhart, *Nitrogen 1s Near-Edge X-ray Absorption Fine Structure Spectroscopy of Amino Acids: resolving Zwitterionic Effects*, J. Phys. Chem. A **110**, 12121 (2006).
- [Pag03] M. Pagliai, G. Cardini, R. Righini, and V. Schettino, *Hydrogen bond dynamics in liquid methanol*, J. Chem. Phys. **119**, 6655 (2003).
- [Pau67] L. Pauling, *The Nature of Chemical Bond*, 3<sup>rd</sup> edition, Oxford University, Oxford (1967).
- [Pen01] M. A. H. du Penhoat, M. A. Huels, P. Cloutier, J. P. Jay-Gerin, and L. Sanche, *Electron stimulated desorption of H- from thin films of thymine and uracil*, J. Chem. Phys. **114**, 5755 (2001).
- [Per86] J. P. Perdew, *Correction*, Phys. Rev. B **34**, 7406 (1986).
- [Pet08] L. G. M. Pettersson, T. Tokushima, Y. Harada, O. Takahashi, S. Shin, and A. Nilsson, *Comment on "Isotope and temperature effects in liquid water probed by x-ray absorption and resonant x-ray emission spectroscopy"*, Phys. Rev. Lett. **100**, 249801 (2008).
- [Ple07] O. Plekan, V. Feyer, R. Richter, M. Coreno, M. de Simone, K. C. Prince, and V. Carravetta, *Investigation of the amino acids glycine, proline, and methionine by photoemission spectroscopy*, J. Phys. Chem. A **111**, 10998 (2007).
- [Ple07\_2] O. Plekan, V. Feyer, R. Richter, M. Coreno, M. de Simone, K. C. Prince, and V. Carravetta, *Photoemission and the shape of amino acids*, Chem. Phys. Lett. **442**, 429 (2007).



- [Pow03] I. Powis, E. E. Rennie, U. Hergenhahn, O. Kugeler, and R. Bussy-Socrate, *Investigation of the gas-phase amino acid alanine by synchrotron radiation photoelectron spectroscopy*, J. Phys. Chem. A **107**, 25 (2003).
- [Rem06] M. Remko and B. M. Rode, *Effect of Metal Ions ( $\text{Li}^+$ ,  $\text{Na}^+$ ,  $\text{Mg}^{2+}$ ,  $\text{Ca}^{2+}$ ,  $\text{Ni}^{2+}$ ,  $\text{Cu}^{2+}$ , and  $\text{Zn}^{2+}$ ) and Water Coordination on the Structure of Glycine and Zwitterionic Glycine*, J. Phys. Chem. A **110**, 1960 (2006).
- [Rob88] M. B. Robin, I. Ishii, R. McLaren, and A. P. Hitchcock, *Fluorination effects on the inner-shell spectra of unsaturated molecules*, J. Electron Spectrosc. Relat. Phenom. **47**, 53 (1988).
- [Rub00] J. E. Rubensson, *RIXS dynamics for beginners*, J. Electron Spectrosc. Relat. Phenom. **110**, 135 (2000).
- [San02] L. Sanche, *Nanosopic aspects of radiobiological damage: Fragmentation induced by secondary low-energy electrons*, Mass Spectrom. Rev. **21**, 349 (2002).
- [San93] A. Sandell, O. Björneholm, A. Nilsson, E. Zdansky, H. Tillborg, J. N. Andersen, N. Mårtensson, *Autoionization as a tool for interpretation of X-ray absorption spectra –  $\text{N}_2/\text{Ni}(100)$* , Phys. Rev. Lett. **70**, 2000 (1993).
- [San97] L. Sanche, *Secondary electrons in radiation chemistry and biology*, Journal de Chimie Physique **94**, 216 (1997).
- [Sar93] S. Sarkar and R. N. Joarder, *Molecular clusters and correlations in liquid methanol at room temperature*, J. Chem Phys. **99**, 2032 (1993).
- [Sch05] A. Schöll, Y. Zou, D. Huebner, S. G. Urquhart, T. Schmidt, R. Fink, and E. Umbach, *A comparison of fine structures in high-resolution x-ray absorption spectra of various condensed organic molecules*, J. Chem. Phys. **123**, 044509 (2005).
- [Sch05] U. Schotte, K. D. Schotte, H.-J. Bleif, M. Kabs, and H. Dachs, *The plastically crystalline phase of NaOH. NaOD, KOH and KOD*, J. Phys.: Condens. Matter **7**, 7453 (1995).
- [Sie85] H. Siegbahn, *Electron-spectroscopy for chemical-analysis of liquids and solutions*, J. Phys. Chem. **89**, 897 (1985).

- 
- [Sig73] H. Siegbahn and K. Siegbahn, *ESCA [Electron Spectroscopy for Chemical Analysis] applied to liquids*, J. Electron Spectrosc. Relat. Phenom **2**, 319 (1973).
- [Sil] Silson Ltd. Homepage: <http://www.silson.com>
- [Sla88] A. R. Slaughter and M. S. Banna, *Core-photoelectron binding-energies of gaseous glycine - correlation with its proton affinity and gas-phase acidity*, J. Phys. Chem. **92**, 2165 (1988).
- [Smi04] J. D. Smith, C. D. Cappa, K. R. Wilson, B. M. Messer, R. C. Cohen, and R. J. Saykally, *Energetics of hydrogen bond network rearrangements in liquid water*, Science **306**, 851 (2004).
- [Spa99] M. Spaeth, K. D. Kreuer, J. Maier, and C. Cramer, *Giant Haven Ration for Proton Transport in Sodium Hydroxide*, J. Solid State Chem. **148**, 169 (1999).
- [Sta08] D. E. Starr, E. K. Wong, D. R. Worsnop, K. R. Wilson, and H. Bluhm, *A combined droplet train and ambient pressure photoemission spectrometer for the investigation of liquid/vapor interfaces*, Phys. Chem. Chem. Phys. **10**, 3093 (2008).
- [Ste70] K. S. Stenn and G. F. Bahr, *A study of mass loss and product formation after irradiation of some dry amino acids, peptides, polypeptides and proteins with an electron beam of low current density*, J. Histochem. Cytochem. **18**, 574 (1970).
- [Stö92] J. Stöhr, *NEXAFS spectroscopy*, Springer, Berlin Heidelberg (1992).
- [Stu93] T. Strunskus, C. Hahn, and M. Grunze, *Mechanism of x-ray-induced degradation of pyromellitic dianhydride*, J. Electron Spectrosc. Relat. Phenom. **61**, 193 (1993).
- [Tab95] J. Taborski, P. Vaterlein, H. Dietz, U. Zimmermann, and E. Umbach, *NEXAFS investigations on ordered adsorbate layers of large aromatic molecules*, J. Electron Spectrosc. Relat. Phenom. **75**, 129 (1995).
- [Tam08] V. Tamenori, K. Okada, O. Takahashi, S. Arakawa, K. Tabayashi, A. Hiraya, T. Gejo, and K. Homma, *Hydrogen bonding in methanol clusters probed by inner-shell photoabsorption spectroscopy in the carbon and oxygen K-edge region*, J. Chem. Phys. **128**, 124321 (2008).

- [Tan01] M. Tanaka, K. Nakagawa, T. Koketsu, A. Agui, and A. Yokoya, *Oxygen K-edge X-ray absorption near edge structures (XANES) of sublimated films of amino acids*, J. Synchrotron Radiat. **8**, 1009 (2001).
- [Tan84] Y. Tanaka, N. Phtomo, and K. Arakawa, *The structure of liquid alcohols by neutron-defraction .1. molecular-structure of methyl-alcohol*, Bull. Chem. Soc. Japn **57**, 644 (1984).
- [Tan93] S. Tanuma, C. J. Powell, and D. R. Penn, *Calculations of Electron Inelastic Mean Free Paths (IMFPs)*, Surface and Interface Anal. **20**, 77 (1993).
- [Tau52] K. J. Tauer and W. N. Lipscomb, *On the crystal structures, residual entropy and dielectric anomaly of methanol*, Acta Crystallogr. **5**, 606 (1952).
- [Tia08] C. Tian, N. Ji, G. A. Waychunas, and Y. R. Shen, *Interfacial Structures of Acidic and Basic Aqueous Solutions*, J. Am. Chem. Soc. **130**, 13033 (2008).
- [Tok08] T. Tokushima, Y. Harada, O. Takahashi, Y. Senba, H. Ohashi, L. G. M. Pettersson, A. Nilsson, and S. Shin, *High resolution X-ray emission spectroscopy of liquid water: The observation of two structural motifs*, Chem. Phys. Lett. **460**, 387 (2008).
- [Tok09] T. Tokushima, Y. Horikawa, Y. Harada, O. Takahashi, A. Hiraya, and S. Shin, *Selective observation of two oxygen atoms at different sites in the carboxyl group (-COOH) of liquid acetic acid*, Phys. Chem. Chem. Phys. **11**, 1679 (2009).
- [Tor89] B. H. Torrie and S.-X. Weng, *Structure of the alpha-phase of solid methanol*, Mol. Phys. **67**, 575 (1989).
- [Tsu99] E. Tsuchida, Y. Kanada, and M. Tsukada, *Density-functional study of liquid methanol*, Chem, Phys. Lett **311**, 236 (1999).
- [Tzv04] G. Tzvetkov, G. Koller, Y. Zubavichus, O. Fuchs, M. B. Casu, C. Heske, E. Umbach, M. Grunze, M. G. Ramsey, and F. P. Netzer, *Bonding and structure of glycine on ordered Al<sub>2</sub>O<sub>3</sub> film surfaces*, Langmuir **20**, 10551 (2004).

- 
- [Umb90] E. Umbach, *Characterization of organic overlayers on well-defined substrates*, Prog. Surf. Sci. **35**, 113 (1990).
- [Umb98] E. Umbach, K. Glöckler, and M. Sokolowski, *Surface “architecture” with large organic molecules: interface order and epitaxy*, Surf. Sci. **404**, 20 (1998).
- [Urq02] S. G. Urquhart and H. Ade, *Trends in the carbonyl core (C 1s, O 1s)  $\rightarrow$   $\pi^*c=O$  transition in the near-edge X-ray absorption fine structure spectra of organic molecules*, J. Phys. Chem. B **106**, 8531 (2002).
- [Vau1806] L. N. Vauquelin and P. J. Robiquet, *The discovery of a new plant principle in Asparagus sativus*, Ann Chim **57**, 88 (1806).
- [Wad84] R. H. Wade, *The temperature-dependence of radiation damage in organic and biological materials*, Ultramicroscopy **14**, 265 (1984).
- [Wei03] L. Weinhardt, M. Bär, H.-J. Muffler, Ch.-H. Fischer, M.C. Lux-Steiner, T.P. Niesen, F. Karg, Th. Gleim, C. Heske, and E. Umbach, *Impact of Cd<sup>2+</sup>-treatment on the band alignment at the ILGAR-ZnO/CuIn(S,Se)<sub>2</sub> heterojunction*, Thin Solid Films **431-432**, 272 (2003).
- [Wei03\_2] L. Weinhardt, Th. Gleim, O. Fuchs, C. Heske, E. Umbach, M. Bär, H.-J. Muffler, Ch.-H. Fischer, M.C. Lux-Steiner, Y. Zubavichus, T.P. Niesen, and F. Karg, *CdS- and Cd(OH)<sub>2</sub>-formation during Cd-treatments of Cu(In,Ga)(S,Se)<sub>2</sub> thin film solar cell absorbers*, Appl. Phys. Lett. **82**, 571 (2003).
- [Wei07] L. Weinhardt, O. Fuchs, E. Umbach, C. Heske, A. Fleszar, W. hanke, and J. D. Denlinger, *Resonant inelastic soft x-ray scattering, x-ray absorption spectroscopy, and density functional theory calculations of the electronic bulk band structure of CdS*, Phys. Rev. B **75**, 165207 (2007).
- [Wei09] L. Weinhardt, O. Fuchs, M. Blum, M. Bär, M. Weigand, J.D. Denlinger, Y. Zubavichus, M. Zharnikov, M. Grunze, C. Heske, and E. Umbach, *Resonant x-ray emission spectroscopy of liquid water: novel instrumentation, high resolution, and the ‘map’ approach*, J. Electron Spectrosc. Rel. Phenom, doi: 10.1016/j.elspec.2009.02.014 (2009).

- [Wer04] P. Wernet, D. Nordlund, U. Bergmann, M. Cavalleri, M. Odelius, H. Ogasawara, L. A. Naslund, T. K. Hirsch, L. Ojamae, P. Glatzel, L. G. M. Pettersson, and A. Nilsson, *The structure of the first coordination shell in liquid water*, *Science* **304**, 995 (2004).
- [Wil04] K. R. Wilson, B. S. Rude, J. Smith, C. Cappa, D. T. Co, R. D. Schaller, M. Larsson, T. Catalano, and R. J. Saykally, *Investigation of volatile liquid surfaces by synchrotron x-ray spectroscopy of liquid microjets*, *Rev. Sci. Instrum.* **75**, 725 (2004).
- [Wil05] K. R. Wilson, M. Cavalleri, B. S. Rude, R. D. Schaller, T. Catalano, A. Nilsson, R. J. Saykally, and L. G. M. Pettersson, *X-ray absorption spectroscopy of liquid methanol microjets: Bulk electronic structure and hydrogen bonding network*, *J. Phys. Chem. B* **109**, 10194 (2005)
- [Wil09] R. G. Wilks, J. B. MacNaughton, H.-B. Kraatz, T. Regier, R. I. R. Blyth, and A. Moewes, *Comparative Theoretical and Experimental Study of the Radiation-Induced Decomposition*, *J. Phys. Chem. A* **113**, 5360 (2009).
- [Win06] B. Winter and M. Faubel, *Photoemission from liquid aqueous solutions*, *Chem. Rev.* **106**, 1176 (2006).
- [Win06] B. Winter, M. Faubel, I. V. Hertel, C. Pettenkofer, S. E. Bradforth, B. Jagoda-Cwiklik, L. Cwiklik, and P. Jungwirth, *Electron binding energies of hydrated  $H_3O^+$  and  $OH^-$ : Photoelectron spectroscopy of aqueous acid and base solutions combined with electronic structure calculations*, *J. Am. Chem. Soc.* **128**, 3864 (2006).
- [Wu87] C. R. Wu, J. O. Nilsson, and W. R. Salaneck, *Photoelectron Spectroscopy of the Absorption of Amino Acids on Surfaces: Glycine on  $Si(O_2)$* , *Physica Scripta* **35**, 586 (1987).
- [Yag04] S. Yagi, Y. Matsumura, K. Soda, E. Hashimoto, and M. Taniguchi, *Interface study for liquid-solid state surface by means of the S K-edge NEXAFS method*, *Surf. Interface Anal.* **36**, 1064 (2004).
- [Yam99] T. Yamaguchi, K. Hidaka, and A. K. Soper, *The structure of liquid methanol revisited: A neutron diffraction experiment at -80 degrees C and +25 degrees C*, *Mol Phys.* **96**, 1159 (1999).

- 
- [Zou06] Y. Zou, L. Kilian, A. Schöll, T. Schmidt, R. Fink, and E. Umbach, *Chemical bonding of PTCDA on Ag surfaces and the formation of interface states*, Surf. Sci. **600**, 1240 (2006).
- [Zub04] Y. Zubavichus, O. Fuchs, L. Weinhardt, C. Heske, E. Umbach, J. D. Denlinger, and M. Grunze, *Soft x-ray-induced decomposition of amino acids: An XPS, mass spectrometry, and NEXAFS study*, Radiat. Res. **161**, 346 (2004).
- [Zub04\_2] Y. Zubavichus, M. Zharnikov, A. Shaporenko, O. Fuchs, L. Weinhardt, C. Heske, E. Umbach, J. D. Denlinger, and M. Grunze, *Soft X-ray induced decomposition of phenylalanine and tyrosine: A comparative study*, J. Phys. Chem. A **108**, 4557 (2004).
- [Zub04\_3] Y. Zubavichus, M. Zharnikov, A. Schaporenko, and M. Grunze, *NEXAFS study of glycine and glycine-based oligopeptides*, J. Electron Spectrosc. Relat. Phenom. **134**, 25 (2004).
- [Zub05] Y. Zubavichus, A. Shaporenko, M. Grunze, and M. Zharnikov, *Innershell absorption spectroscopy of amino acids at all relevant absorption edges*, J. Phys. Chem. A **109**, 6998 (2005).
- [Zub05\_2] Y. Zubavichus, M. Zharnikov, Y. J. Yang, O. Fuchs, C. Heske, E. Umbach, G. Tzvetkov, F. P. Netzer, and M. Grunze, *Surface chemistry of ultrathin films of histidine on gold as probed by high-resolution synchrotron photoemission*, J. Phys. Chem. B **109**, 884 (2005).
- [Zub06] Y. Zubavichus, A. Shaporenko, M. Grunze, and M. Zharnikov, *Solid-state near-edge X-ray absorption fine structure spectra of glycine in various charge states*, J. Phys. Chem. B **110**, 3420 (2006).
- [Zub07] Y. Zubavichus, A. Shaporenko, M. Grunze, and M. Zharnikov, *NEXAFS spectroscopy of homopolypeptides at all relevant absorption edges: Polyisoleucine, polytyrosine, and polyhistidine*, J. Phys. Chem. B **111**, 9803 (2007).

## Own Publications

---

- [A01]      *“SALSA – a soft x-ray spectroscopy endstation with a novel flow-through liquid cell”*  
M. Blum, L. Weinhardt, O. Fuchs, M. Bär, Y. Zhang, M. Weigand, S. Krause, S. Pookpanratana, T. Hofmann, W. Yang, J. D. Denlinger, E. Umbach, and C. Heske  
Rev. Sci. Instrum. **80**, 123102 (2009).
- [C01]      *“Resonant x-ray emission spectroscopy of liquid water: novel instrumentation, high resolution, and the map approach”*  
L. Weinhardt, O. Fuchs, M. Blum, M. Bär, M. Weigand, J.D. Denlinger, Y. Zubavichus, M. Zharnikov, M. Grunze, C. Heske, and E. Umbach, J. El. Spectrosc. Rel. Phenom., doi: 10.1016/j.elspec.2009.02.014 (2009).
- [C02]      *“High-resolution, high-transmission soft x-ray spectrometer for the study of biological samples”*  
O. Fuchs, L. Weinhardt, M. Blum, M. Weigand, E. Umbach, M. Bär, C. Heske, J. Denlinger, Yi-De Chuang, W. McKinney, Z. Hussain, E. Gullikson, M. Jones, P. Batson, B. Nelles, and R. Follath, Rev. Sci. Instrum. **80**, 063103 (2009).
- [C02]      *“Resonant inelastic soft x-ray scattering map of CdS”*  
L. Weinhardt, O. Fuchs, A. Fleszar, M. Bär, M. Blum, M. Weigand, J.D. Denlinger, W. Yang, W. Hanke, E. Umbach, and C. Heske, Phys. Rev. B **79**, 165305 (2009).
- [C03]      *“Impact of air-exposure on the chemical and electronic structure of ZnO:Zn<sub>3</sub>N<sub>2</sub> thin films”*  
M. Bär, K.-S. Ahn, Y. Yan, L. Weinhardt, O. Fuchs, M. Blum, K. George, S. Pookpanratana, W. Yang, J.D. Denlinger, M. Al-Jassim, and C. Heske, Appl. Phys. Lett. **94**, 012110 (2009).
- [C04]      *“Depth-resolved band gap energies in Cu(In,Ga)(S,Se)<sub>2</sub> thin films”*  
M. Bär, L. Weinhardt, S. Pookpanratana, C. Heske, S. Nishiwaki, W. Shafarman, O. Fuchs, M. Blum, W. Yang, and J.D. Denlinger, Appl. Phys. Lett. **93**, 244103 (2008).

- 
- [C05]      *“Isotope and temperature effects in liquid water probed by x-ray absorption and resonant x-ray emission spectroscopy”*  
O. Fuchs, M. Zharnikov, L. Weinhardt, M. Blum, M. Weigand, Y. Zubavichus, M. Bär, F. Maier, W. Yang, J. D. Denlinger, C. Heske, M. Grunze, and E. Umbach,  
Phys. Rev. Lett. **100**, 027801 (2008).
- [C06]      *Comment on Phys. Rev. Lett. 100, 027801 (2008)*  
O. Fuchs, M. Zharnikov, L. Weinhardt, M. Blum, M. Weigand, Y. Zubavichus, M. Bär, F. Maier, W. Yang, J. D. Denlinger, C. Heske, M. Grunze, and E. Umbach,  
Phys. Rev. Lett. **100**, 249802 (2008).
- [C07]      *“Intermixing and chemical structure at the interface between n-GaN and V-based contacts”*  
S. Pookpanratana, R. France, M. Bär, L. Weinhardt, O. Fuchs, M. Blum, W. Yang, J. D. Denlinger, T. D. Moustakas, and C. Heske,  
Appl. Phys. Lett. **93**, 172106 (2008).
- [C08]      *“Electronic surface level positions of WO<sub>3</sub> thin films for photoelectrochemical hydrogen production”*  
L. Weinhardt, M. Blum, M. Bär, C. Heske, B. Cole, B. Marsen, and E.L. Miller,  
J. Phys. Chem. C **112**, 3078 (2008).
- [C09]      *“A liquid flow cell to study the electronic structure of liquids with soft X-rays”*  
O. Fuchs, F. Maier, L. Weinhardt, M. Weigand, M. Blum, M. Zharnikov, J. Denlinger, M. Grunze, C. Heske, and E. Umbach,  
Nucl. Instrum. Meth. A **585**, 172 (2008).
- [C10]      *“Chemical properties of the Cu(In,Ga)Se<sub>2</sub>/Mo/glass interfaces in thin film solar cells”*  
L. Weinhardt, M. Blum, M. Bär, C. Heske, O. Fuchs, E. Umbach, J.D. Denlinger, K. Ramanathan, and R. Noufi,  
Thin Solid Films **515**, 6119-6122 (2007).



# Curriculum Vitae

---

## Persönliche Daten

[Name]	Blum
[Vornamen]	<u>Monika</u> Annette
[Geburtsdatum]	10. August 1982
[Geburtsort]	Aschaffenburg
[Familienstand]	ledig

## Ausbildung und Beruf

[09/1992 – 07/2001]	Maria-Ward-Schule Aschaffenburg – Abitur
[10/2001 – 04/2006]	Julius-Maximilians Universität Würzburg – Studium der Nanostrukturtechnik Thema der Diplomarbeit: <i>“X-ray and Electron Spectroscopy of WO<sub>3</sub> and CdS/Cu(In,Ga)Se<sub>2</sub> thin films for photoelectrochemical and photovoltaic devices”</i>
[07/2005 – 04/2006]	University of Nevada Las Vegas, USA – Auslandsaufenthalt
[07/2006 – 09/2009]	Julius-Maximilians Universität Würzburg - Doktorarbeit Experimentelle Physik II
[seit 10/2009]	University of Nevada Las Vegas, USA und Lawrence Berkeley National Laboratory, CA, USA – Anstellung

## Stipendien

[02/2004 – 04/2006]	Infineon Technologies AG – Student MemberChip Program
[11/2006 – 10/2009]	Stiftung der Deutschen Wirtschaft – Promotionsförderung

---

# Acknowledgment

---

Nach drei Jahren ist es Zeit einmal bei allen “DANKE” zu sagen, die einen erheblichen Beitrag zum Entstehen dieser Doktorarbeit geleistet haben.

Besonderer Dank gilt meinem Doktorvater **Prof. Dr. Eberhard Umbach**, der mich fachlich und auch persönlich geprägt hat. Mit der Aufnahme in seine Arbeitsgruppe bekam ich die Möglichkeit in einem doch eher seltenen (dafür umso spannenderen) Forschungsgebiet zu arbeiten und meine Begeisterung für Instrumentierung zu entdecken.

Genauso herzlich möchte ich mich bei meinem „Ersatz-Doktorvater“ **Prof. Dr. Clemens Heske** bedanken, der mich auch über den großen Teich hinweg unterstützt und gefördert hat und mir ein zweites Zuhause in seiner Arbeitsgruppe gab.

**Prof. Dr. Kai Fauth** danke ich für die Übernahme des Zweitgutachtens, das in Rekordzeit angefertigt werden musste, und für die nächtlichen Aufmunterungsbesuche an der Beamline während meiner BESSY Messzeit.

Bei **PD Dr. Reinhold Fink** möchte ich mich bedanken, dass er sich bereit erklärt hat mein Drittprüfer in der Verteidigung zu sein.

Dank **Prof. Dr. Friedel Reinert** und seinen unzähligen Gutachten war mein Geldgeber, die Stiftung der Deutschen Wirtschaft, immer glücklich.

Meinen zwei Super-Post-Docs **Marcus Bär** und **Lothar Weinhardt** ein ganz dickes DANKE für tolle Messzeiten und für alles was ich von ihnen lernen durfte. Lothar gilt noch zusätzlich mein Dank für die vielen Diskussionen, die Inspirationen und die schöne Zeit im Büro (Immer schön ans Blumengießen denken!).

**Oliver Fuchs** (meinem Vorgänger) danke ich, dass er mich in die Welt der Flüssigkeiten eingeführt hat.

**Michael Odelius** gilt mein Dank für die theoretische Unterstützung und die unzähligen Rechnungen die er für mich gemacht hat. Michael, tack så mycket för beräkningar som räddade mitt aminosyrakapitel. Jag ser redan fram emot att samarbeta med dig igen!

Mit **Florian Holch** und **Franziska Niederdraenk** habe ich mir gegen Ende meiner Arbeit öfters die Nächte um die Ohren geschlagen und lustige Kaffeerunden nachts um zwei erlebt. Vielen Dank euch, es war immer eine schöne Abwechslung. Flo gilt noch mein besonderer Dank, da er nicht nur meine Arbeit gedruckt sondern mich auch zur Doktorprüfung angemeldet hat. Danke!

Ich hatte das Glück während meiner Arbeit in zwei Arbeitsgruppen eingebunden zu sein. Daher danke ich allen Kollegen und Freunden aus der **EPII** und der **UNLV group** sehr herzlich für das angenehme Arbeitsklima und die schöne Zeit.

Für das Bereitstellen der Kohlenstoffmembranen danke ich **Joakim Andersson**. Joakim, dina membraner är världsklassa! Tack att jag fick testa dem. Lycka till med ditt företag!

---

Ohne die **Mechanikwerkstatt** der Physik wäre SALSA und somit ein Teil meine Arbeit in diesem Maße nie entstanden. Besonders **Rainer Brauner** und **Günter Carl** haben immer das Unmögliche für mich möglich gemacht auch wenn es sehr, sehr kurzfristig war.

Es gibt noch ein paar Menschen, denen ich recht herzlich danken möchte, da sie mich unbewusst mehr unterstützt haben, als sie vielleicht denken. Dazu gehören meine **Freunde** (ich glaube, sie wissen alle auch ohne Namen, dass sie gemeint sind), die mich mit Abendprogramm, Kochen, Kickern oder einfach nur Reden abgelenkt haben. **Katha** und **Günther** die meinen „Werdegang“ immer verfolgt haben. **Anette, Louisa, Johann** und **Clara**, die für mich meine amerikanische Ersatzfamilie sind. Und natürlich meine **Eltern**, meine **Schwester** und mein **Schwager**, die immer an mich geglaubt haben.